PERFORMANCE ANALYSIS OF OPTICAL IMPLEMENTATION OF LMS AND KALMAN FILTER BASED ADAPTIVE NOISE CANCELER

By

Sudesh K Pandit

DEPARTMENT OF NUCLEAR ENGINEERING & TECHNOLOGY
INDIAN INSTITUTE OF TECHNOLOGY KANPUR
JULY, 2003

22 SEP 2003 / NET
पुरुषोत्तम काशीनाथ केलकर पुस्तकालय
भारतीय प्रौद्योगिकी संस्थान कानपुर
अवाप्ति क्र० A 145006

A145006

THESIS SUBMITTED
ON 30-7-03
I.I.T., KANPUR 16

CERTIFICATE

This is to certify that the thesis work entitled "***Performance Analysis of Optical Implemenattion of LMS and Kalman Filter based Adaptive Noise Canceler***", by Mr. **Sudesh K Pandit** (Roll. No. Y111506) has been carried out under my supervision and the same has not been submitted elsewhere for a degree.

30 July 2003

Dr. Anjan K. Ghosh
Professor & Head
Department of Electrical Engineering
Indian Institute of Technology Kanpur
208016.

Offered with utmost humility at the feet of
Swami Vivekananda

ACKNOWLEDGEMENT

I take this opportunity to express my gratitude to my thesis supervisor, Prof. Anjan K Ghosh, for his guidance and sharing his knowledge with me. Particularly his generous nature towards me helped me in carrying out the research without much difficulty. His continuous support, advices, and discussions were invaluable to the preparation of the thesis.

There are many people whom I am aware of, and also many people whom I am unaware of, who directly or indirectly helped me in carrying out the completion of my thesis work. I feel it to be a sort of partiality in naming anybody's name over here. So without writing anybody's name let me express my gratefulness to all of them.

I am also thankful to Bhabha Atomic Research Center (BARC), Mumbai for the financial support of this research work. Finally, I express my regards to the Professors, particularly Prof. P. Munshi and Prof. M. S. Kalra, and Staffs of Department of Nuclear Engineering & Technology Programme, IIT Kanpur, for their time to time needful help.

Sudesh K Pandit

Abstract

The photonics technology is playing an important role in providing enormous bandwidth in communication and signal processing applications. The recent trend in high speed optical communication and signal processing systems is to use several photonic devices and as few electronic systems as possible in order to fully achieve the high bandwidth that photonics offers. Presence of noise in the system degrades its performance. Noise combating through an Adaptive Noise Cancellation method seems to be very promising in several cases.

The present thesis explored the Adaptive Noise Cancellation method based on least-mean-square and Kalman filter algorithms to remove the noise from optical signals. The methods presented can directly process the optical signals from optical fibers by using spatial light modulators or acousto-optic cells, lenses, detectors and a few minimum electronic components. Error and noise models of photonic processors that can realize the noise canceling algorithms are developed. Detailed computer simulations were carried out to analyze the performance of the noise canceling algorithms in presence of optical hardware errors, and under different choices of system parameters. Results obtained give guidelines on the design of such systems. High quality spatial light modulators and acousto-optic cells should be employed and the number of taps of the filter should be kept below 10. In case of least-mean-square algorithm the effects of optical hardware errors can be further reduced by an optimum selection of its parameters.

Contents

Certificate i
Acknowledgement iii
Abstract iv
List of Figures vii
List of Tables xi
Nomenclature xii

1 Introduction 1
- 1.1 Motivation 2
- 1.2 About the thesis and objectives 2
- 1.3 Thesis layout 3

2 Adaptive Noise Cancellation 5
- 2.1 Basic Concept 5
- 2.2 Basic Theory of LMS based ANC 8
  - 2.2.1 Derivation of time constant 9
  - 2.2.2 Bounds on μ 10
  - 2.2.3 Covariance of gradient of $|\varepsilon_k|^2$ under noisy condition 10
  - 2.2.4 Derivation of excess mean-square-error and *Misadjustment* 13
- 2.3 Theoretical background on Kalman Filter 15
  - 2.3.1 Estimation and optimization of state 16
  - 2.3.2 Summary of Equations for Discrete-Time Kalman Estimator: . . . 20
- 2.4 Mathematics of Kalman filter when applied to ANC 21
  - 2.4.1 Study of convergence of Kalman filter algorithm in ANC 24
  - 2.4.2 Derivation of *excess-mean-square-error* and *Misadjustment* 26
- 2.5 Review of results with both algorithm 27
  - 2.5.1 Case study and general simulation idea 27
  - 2.5.2 Results with LMS filter 32
  - 2.5.3 Results with Kalman filter approach 42
  - 2.5.4 Comparison of results of LMS and Kalman filter 50
  - 2.5.5 Conclusions made on these results 55

3 **Optical Implementation of LMS filter** 57

3.1 Elements for optical realization 57

3.2 Optical LMS algorithm 63

3.3 Handling negative values 66

4 **Performance of LMS algorithm in presence of Optical Errors** 67

4.1 Error source identification & modeling 67

4.2 Derivation of MSE, *Misadjustment* and Signal to Noise Ratio 69

4.3 Performance optimization 74

5 **Optical realization of Kalman filter** 76

5.1 Acousto-optic Systems 76

5.2 Basic algebraic calculations using AO cell 80

5.2.1 Matrix-vector multiplication 80

5.2.2 Matrix-matrix multiplication 81

5.2.3 Vector outer product 81

5.3 Optical Kalman filter 82

6 **Optical Error and Noise Modeling in Kalman Filter algorithm** 87

6.1 Error source modeling of AO cell 87

6.2 Error source modeling of optical Kalman filter 89

7 **Simulation and results** 94

7.1 Signal modeling 94

7.2 Results of LMS implementation 94

7.3 Results of Kalman filter implementation 102

8 **General discussion on optical system** 108

8.1 Merits and limitations of optical system 108

8.2 Current technology 110

9 **Summary and Conclusions** 111

9.1 Main contributions 111

9.2 Conclusions 111

9.3 Future work 112

Bibliography **114**

List of Figures

2.1 Block diagram of adaptive noise cancellation system. 6

2.2 An N tapped or $(N-1)^{th}$ order transversal filter applied to ANC system. 7

2.3 Block diagram of system, measurement model, and discrete-time Kalman filter. 21

2.4 (a) Variation of *Misadjustment* with the noise level l ($N = 2$, $\mu = 0.002$, and $cc = 1$). (b) zoomed view to show discrepancy between theoretical M and practically measured M. 33

2.5 Variation of SNR of output signal with noise level l ($N = 2$, $\mu = 0.002$, and $cc = 1$). 34

2.6 Frequency response of output signals for different values of noise level l ($N = 2$, $\mu = 0.002$, and $cc = 1$). 35

2.7 Variation of M with number of taps N ($l = 1$, $\mu = 0.002$, and $cc = 1$). 36

2.8 Variation of SNR of output signal with number of taps N ($l = 1$, $\mu = 0.002$, and $cc = 1$). 36

2.9 Frequency response of output signals for different number of taps N ($l = 1$, $\mu = 0.002$, and $cc = 1$). 37

2.10 FFT of weight vectors for different filter length ($l = 1$, $\mu = 0.002$, and $cc = 1$). 37

2.11 Variation of M versus the adaptive gain constant μ ($l = 1$, $N = 2$, and $cc = 1$). 39

2.12 Plots showing variations of the theoretical and measured SN with μ ($l = 1$, $N = 2$, and $cc = 1$). 39

2.13 Frequency response of output signals for different μ, ($l = 1$, $N = 2$, and $cc = 1$). 40

2.14 Variation of PF with μ ($l = 1$, $N = 2$, and $cc = 1$). 41

2.15 Spectrum of pure, primary and output signals ($\mu = 0.002$, $l = 1$, $N = 2$, and $cc = 1$). 42

2.16 Variation of M with the correlation coefficient cc ($N = 2$, $\mu = 0.002$, and $l = 1$). 43
2.17 Plots showing the SNR of the output signal with cc for two different values of number of taps, $N = 2$ and 6 ($l = 1$ and $\mu = 0.002$). 43
2.18 Frequency response of output signals for different cc ($l = 1$, $N = 2$, and $\mu = 0.002$). 44
2.19 Variation of M with the noise level, l ($N = 2$ and $cc = 1$, Kalman filter). 45
2.20 Plots showing variations of SNR of the output signal with the noise level l ($N = 2$ and $cc = 1$, Kalman filter). 45
2.21 Spectrum of the output signals at different noise level l ($N = 2$ and $cc = 1$, Kalman filter). 46
2.22 Variation of M with N ($l = 1$ and $cc = 1$, Kalman filter). 47
2.23 Plots showing the variations SNR of the output signal with N ($l = 1$ and $cc = 1$, Kalman filter). 48
2.24 Frequency response of the output signal for different values of N ($l = 1$ and $cc = 1$, Kalman filter). 48
2.25 Plots of M versus cc ($l = 1$ and $N = 2$, Kalman filter). 49
2.26 Plots of SNR of the output signal versus correlation coefficient, cc for two different values of $N = 2$ and 6 ($l = 1$, Kalman filter). . . . 49
2.27 Spectrum of the output signals for various values of cc ($l = 1$ and $N = 2$, Kalman filter). 50
2.28 Comparison of *Misadjustment* in LMS and Kalman implementations when noise level l is varied. ($N = 2$ and $cc = 1$, in both case.) . . . 51
2.29 Comparison of SNR of outputs obtained from LMS and Kalman implementations of ANC when noise level l is varied ($N = 2$ and $cc = 1$, in both case). 52
2.30 Comparison of *Misadjustment* in LMS and Kalman filter implementations when number of taps N is varied ($l = 1$ and $cc = 1$, in both case). 53
2.31 Comparison of the output SNR obtained in LMS and Kalman filter, for different number of taps ($l = 1$ and $cc = 1$, in both case). 53
2.32 Comparison of *Misadjustment* in LMS and Kalman implementations when cc is varied ($N = 2$ and $l = 1$, in both case). 54
2.33 Plots showing the comparison of output SNR in LMS and Kalman filter implementations when cc is varied ($N = 2$ and $l = 1$, in both case). 55

3.1 Optical fiber delay lines: (a) Fiber bundle type tapped delay line; (b) Longitudinal tapped delay line 58
3.2 Major SLM functional structures [A indicates optical wave amplitudes and I the intensities or currents]. (a,b) Signal multiplying and amplifying type SLM; (c) Self-modulating type SLM; (d) Self-emissive type SLM. 60
3.3 Optoelectronic transversal filter based on MSM photo-diode. 62
3.4 Fiber optic based ANC using fiber-bundle type FOTDL. 63
3.5 Scheme to illustrate the arrangement of SLM in Figure 3.4. 64
3.6 Fiber optic based ANC using a LACE processed FOTDL. 65

4.1 Schematic diagram of fiber optic LMS algorithm for ANC with dominant error sources. 68

5.1 Bragg cell used as (a) light-beam modulator and (b) light-beam deflector. Input beam enter from the left at angle satisfying condition for Bragg diffraction. 77
5.2 Schematic diagram shows the use of AO Bragg cell to produce amplitude modulated light. 78
5.3 Multiple input-output beam (a) modulation and (b) deflection. Optical stop in (a) prevents undiffracted light from reaching image plane. 79
5.4 Basic space-, time-, and frequency-multiplexed optical systolic matrix-vector or matrix-matrix processor system. 80
5.5 A schematic diagram of an optical processor for calculating outer product between a column and a row vector. 82
5.6 Optical Implementation of a Kalman filter for ANC using fiber bundle FOTDL and AO Bragg cells. (Thick lines are for the optical signal while thin line shows the electrical path.) 84
5.7 Scheme to illustrate the optical computations of three quantity simultaneously using a 3-channel AO cell. 85

6.1 Schematic diagram of error model with dominant error sources in realizing optical Kalman filter based ANC. 92
6.2 Positions of elements of X_k while handling bipolar data. Only alternate positions of the AO cell is illuminated by the signal. 93

7.1 Variation of SNR of output signal with cc for different levels of optical errors (number of taps=2 and $\mu = 0.002$). 95

7.2 Variation of SNR of output signal with optical error σ_0 for different values of cc (number of taps=2 and $\mu = 0.002$). 96
7.3 Variation of SNR of output signal with adaptive gain μ for different levels of optical errors (number of taps, N=2 and $cc = 1$). 97
7.4 Variation of SNR of output signal with adaptive gain μ for different number of taps ($\sigma_0 = 10^{-3}$ and $cc = 1$). 98
7.5 Variation of SNR of output signal with detector noise σ_{det}, at different values of spatial error σ_{spa} (Number of taps, $N = 2$, adaptive gain constant $\mu = 0.002$, $cc = 1$, and $\sigma_{tap} = 10^{-5}$). 100
7.6 Variation of SNR of output signal with spatial error σ_{spa}, at different values of detector noise σ_{det} (Number of taps, $N = 2$, adaptive gain constant $\mu = 0.002$, $cc = 1$, and $\sigma_{tap} = 10^{-5}$). 101
7.7 Variation of SNR of output signal with correlation coefficient cc, at different levels of optical error σ_0 (Number of taps, $N = 2$, Kalman filter). 103
7.8 Variation of SNR of output signal with optical error σ_0, for different values of correlation coefficient cc (Number of taps, $N = 2$, Kalman filter). 104
7.9 Variation of SNR of output signal with number of taps N, at various levels of optical error σ_0 ($cc = 1$, Kalman filter). 105
7.10 Variation of SNR of output signal with optical error σ_0 for different values of number of taps N ($cc = 1$, Kalman filter). 106
7.11 Variation of SNR of output signal with additive error, σ_a for different levels of multiplicative error σ_m ($cc = 1$, $N = 2$, Kalman filter). . . . 106
7.12 Variation of SNR of output signal with multiplicative error, σ_m for different levels of additive error σ_a ($cc = 1$, $N = 2$, Kalman filter). . 107

List of Tables

2.1 Discrete-time Kalman filter equations 20
2.2 Discrete-time Kalman filter equations for ANC 24

3.1 Underlying techniques for spatial light modulation. 60

6.1 Error source model for matrix vector multiplier. 90

7.1 Comparison of theoretical and simulated values of μ_{opt} at different levels of optical error. 98
7.2 Comparison of theoretical and simulated values of μ_{opt} for different number of taps. 99

Nomenclature

Abbreviations

ANC	Adaptive Noise Cancellation
AO	Acousto-Optic
CRT	Cathode Ray Tube
DC	Direct Current
ECG	Electro-Cardio-Graph
FFT	Fast Fourier Transform
FOSP	Fiber Optic Signal Processor
FOTDL	Fiber-Optic Time Delay Line
FR	Frequency Response
FT	Fourier Transform
FWHM	Full Width Half Maximum
IIR	Infinite Impulse Response
I/P	Input
LACE	Laser Ablative Chemical Etching
LED	Light Emitting Diode
LMS	Least Mean Square
MSM	Metal Semiconductor Metal
OLAP	Optical Linear Algebra Processor
O/P	Output
PMT	Photo-Multiplier-Tube
RADAR	Radio Detection And Ranging
RF	Radio Frequency
RMS	Root Mean Square
SLM	Spatial Light Modulator
SNR	Signal to Noise Ratio
std.	Standard Deviation
VLSI	Very Large Scale Integration

Important Dimensional Symbols[1]

X_k	Input signal vector

---

[1] Some symbols are repeated, but it will not create problem in undersatnding

W_k	Weight vector
W^*	Weiner weight vector
P	Cross-correlation matrix, and Error covariance matrix
R	Auto-correlation matrix
U_k, V_k	Weight error vector between Weiner and actual weights
Λ	Transformed matrix R, in Principal co-ordinate system
Q	Eigen vector matrix of R, and Auto-covariance matrix of Π_k
∇_k	Gradient vector of $\lvert\varepsilon_k^2\rvert$
N_k	Gradient vector of noise under noisy estimate
$\widehat{\nabla}_k$	Total gradient vector of $\lvert\varepsilon_k^2\rvert$
S_k	State vector
Z_k	Measurement vector
Φ_k	State transition matrix
H_k	Measurement sensitivity matrix
G_k	Process noise coupling matrix
Π_k	Plant noise process
Ξ_k	Measurement noise process
L	Auto-covariance matrix of Ξ_k, and Vector having all elements $= 1$
M	Cross-covariance matrix between Π_k and Ξ_k
K_k	*Kalman gain*
Γ_k	State estimation error
Σ_k	Estimation error in measurement
δX_k	Tap position error
ΔW_k	Total inaccuracy in optically computed weight
δW_k	Spatial error in weight
$1 + \delta Mul$	Total residual multiplicative error
δAdd	Total residual additive error

Important Non-Dimensional Symbols

d_k	Desired signal or Primary signal
s_k	Pure signal
$(n_o)_k$	Noise signal interfering with pure signal
$(n_1)_k$	Noise signal or Reference Signal
y_k	Filter output
ε_k	Error signal or output signal
cc	Correlation coefficient between $(n_o)_k$ and $(n_1)_k$
N	Number of taps
x_k	Reference Signal
w_k	Element of weight vector
N_k	Gradient vector of noise under noisy estimate
μ	Adaptive gain constant
τ_n	Time constant
λ_n	Eigen value of R
ξ	Mean-square-error

χ	*Excess-mean-square-error*
u_{nk}	Element of vector U_k
M	*Misadjustment*
SN	Signal to noise ratio
w^*	Element of Weiner vector
v_{nk}	Element of vector V_k
PF	*Performance Factor*
CT	*Convergence time*
Φ_{dd}	Auto-correlation function of primary signal
Φ_{xx}	Auto-correlation function of reference signal
Φ_{dx}	Cross correlation function between primary and reference signals
l	Noise level
$dnoise$	Standard deviation of noise in output
dop	Standard deviation of output signal
$dpure$	Standard deviation of pure signal
x(t)	Time varying signal
β_k, φ_k	Detector noise
σ	Standard deviation of different optical errors
$\Delta\varepsilon_k$	Difference between ε_k and optically computed $\varepsilon_k^{'}$
D	DC value
λ	Wavelength of light
Υ	Wavelength of acoustic wave
θ	Bragg's angle
f	Frequency
T_B	Bit time

Special Symbols

$E\langle\cdots\rangle$	Expected value
Z^{-1}	Delay by 1 sample
$trace(..)$	Trace of matrix
$cov[..]$	Covariance of matrix
$\aleph(..)$	Normal Gaussian Process
$Ztransform[..]$	Z-Transform of signal
$\|..\|$	Norm of a quantity
$\hat{\cdot}$	Estimated value
$(-)$	*a priori value*
$(+)$	*a posteriori value*

Subscript

k	k^{th} sample of the signal
i	Delay of i^{th} sample
n	n^{th} elemental value

min	Minimum value
max	Maximum value
$total$	Total value
opt	Optimum value
spa	Spatial error
tap	Tap position error
det	Detector error
mul	Multiplication error of LMS algorithm
ofa	Optical fiber amplifier error
$coup$	Coupling error
amp	Amplifier error
$AOfreq$	Error due to frequency response of AO cell
$AOatten$	Attenuation error of AO cell
$AOspa$	Spatial error in AO cell
$DFspa$	Detector or Fiber spatial error
$dark$	Dark current error
a	Additive errors
m	Multiplicative error

Superscript

T	Transpose
$'$	Value after transforming to principal coordinate system, And also, value under optical noise or errors
LMS	For LMS algorithm
Kal	For Kalman filter algorithm

Chapter 1

Introduction

Noise combating is one of the most challenging problems in signal processing, communication system or networking. Electrical noise is present in every electrical system. The information carried by a signal can be misinterpreted because of the presence of noise. Therefore in all signal processing and communication systems, it is important to reduce or eliminate the noise. There are two broad classes of methods to eliminate noise from a signal. First method is the filtering process. This method removes the noise from the signal by suppressing certain frequencies. However, it may also remove an important part of the information carried by the signal. The second method is Adaptive Noise Cancellation (ANC). The subject of Adaptive Noise Cancellation was introduced and is treated extensively by Widrow *et al.* [1]. In this method, first the noise present in the system is estimated and then this estimated noise is subtracted from the received signal.

At first glance, the idea of subtracting noise from the received signal seems to be dangerous as its improper implementations may increase output noise power. However, if, filtering and subtraction are controlled by an appropriate adaptive process, noise reduction, in many cases be accomplished with little risk of distorting the signal or increasing output noise level. In circumstances, where ANC is applicable, we can often achieve a degree of noise rejection that would be difficult or impossible to achieve by direct filtering. This method effectively removes the noise even if the noise has the frequencies same as those present in the signal. The ANC also allows processing of input signals whose properties are unknown and non-stationary. These are the major advantages of ANC.

ANC based filtering is employed where there is an available signal, which is highly correlated with the interfering noise. Since the advent of this method it has been tried and used in many areas. Initially it was employed to remove the hum in

ECG signals [1]. Then it has been extensively used for speech signals, like reduction of acoustic noise in speech [2], [3], speech enhancement [4], and echo cancellation in long distance telephone lines [5]. Another major area of application is in adaptive beam-forming in RADAR [6], [7]. Some of the other applications of ANC are computerized tomography [8], inspection of magnetic flux leakage obtained from gas pipeline [9], geophysical signal detection [10].

1.1 Motivation

While dealing with the problems in Gamma Ray Bursts detection, we thought it fruitful to apply ANC technique to see its utility in eliminating the noise. Gamma Ray Bursts [11] are the bursts of light that appears due to the interaction of gamma rays coming from the cosmic sources with the nitrogen present in the atmosphere of earth. These bursts are detected with the help of Photo-Multiplier-Tubes (PMTs). The output of a PMT consists of two dominant sources of noise: the noise due to the background light of night sky and the shot noise of the PMT [11]. The occurrence of bursts are non-stationary in nature. Therefore the signal from the PMT are also non-stationary. A fixed filter cannot solve the problem of extracting the burst signal buried in noise. Hence, there is a scope of using ANC to combat the noise in Gamma Ray Burst detection. With this idea we carried on, and found it very interesting to implement a generalized ANC system in optical domain, as an optical system has many advantages over electronic realizations such as parallel operation and high speed of processing [12], [13]. Optical processing is especially suitable for signals that are optical in nature such as the Gamma Ray Bursts or light-wave signals transmitted through optical fibers for long distance communication [12].

1.2 About the thesis and objectives

Earlier, many attempts have been made to optically implement adaptive system identification [14], adaptive equalizers [15], IIR filters [16], [17], Adaline neural networks [18], delay line filters [19], and switches [20]. Based on these ideas, the present research focuses on the implementation of ANC system in optical domain. Our design employs as few electronic devices as possible and utilizes the processing speed, parallelism, and interconnection capabilities of optics for signal computations [21]. It relies upon optical matrix-matrix, matrix-vector or vector multipliers to take advantage of speed and efficiency associated with light-wave communication and optical data processing. Fiber optical delay lines (FOTDLs) are used for sampling the guided light-wave signal.

We considered optical realization based implementation of ANC with two popular adaptive methods: least-mean-square (LMS) algorithm and Kalman filter algorithm. LMS algorithm is a simple algorithm whereas computational complexities are more in Kalman filter algorithm. Through simulations and numerical experiments with a detailed model of the optical system we tried to determine the feasibility and effectiveness of optical implementation of the ANC algorithms. We considered the performance analysis of both systems in the presence of hardware round-off errors or optical errors. In LMS case, the signals from FOTDLs are processed in free space using lenses and spatial light modulators (SLMs). While in the Kalman case, SLMs are replaced by acousto-optic (AO) cells. The reasons for this choice will be explained in their respective chapters. Optical structures for LMS and Kalman filter based ANC presented are for incoherent optical signals.

1.3 Thesis layout

In this thesis, Chapter 2 reviews the basic concepts of ANC method of eliminating noise. The theoretical backgrounds on LMS and Kalman filter algorithms are given. The effects of various parameters of the algorithms such as adaptive gain constant on the signal to noise ratio (SNR) of output signal are then brought forward. Results obtained from simulations are reviewed. Chapter 3 focuses on the optical realization of LMS based ANC. This chapter begins with a discussion on various optical components that can replace the components of electronic realizations of ANC system. Following it, the optical realization of LMS algorithm is presented. In Chapter 4, the error and noise sources of the optical hardware are modeled and then the analysis of mean square error is carried out. The method of performance optimization is discussed thereafter. Chapter 5 is dedicated to the optical realization of Kalman filter algorithm. Basic operation of acousto-optic (AO) Bragg cells are discussed. Following it, the optical computations using AO cells are illustrated. Thereafter, the details of the possible optical realization of Kalman filter algorithm is exemplified. The error and noise source identification and its modeling is the topic of Chapter 6. Error source modeling of simple AO cell is first figured out, and this concept is extended to model the dominant errors of optical Kalman filter. Chapter 7 explores the problems that are solved through computer simulations for both optical LMS and optical Kalman filter based ANC. General idea on simulation is explained, and also, the method to calculate the signal to noise ratio of the output signal is detailed. Results obtained from simulations are expounded and illustrated in Chapter 7. The general overview of optical systems along with its merits and limitations and some recent technology for optical computations are the matters of Chapter 8. Finally, in Chapter 9 the main contributions of the thesis are discussed, some important conclusions are made, certain limitations of the work are identified, while the scope for future research is also brought forward.

Chapter 2

Adaptive Noise Cancellation

2.1 Basic Concept

Adaptive noise cancellation (ANC) is a technique to remove noise or interference from a mixture of desired and noise signals [22]. ANC uses an additional reference input that should contain a sample of noise field and as little the pure signal as possible. The noise reference is then filtered and subtracted from the signal that contains both desired and noisy signals to get the error signal or output signal. The filtering and subtraction are controlled by an adaptive process that minimizes the mean square of this error signal. The idea is shown in Figure 2.1. From this figure, we observe that the primary sensor receives desired signal interfered with signal from noisy source, the signal from the primary sensor will be called as primary signal, d_k. And the reference sensor receives noise signal from the noisy source which will be called as reference signal, x_k. The subscript k indicates the k^{th} sample of the signal. The reference signal is input to the transversal filter, output of the filter, y_k, is subtracted from d_k to obtain error signal, ε_k which controls the adaptive process.

Basically, an ANC is a dual input, closed-loop adaptive control system. The two inputs are derived from a pair of sensors: a primary sensor and a reference sensor. Referring to Figure 2.1, specifically we have the following:

- The primary signal, d_k receives an information bearing signal (pure signal) s_k corrupted by an additive noise $(n_0)_k$, i.e.,

  $$d_k = s_k + (n_o)_k.$$

  And both s_k and $(n_0)_k$ are assumed to be uncorrelated [23] with each other,

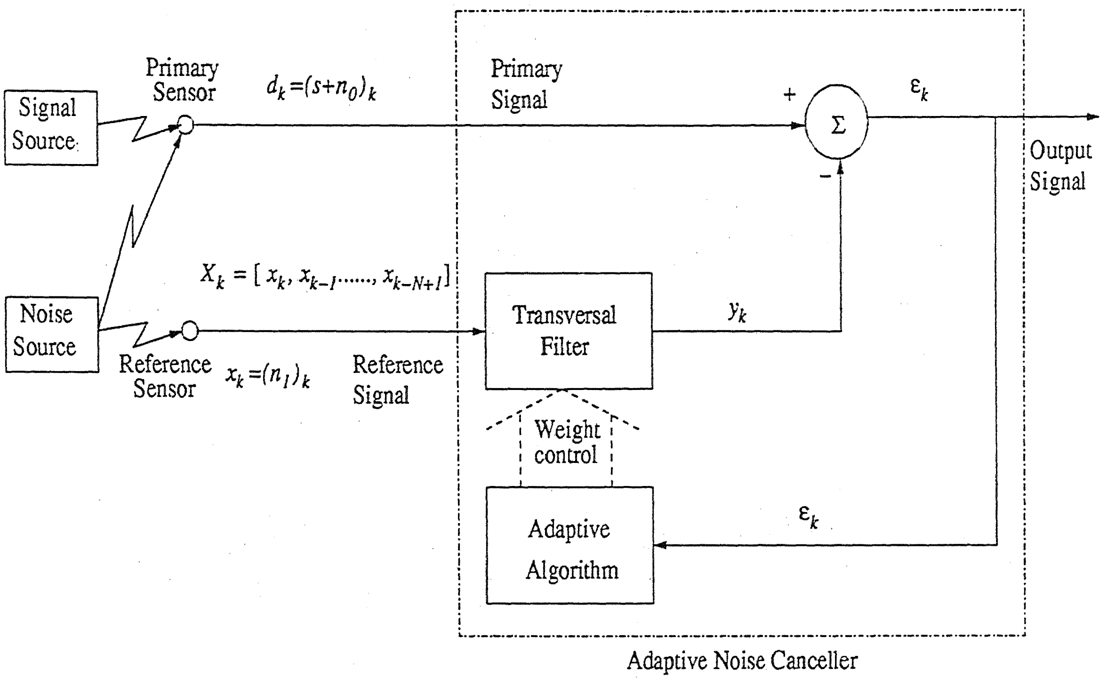

Figure 2.1: Block diagram of adaptive noise cancellation system.

i.e.,

$$E\langle s_k(n_0)_k\rangle = 0, \quad for\, all\, k$$

where, s_k and $(n_0)_k$ are assumed to be real valued, and $E\langle\cdots\rangle$ denotes the ensemble expected value, for ergodic processes it also denotes the expected value over time [23] .

- The reference sensor receives a noise, $x_k = (n_1)_k$ that is assumed to be uncorrelated with the signal, s_k. Since noise source is the same so we assume $(n_1)_k$ to be correlated with the noise $(n_0)_k$ in the primary sensor output. Let the correlation coefficient between them be cc and there is a time delay of i sample between them. Hence we have

$$E\langle s_k(n_1)_k\rangle = 0, \quad for\, all\, k$$

and

$$E\langle (n_1)_k(n_0)_{k-i}\rangle = cc_i$$

where, as before the signals are real valued.

Figure 2.2 shows the schematic diagram of a transversal filter used in the adaptive filter of ANC. The number of taps of the filter is chosen to be N. The reference signal x_k is fed serially to the filter, it is delayed and stored successively. A set

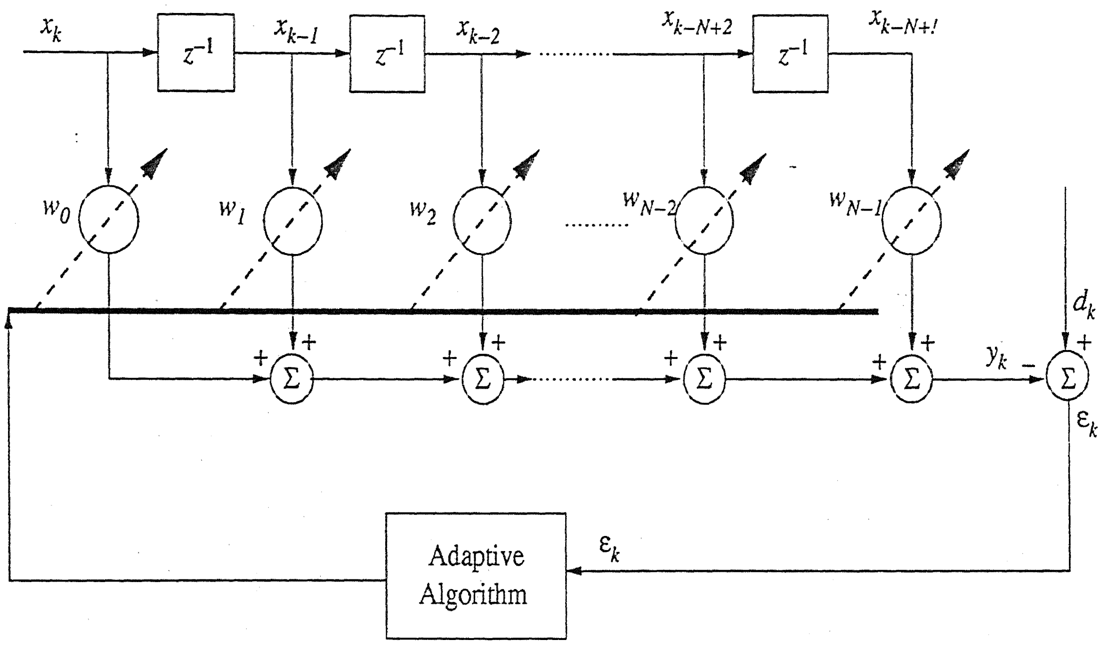

Figure 2.2: An N tapped or $(N-1)^{th}$ order transversal filter applied to ANC system.

of last N samples of x_k is stored as X_k and a set of N elements of weight form weight vector W_k. Each sample of X_k is multiplied with the corresponding element of W_k. The result after multiplication is added to the filter output signal y_k. Mathematically the filter output is expressed as:

$$y_k = W_k^T X_k$$

where, X_k is an $N \times 1$ column vector of reference signal at k^{th} iteration, defined as

$$X_k = [x_k,\ x_{k-1}, ...,\ x_{k-N+1}]^T,$$

and W_k is an $N \times 1$ column vector of transversal filter weights at k^{th} iteration defined as:

$$W_k = [w_0,\ w_1, ...,\ w_{N-1}]^T,$$

and a scalar quantity y_k is the filter output at k^{th} iteration. The filter output is subtracted from the primary signal d_k.The error signal so generated is given by

$$\varepsilon_k = d_k - y_k = s_k + (n_0)_k - y_k$$

The objective of ANC is to produce a system output, an error signal ε_k, that is a best fit in least-square sense to the signal s_k. Assuming that all signals are statistically stationary and have zero mean, squaring the output and taking its expected value we obtain

$$E\left\langle\varepsilon_k^2\right\rangle = E\left\langle s_k^2\right\rangle + E\left\langle((n_0)_k - y_k)^2\right\rangle.$$

The signal power of s will be unaffected as the filter is adjusted to minimize $E\left\langle\varepsilon_k^2\right\rangle$ over all k. When the filter is adjusted so that $E\left\langle\varepsilon_k^2\right\rangle$ is minimized, $E\left\langle[(n_0)_k - y_k]^2\right\rangle$ is also get minimized. Accordingly the minimum output power is

$$E_{min}\left\langle\varepsilon_k^2\right\rangle = E\left\langle s_k^2\right\rangle + E_{min}\left\langle((n_0)_k - y_k)^2\right\rangle,$$

where, $E_{min} = min\, E\left\langle\right\rangle$ over all k. Hence the output signal-to-noise ratio is maximized. The filter output is then a best least-square estimate of the primary noise $(n_0)_k$.

The smallest possible output power is $E_{min}\left\langle\varepsilon_k^2\right\rangle = E\left\langle s_k^2\right\rangle$. This is achievable when $E\left\langle[(n_0)_k - y_k]^2\right\rangle = 0$ or $y_k = (n_0)_k$, and the output signal becomes perfectly free of noise.

On the other hand, when reference input is completely uncorrelated with the primary noise n_0, then filter will "*turn itself off*" and will not increase output noise. The output power in this case will be

$$E\left\langle\varepsilon_k^2\right\rangle = E\left\langle(s_k + (n_0)_k)^2\right\rangle + E\left\langle y_k^2\right\rangle.$$

Minimizing output power requires that $E\left\langle y_k^2\right\rangle$ be minimized, which is accomplished by making all weights zero, bringing $E\left\langle y_k^2\right\rangle$ to zero.

2.2 Basic Theory of LMS based ANC

Based on the configuration of Figure 2.2, we can write the LMS algorithm as [22]-[24]:

$$y_k = X_k^T W_k \tag{2.1}$$

$$\varepsilon_k = d_k - y_k \tag{2.2}$$

$$W_{k+1} = W_k + \mu\varepsilon_k X_k \tag{2.3}$$

where, X_k, W_k, y_k and ε_k are the same as described before and the scalar quantity μ is called adaptive gain constant. From Equation (2.3), we see that weights change after each iteration. We can write its expected value as:

$$E\left\langle W_{k+1}\right\rangle = E\left\langle W_k\right\rangle + E\left\langle \mu\varepsilon_k X_k\right\rangle \tag{2.4}$$

From Equation (2.2) it becomes

$$E\left\langle W_{k+1}\right\rangle = E\left\langle W_k\right\rangle + \mu E\left\langle d_k X_k\right\rangle - \mu E\left\langle X_k X_k^T W_k\right\rangle \tag{2.5}$$

Assuming that the algorithm converges and if the number of iterations is large, then the error becomes very small in Equation (2.2), and weight remains approximately constant even after the updating. It is tantamount to independence of X_k and W_k. Now we can modify Equation (2.5) as

$$E\left\langle W_{k+1}\right\rangle = E\left\langle W_k\right\rangle + \mu P - \mu R E\left\langle W_k\right\rangle \tag{2.6}$$

where, $P = E\left\langle d_k X_k\right\rangle$ is a $N \times 1$ cross-covariance vector between primary and reference signal, and $R = E\left\langle X_k X_k^T\right\rangle$ is the $N \times N$ auto-covariance matrix of the reference signal. The weight vector, which minimizes the mean square error of Equation (2.2), is given by Weiner weight (W^*) [22] as:

$$W^* = R^{-1}P. \tag{2.7}$$

Using Equation (2.7) we can modify Equation (2.6) as:

$$E\left\langle W_{k+1}\right\rangle = \left(I - \mu R\right) E\left\langle W_k\right\rangle + \mu R W^* \tag{2.8}$$

2.2.1 Derivation of time constant

We can solve Equation (2.8) by transforming it to the principal coordinate system or orthogonal system [22], [25]. First we translate it, using $U = W - W^*$, so that Equation (2.8) becomes

$$U_{k+1} = \left(I - \mu R\right) U_k, \tag{2.9}$$

then by rotating Equation (2.9) to the principal axis using a transformation matrix, i.e., a matrix which transforms R into a diagonal matrix, Λ we get

$$U'_{k+1} = \left(I - \mu\Lambda\right) U'_k \tag{2.10}$$

where, $U' = Q^{-1}U$ and $\Lambda = Q^{-1}RQ$. The matrix Q is the eigen vector matrix of R. (Note: All the primed variables are in principal coordinate system.)

The solution to Equation (2.10) can be written in the form

$$U'_k = (I - \mu\Lambda)^k U'_0 \tag{2.11}$$

where, U'_0 is the initial weight vector in principal coordinate system. Now with the help of Equation (2.11), we can define the time constants of the algorithm as

$$\tau_n = \frac{1}{\mu\lambda_n} : n = 1, 2, 3, ...N \tag{2.12}$$

where, λ_n is the n^{th} eigen value of matrix R and τ_n is the time constant of n^{th} element of the weight vector [22].

2.2.2 Bounds on μ

From Equation (2.11), it can be observed that the algorithm is stable when

$$lim_{k\to\infty} (I - \mu\Lambda)^k = 0.$$

This condition is obtained when

$$0 < \mu < \frac{1}{\lambda_{max}} \tag{2.13}$$

where, λ_{max} is the largest eigen value of R. A much less stringent condition would be

$$0 < \mu < \frac{1}{trace(R)}. \tag{2.14}$$

2.2.3 Covariance of gradient of $|\varepsilon_k|^2$ under noisy condition

Gradient estimate [22] of the square of the error ε_k in LMS algorithm can be written as

$$\nabla_k = -2\varepsilon_k X_k. \tag{2.15}$$

Using Equation (2.2), the expected value of this gradient can be written as

$$E\langle\nabla_k\rangle = -2E\langle\varepsilon_k X_k\rangle = 2R\left(E\langle W_k\rangle - W^*\right) \tag{2.16}$$

$$\Rightarrow \; E\left\langle \nabla_k \right\rangle = 2RU \tag{2.17}$$

Under erroneous measurement conditions, the measured gradient is not equal to the true gradient. There are fluctuations around the true gradient. Let us denote this fluctuations as N_k, thus we can write the total gradient estimate of $|\varepsilon_k|^2$, i.e., $\widehat{\nabla}_k$ as the addition of true gradient and N_k, i.e.,

$$\widehat{\nabla}_k = \nabla_k + N_k. \tag{2.18}$$

Assuming that μ is sufficiently small and the algorithm has converged, i.e., weight vector is close to the optimum solution we can assume that $\nabla_k \approx 0$. Now using Equation (2.15) and Equation (2.18) we find

$$\widehat{\nabla}_k = N_k = -2\varepsilon_k X_k \tag{2.19}$$

Having obtained this result we can calculate the covariance of N_k as

$$cov\left[N_k\right] = E\left\langle N_k N_k^T \right\rangle = 4E\left\langle \varepsilon_k^2 X_k X_k^T \right\rangle \tag{2.20}$$

When the algorithm converges and W_k approaches W^*, then the error ε_k becomes very small and it does not depend on X_k. We can assume that ε_k^2 and X_k to be independent. Then from Equation (2.20)

$$cov\left[N_k\right] \approx 4E\left\langle \varepsilon_k^2 \right\rangle E\left\langle X_k X_k^T \right\rangle$$

$$\Rightarrow \; cov\left[N_k\right] \approx 4\xi_{min} R \tag{2.21}$$

where, ξ_{min} is minimum value of mean square error given as $\xi_{min} = E\left\langle \varepsilon_k^2 \right\rangle$. $E\left\langle \varepsilon_k^2 \right\rangle$ comes out to be minimum because we have assumed that the algorithm has nearly reached to its optimal value.

In the same way as discussed already, we can transform matrix $cov[N_k]$ to the principal coordinate system and rewrite Equation (2.21) as

$$cov\left[N_k^{'}\right] \approx 4\xi_{min}\Lambda \tag{2.22}$$

where, $N_k^{'}$ is the gradient of noise vector in principal coordinate system.

For small values of μ, the LMS and steepest descent method follow approximately the same gradient curve to reach the optimum value [26]. The derivation of closed form mathematical expression of weight error, i.e., $(W_k - W^*)$ in terms of initial weight vector W_0 is simple in steepest descent method. So we can use steepest descent method to derive the covariance of W_k. Although not perfectly accurate it provides many of the answers we seek. Weight updating equation in steepest descent algorithm is given by [22]

$$W_{k+1} = W_k - \mu \nabla_k. \tag{2.23}$$

Here,

$$\nabla_k = -P + 2RW_k \tag{2.24}$$

Using Equation (2.24) as the true gradient, the total gradient of LMS algorithm under the erroneous condition, i.e., Equation (2.18) can be approximated as

$$\widehat{\nabla}_k = -P + 2RW_k + N_k \tag{2.25}$$

Thus, by using Equation (2.25), the weight updating equation for LMS algorithm can be approximated as

$$W_{k+1} = (I - \mu R)W_k + \mu(P + N_k). \tag{2.26}$$

Now, we can manipulate Equation (2.26) using Equation (2.17) and Equation (2.18) with same approximations and in the same way as was done to obtain Equation (2.11). Thus Equation (2.26) becomes

$$U_k^{'} = (I - \mu\Lambda)^k U_0 - \frac{\mu}{2} \sum_{n=0}^{k-1} (I - \mu\Lambda)^k \left(N_{k-n-1}^{'}\right). \tag{2.27}$$

If the number of iteration $k \to \infty$, the first term on RHS of Equation (2.27) becomes negligible and steady-state solution becomes

$$U_k^{'} = -\frac{\mu}{2} \sum_{n=0}^{k-1} (I - \mu\Lambda)^k N_{k-n-1}^{'}. \tag{2.28}$$

Covariance of this weight error vector is given by

$$cov\left[U_k^{'}\right] = E\left\langle U_k^{'} U_k^{'T} \right\rangle$$

$$= E \left\langle \begin{array}{l} (I - \mu\Lambda) U_{k-1}^{'} U_{k-1}^{'T} (I - \mu\Lambda)^T + \frac{\mu^2}{4} N_{k-1}^{'} N_{k-1}^{'T} - \\ \frac{\mu}{2} \left\{ (I - \mu\Lambda) U_{k-1}^{'} N_{k-1}^{'T} + N_{k-1}^{'} N_{k-1}^{'} (I - \mu\Lambda)^T \right\} \end{array} \right\rangle. \tag{2.29}$$

Since $(I - \mu\Lambda)$ is a diagonal and expected cross products (between U_k' and N_k') will vanish because of non-correlation between them, Equation (2.29) becomes

$$cov\left[U_k'\right] = \frac{\mu}{8}\left(\Lambda - \frac{\mu}{2}\Lambda^2\right)^{-1} cov\left[N_k'\right]. \tag{2.30}$$

Using Equation (2.22) and Equation (2.30), we get the final expression of covariance of weight vector as

$$cov\left[U_k'\right] = \frac{\mu}{2}\xi_{min}\left(\Lambda - \frac{\mu}{2}\Lambda^2\right)^{-1} \Lambda. \tag{2.31}$$

2.2.4 Derivation of *excess-mean-square-error* and *Misadjustment*

In LMS algorithm the estimate of gradient taken to update the weights, i.e., $-\varepsilon_k X_k$ is not equal to the actual gradient, i.e., $-2P + RW_k$. Therefore it suffers from gradient noise and the even after the convergence it causes the steady-state weight vector solution to vary randomly about the minimum point of the mean-square-error surface [22]. This results in an increase in the value of minimum mean-square-error, ξ_{min} which is obtained when there is no error in gradient estimate of $|\varepsilon_k|^2$. This increment is known as *excess-mean-square-error.* The mean-square-error at k^{th} iteration is defined as the expected value of $|\varepsilon_k|^2$ with the weight vector fixed at U_k. So we can define *excess mean-square-error* as

$$\chi = E\left\langle \xi_k - \xi_{min} \right\rangle \tag{2.32}$$

also, the mean-square-error in terms of minimum mean-square-error at k^{th} iteration is given as [22]

$$\xi_k = \xi_{min} + U_k'^T \Lambda U_k'. \tag{2.33}$$

Therefore, using Equation (2.33), Equation (2.32) becomes

$$\chi = E\left\langle U_k'^T \Lambda U_k' \right\rangle \tag{2.34}$$

This definition is applicable only where U_k' undergoes a statistically stationary process over k, i.e., where the gradient of noise N_k, as well as the reference signal vector X_k and the primary signal d_k are statistically stationary. Thus it is applicable only in steady state after adaptive transients have died out.

$$\chi = \sum_{n=1}^{N} \lambda_n E\left\langle u_{nk}^{'2} \right\rangle \tag{2.35}$$

where, $u_{nk}^{'}$ is the n^{th} element of $U_k^{'}$. After convergence $E\left\langle u_{nk}^{'2} \right\rangle$ can be equated to the n^{th} diagonal element of the diagonal matrix *cov* $\left[U_k^{'}\right]$, thus by using Equation (2.31) it can be expressed as

$$E\left\langle u_{nk}^{'2} \right\rangle = \frac{\mu \xi_{min}}{(2 - \mu\lambda_n)} \tag{2.36}$$

where, λ_n is the n^{th} eigen value of matrix R or Λ. Hence, by combining Equation (2.35), Equation (2.36) we get

$$\chi = \mu\xi_{min} \sum_{n=1}^{N} \frac{\lambda_n}{(2 - \mu\lambda_n)}. \tag{2.37}$$

The total mean-square-error is given by

$$\xi_{total} = \xi_{min} + \mu\xi_{min} \sum_{n=1}^{N} \frac{\lambda_n}{(2 - \mu\lambda_n)}. \tag{2.38}$$

Using the *excess-mean-square-error,* we can define another parameter *Misadjustment* M, which is useful in design of the adaptive processes. Mathematically can be M is defined as

$$M = \frac{\chi}{\xi_{min}}. \tag{2.39}$$

Thus, after substituting for χ from Equation (2.37) in Equation (2.39) we get

$$M = \mu \sum_{n=1}^{N} \frac{\lambda_n}{(2 - \mu\lambda_n)}. \tag{2.40}$$

We can also approximate Equation (2.40) to

$$M = \frac{\mu\, trace(R)}{2 - \mu\, trace(R)} \tag{2.41}$$

The excess in the value of mean-square-error can be seen in other words as the variance of noise present at the output signal. When χ is zero, it means the minimum possible value of the variance of noise at output is ξ_{min}. If we relate ξ_{min} to variance of a signal then χ corresponds to the variance of error in the same signal. Thus Signal to Noise Ratio (SNR) will be given by χ/ξ_{min}. Therefore from this reasoning and using Equation (2.39), we can equivalently express the SNR of output signal as

$$SN = 10 \log \left(\frac{1}{M} \right). \tag{2.42}$$

2.3 Theoretical background on Kalman Filter

In 1960, R.E. Kalman published his famous paper [27] describing a recursive solution to the discrete-data linear filtering problem. This paper led to an advancement in the area of smoothing, filtering and prediction. The Kalman filter has been the the subject of extensive research and application, particularly in area of autonomous or assisted navigation [28], [29]. Other areas include sensor calibration [30], radar tracking [31], [32], channel equalization [33]. Few references on Kalman filter include [34], [35]. A brief introduction can also be found in [36].

Application of Kalman filter supposes the studied system to be described by a set of linear differential equations for continuous time case and linear difference equations in the case of discrete time systems. Difference equations involving random processes are called *stochastic difference* equation. A vector discrete-time recursive difference equation for modeling a random process can be given in the form [34]

$$S_k = \Phi_k S_{k-1} + G_{k-1} \Pi_k \tag{2.43}$$

$$Z_k = H_k S_k + \Xi_k, \tag{2.44}$$

where the variable

S_k is a $n \times 1$ state vector
Z_k is a $l \times 1$ measurement vector
Φ_k is a $n \times n$ time-varying dynamic coefficient matrix (state transition matrix)
H_k is a $l \times n$ time-varying measurement sensitivity matrix
G_{k-1} is a $n \times r$ time varying process noise coupling matrix
Π_k is a $r \times 1$ zero-mean uncorrelated "plant noise" process
Ξ_k is a $l \times 1$ zero-mean uncorrelated "measurement noise" process,

and the expected values

$$E \langle \Pi_k \rangle = 0$$

$$E \langle \Xi_k \rangle = 0$$

$$E\left\langle \Pi_{k_1}\Pi_{k_2}^T \right\rangle = Q_{k_1}\Delta(k_2 - k_1)$$
$$E\left\langle \Xi_{k_1}\Xi_{k_2}^T \right\rangle = L_{k_1}\Delta(k_2 - k_1)$$
$$E\left\langle \Pi_{k_1}\Xi_{k_2}^T \right\rangle = M_{k_1}\Delta(k_2 - k_1).$$

The symbols Q and L are $r \times r$ and $l \times l$ dimensional auto-covariance matrices of Π_k and Ξ_k respectively, M^1 is the $r \times l$ dimensional cross-covariance matrix of Π_k and Ξ_k. Both Π_k and Ξ_k have normal probability distributions and Δ represents the Kronecker delta function defined by

$$\Delta(k) = \begin{cases} 1 \; if \; k = 0 \\ 0 \; otherwise. \end{cases}$$

2.3.1 Estimation and optimization of state

Suppose that a measurement has been made at time t_k, and that the information that it provides is to be applied in updating estimate of the state x at time t_k. Therefore it suffices to seek an updated estimate $\widehat{S}_k(+)$; based on the information Z_k; i.e. a linear function of the *a priori* estimate and the measurement Z:

$$\widehat{S}_k(+) = \Theta_k \widehat{S}_k(-) + K_k Z_k, \tag{2.45}$$

where $\widehat{S}_k(-)$ is the a priori estimate of S_k and $\widehat{S}_k(+)$ is the a posteriori value of the estimate. We seek those values of Θ_k and K_k such that new estimate $\widehat{S}_k(+)$ will satisfy the orthogonality condition i.e.

$$E\left\langle \left[S_k - \widehat{S}_k(+)\right] Z_i^T \right\rangle = 0, \;\; i = 1, 2, ..., k \tag{2.46}$$

As noises are uncorrelated, one can obtain the following relation using Equation (2.43), Equation (2.45) and Equation (2.46).

$$E\left\langle \Phi_{k-1}S_{k-1} + \Pi_{k-1} - \Theta_k\widehat{S}_k(-) - K_k Z_k \right\rangle Z_i^T = 0, \; i = 1, 2, ..., k-1. \tag{2.47}$$

Using Equation (2.44), Equation (2.47) becomes

$$E\left\langle \Phi_{k-1}S_{k-1} - \Theta_k\widehat{S}_k(-) - K_k H_k S_k - K_k \Xi_k \right\rangle Z_i^T = 0, \; i = 1, 2, ..., k-1. \tag{2.48}$$

---

[1] This M should not be confused with the scalar M which is meant for *Misadjustment*

We know that Equation (??) holds at the previous step, i.e.,

$$E\left\langle \left[S_{k-1} - \widehat{S}_{k-1}(+)\right] Z_i^T \right\rangle = 0,\ \ i = 1, 2, \ldots.., k-1.$$

and

$$E\left\langle \Xi_k Z_i^T \right\rangle = 0,\ \ i = 1, 2, \ldots.., k-1.$$

Then Equation (2.48) can be reduced to the form

$$[\Phi_{k-1} E\left\langle S_{k-1} Z_i^T \right\rangle - \Theta_k E\left\langle \widehat{S}_k(-) Z_i^T \right\rangle - K_k H_k \Phi_{k-1} E\left\langle S_{k-1} Z_i^T \right\rangle - K_k E\left\langle \Xi_k Z_i^T \right\rangle] = 0$$

$$\begin{aligned}
&\Rightarrow [\Phi_{k-1} E\left\langle S_{k-1} Z_i^T \right\rangle - \Theta_k E\left\langle \widehat{S}_k(-) Z_i^T \right\rangle - K_k H_k \Phi_{k-1} E\left\langle S_{k-1} Z_i^T \right\rangle] = 0 \\
&\Rightarrow E\left\langle [S_k - K_k H_k S_k - \Theta_k S_k] - \Theta_k \left(\widehat{S}_k(-) - S_k\right) \right\rangle Z_i^T = 0 \\
&\Rightarrow [I - \Theta_k - K_k H_k]\, E\left\langle S_k Z_i^T \right\rangle = 0.
\end{aligned} \qquad (2.49)$$

Since $E\left\langle S_k Z_i^T \right\rangle$ cannot be equal to zero, [see Equation (2.43, and Equation (2.44)], therefore, Equation (2.49) is satisfied for any given S_k if

$$\Theta_k = I - K_k H_k. \qquad (2.50)$$

Let us define some more terms for further analysis.

$$\Gamma_k(+) \ \underline{\Delta}\ \ \widehat{S}_k(+) - S_k \qquad (2.51)$$

$$\Gamma_k(-) \ \underline{\Delta}\ \ \widehat{S}_k(-) - S_k \qquad (2.52)$$

$$\begin{aligned}
\Sigma_k \ &\underline{\Delta}\ \ \widehat{Z}_k(-) - Z_k \\
&= \ H_k \widehat{S}_k(-) - Z_k,
\end{aligned} \qquad (2.53)$$

where, vectors $\Gamma_k(+)$ and $\Gamma_k(-)$ are the state estimation errors after and before the updates, and vector Σ_k is the estimation error in measurement. The term $\widehat{S}_k(-) = H_k \widehat{S}_k(-)$ is called *"a priori* measurement". From Equation (2.46), Equation (2.44), Equation (2.45) and the definition of Σ_k, we find

$$E\left\langle \left[S_k - \widehat{S}_k(+)\right] \Sigma_k^T \right\rangle = 0. \qquad (2.54)$$

Substituting for S_k, $\widehat{S}_k(+)$ and Σ_k in Equation (2.54), from Equation (2.43), Equation (2.45) and Equation (2.53) respectively, we obtain

$$E\left\langle \left[\Phi_{k-1} S_{k-1} + G_{k-1} \Pi_k - \Theta_k \widehat{S}_k(-) - K_k Z_k\right] \left[H_k \widehat{S}_k(-) - Z_k\right]^T \right\rangle = 0. \qquad (2.55)$$

However, by the system structure

$$E\left\langle \Pi_k Z_k^T \right\rangle = E\left\langle \Pi_k \widehat{S}_k^T \right\rangle = 0$$

so Equation (2.55) becomes

$$E\left\langle \left[\Phi_{k-1}S_{k-1} - \Theta_k \widehat{S}_k(-) - K_k Z_k\right]\left[H_k\widehat{S}_k(-) - Z_k\right]^T \right\rangle = 0 \tag{2.56}$$

Substituting for Θ_k, Z_k, and $\Gamma_k(-)$ from Equation (2.50), Equation (2.44) and Equation (2.52) respectively, and using the fact that $E\left\langle \Gamma_k(-)\Xi_k^T \right\rangle = 0$, Equation (2.56) can be modified as follows:

$$\begin{aligned} E\Big\langle [\Phi_{k-1}S_{k-1} + \widehat{S}_k(-) + K_kH_k\widehat{S}_k(-) - K_kH_kS_k - K_k\Xi_k] & \\ [H_k\widehat{S}_k(-) - H_kS_k - \Xi_k]^T \Big\rangle &= 0 \end{aligned}$$

$$\Rightarrow E\left\langle \left[\left(S_k - \widehat{S}_k(-)\right) - K_kH_k\left(S_k - \widehat{S}_k(-)\right) - K_k\Xi_k\right][H_k\Gamma_k(-) - \Xi_k]^T \right\rangle = 0$$

$$\Rightarrow E\left\langle [\Gamma_k(-) - K_kH_k\Gamma_k(-) - K_k\Xi_k][H_k\Gamma_k(-) - \Xi_k]^T \right\rangle = 0. \tag{2.57}$$

Let us define a term, *a priori* error covariance matrix, $P_k(-)$, i.e., the error covariance matrix before the update as

$$P_k(-) = E\left\langle \Gamma_k(-)\Gamma_k^T(-) \right\rangle. \tag{2.58}$$

Using this definition, Equation (2.57) can be modified to

$$[I - K_kH_k]\, P_k(-)H_k^T - K_kL_k = 0, \tag{2.59}$$

and therefore, K_k from Equation (2.59) can be expressed as

$$K_k = P_k(-)H_k^T\left[H_kP_k(-)H_k^T + L_k\right]^{-1}, \tag{2.60}$$

which is the solution we seek for the K_k as a function of *a priori* error covariance. K_k is also known as "*Kalman gain*".

Similarly for *a posteriori* error covariance (the error covariance matrix after update), which is defined as

$$P_k(+) = E\left\langle \Gamma_k(+)\Gamma_k^T(+) \right\rangle. \tag{2.61}$$

By substituting Equation (2.50) into Equation (2.45) we get

$$\widehat{S}_k(+) = (I - K_k H_k)\,\widehat{S}_k(-) + K_k Z_k$$

$$\Rightarrow \widehat{S}_k(+) = \widehat{S}_k(-) + K_k\left[Z_k - H_k\widehat{S}_k(-)\right]. \tag{2.62}$$

Subtract S_k from both sides of equation Equation (2.62) to obtain

$$\widehat{S}_k(+) - S_k = \widehat{S}_k(-) + K_k H_k S_k + K_k \Xi_k - K_k H_k \widehat{S}_k(-) - S_k$$

$$\Rightarrow \Gamma_k(+) = [I - K_k H_k]\,\Gamma_k(-) + K_k \Xi_k. \tag{2.63}$$

Using Equation (2.61) and Equation (2.63) and noting that $E\left\langle \Gamma_k(-)\Xi_k^T \right\rangle = 0$, we get

$$\begin{aligned} P_k(+) &= E\left\langle (I - K_k H_k)\,\Gamma_k(-)\Gamma_k^T(-)\,(I - K_k H_k)^T + K_k \Xi_k \Xi_k^T K_k^T \right\rangle \\ &= (I - K_k H_k)\,P_k(-)\,(I - K_k H_k)^T + K_k L_k K_k^T \end{aligned} \tag{2.64}$$

Now substituting for K_k from Equation (2.60), Equation (2.64) becomes

$$P_k(+) = (I - K_k H_k)\,P_k(-), \tag{2.65}$$

This implements the effect that conditioning on measurement has on the error covariance matrix of estimation uncertainty.

Error covariance extrapolation models the effects of time on the error covariance matrix of estimation uncertainty, which is reflected in the *a priori* values of the error covariance and state estimates, i.e.,

$$\widehat{S}_k(-) = \Phi_{k-1}\widehat{S}_{k-1}(+), \tag{2.66}$$

respectively. Subtract S_k from both sides of the Equation (2.66) it becomes

$$\Gamma_k(-) = \Phi_{k-1}\Gamma_{k-1}(+) - G_{k-1}\Pi_{k-1} \tag{2.67}$$

Post-multiply Equation (2.67) by $\Gamma_k^T(-)$ on both sides and taking its expected values and using the fact that $E\left\langle \Gamma_{k-1}\Pi_{k-1}^T \right\rangle = 0$ it can be modified to

$$P_k(-) = \Phi_{k-1}P_{k-1}(+)\Phi_{k-1}^T + Q_{k-1}, \tag{2.68}$$

which gives the *a priori* value of the error covariance matrix of estimation uncertainty as a function of the previous *a posteriori* value.

Table 2.1: Discrete-time Kalman filter equations

State Dynamic model:

$$\begin{aligned} S_k &= \Phi_{k-1}S_{k-1} + G_{k-1}\Pi_{k-1} \\ \Pi_k &\sim \aleph\left(0,\, Q_k\right) \end{aligned}$$

Measurement model:

$$\begin{aligned} Z_k &= H_k S_k + \Xi_k \\ \Xi_k &\sim \aleph\left(0,\, L_k\right) \end{aligned}$$

Initial conditions:

$$\begin{aligned} E\left\langle S_0 \right\rangle &= \widehat{S}_0 \\ E\left\langle \Gamma_0 \Gamma_0^T \right\rangle &= P_0 \end{aligned}$$

Independence assumption:

$$E\left\langle \Pi_k \Xi_j^T \right\rangle = 0 \text{ for all } k \neq j$$

State estimate extrapolation:

$$\widehat{S}_k(-) = \Phi_{k-1}\widehat{S}_{k-1}(+)$$

Error covariance extrapolation:

$$P_k(-) = \Phi_{k-1}P_{k-1}(+)\Phi_{k-1}^T + Q_{k-1}$$

State estimate observational update:

$$\widehat{S}_k(+) = \widehat{S}_k(-) + K_k\left[Z_k - H_k\widehat{S}_k(-)\right]$$

Error covariance update:

$$P_k(+) = \left(I - K_k H_k\right)P_k(-)$$

Kalman gain matrix:

$$K_k = P_k(-)H_k^T\left[H_k P_k(-)H_k^T + L_k\right]^{-1}$$

2.3.2 Summary of Equations for Discrete-Time Kalman Estimator:

The summary of discrete-time Kalman filter equations are given in Table 2.1. The relation of the filter to the system is illustrated in the block diagram of Figure 2.3. The basic steps of the computational procedure for the discrete-time Kalman filter are as follows:

1. Compute $P_k(-)$ using $P_{k-1}(+)$, $\Phi_{k-1}$and Q_{k-1}.
2. Compute K_k using $P_k(-)$ (computed in step 1), H_k, and, L_k.
3. Compute $P_k(+)$ using K_k (computed in step 2) and $P_k(-)$ (step 1).
4. Compute successive values of $\widehat{S}_k(+)$ recursively, using the computed values of K_k (from step 3), the given initial estimate $\widehat{S}_0$, and the input data Z_k.

These steps leads to the minimization of the trace of the error covariance matrix.

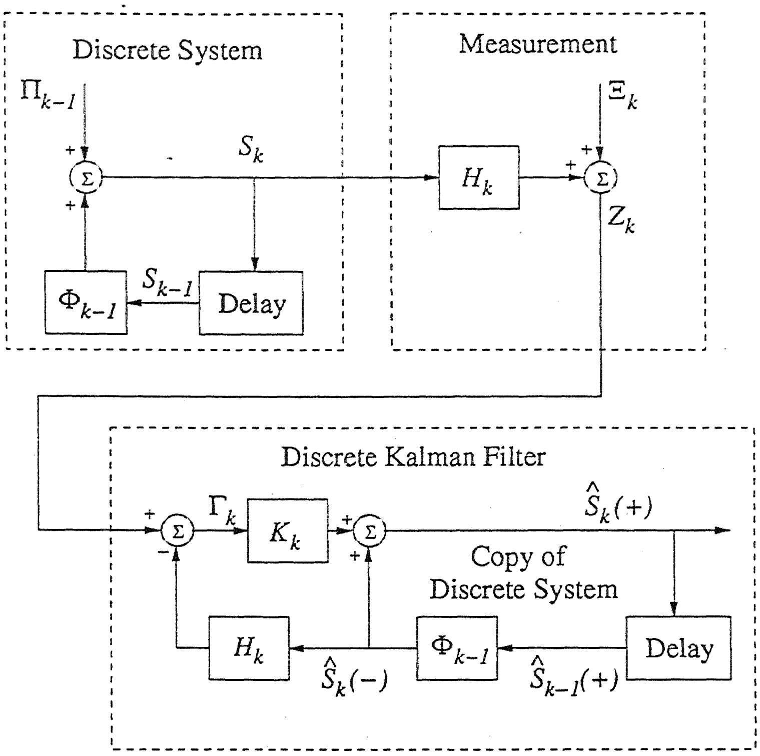

Figure 2.3: Block diagram of system, measurement model, and discrete-time Kalman filter.

2.4 Mathematics of Kalman filter when applied to ANC

An Adaptive Noise Canceler is basically an N-tapped delay line filter. Referring to the block diagram of Figure 2.2, the input to the adaptive filter is the noise sequence n_1. Let us assume the noises n_0 and n_1 be stationary. Output from the adaptive filter can be written in the same way as explained in Section 2.2, i.e.,

$$y_k = X_k^T W_k$$

We choose as the error criterion the minimization of the expected mean-square-error [33]

$$\xi_k = E\left\langle \varepsilon_k^2 \right\rangle . \tag{2.69}$$

The sequence n_1 is assumed to be stationary so, ξ does not depend on k for a given tap gain setting. For the optimal weight, i.e., Weiner weight (W^*) the mean-square-error reaches its minimum value ξ_{min}. Even if there is no noise in the system, ξ_{min} is not zero because of the finiteness of filter order. So for Weiner weight, we can write Equation (2.2) as:

$$\varepsilon_{k_{min}} = d_k - X_k^T W^*$$

or

$$d_k = X_k^T W^* + \varepsilon_{k_{min}} \tag{2.70}$$

where d_k and X_k are the same as defined in Section 2.2, $\varepsilon_{k_{min}}$ is the error at k^{th} iteration for the optimal weight vector. At k^{th} iteration mean-square error can be written as:

$$\xi_k = E\left\langle \left\{ X_k^T (W^* - W_k) + \varepsilon_{k_{min}} \right\}^2 \right\rangle . \tag{2.71}$$

Assuming $E\left\langle \varepsilon_{k_{min}} X_k \right\rangle = 0$, i.e., the two terms in Equation (2.71) are uncorrelated, so it can be expanded as

$$\xi_k = E\left\langle \left\{ (W^* - W_k)^T X_k X_k^T (W^* - W_k) \right\} \right\rangle + \xi_{min}. \tag{2.72}$$

In Section 2.3, we denoted state error covariance matrix by P_k, here, let us treat weight vector as the state vector of the Kalman filter and define weight error covariance matrix, V_k as

$$V_k = E\left\langle \left\{ (W^* - W_k)(W^* - W_k)^T \right\} \right\rangle . \tag{2.73}$$

After the algorithm has converged one can assume the independence between X_k and W_k, hence, we can write Equation (2.72) as:

$$\xi_k = trace(V_k R) + \xi_{min}. \tag{2.74}$$

where, R is the same matrix as defined in Section 2.2.

Now, having obtained these results, let us try to find out the equations that are meant for the Kalman filter algorithm as quoted in Table 2.1. Here, the aim of the Kalman filter would be to identify the optimal weight characterized by the constant state variable W^*, under the condition that output signal satisfies

$$d_k = X_k^T W^* + \varepsilon_{k_{min}}$$

Referring Equation (2.43), Equation (2.44), and block diagram of Figure 2.2, we see that the state transition matrix Φ_k will be an identity matrix. Equation (2.70) is equivalent to the measurement equation, i.e., Equation (2.44). The mean of $\varepsilon_{k_{min}}$ will be approximately equal to zero since the d_k is taken to be zero-mean signal. While we were deriving equations for Kalman filter, we assumed the measurement noise process to be a white noise process. Here also, it is reasonable to approximate $\varepsilon_{k_{min}}$, to be a white noise process. It is because the optimal mean-square error is usually small and the correlation between successive samples of noise may be neglected. Thus the linear difference equations for dynamic model of ANC, in the context of Kalman filter becomes

$$W_k = W_{k-1} \tag{2.75}$$

(note: here the process noise term is absent) and

$$d_k = X_k^T W^* + \varepsilon_{k_{min}}$$

where, the meanings and dimensions of each term are the same as described earlier. Using Equation (2.73), the *a priori* covariance matrix can be expressed as

$$V_k(-) = E\left\langle \left(W^* - \widehat{W}_k(-)\right) \left(W^* - \widehat{W}_k(-)\right)^T \right\rangle . \tag{2.76}$$

Since Φ is a unity matrix, so referring Equation (2.66), the *a priori* weight vector is written as

$$\widehat{W}_k(-) = \widehat{W}_{k-1}(+), \tag{2.77}$$

and from Equation (2.68) *a priori* error covariance matrix in terms of the *a posteriori* becomes

$$V_k(-) = V_{k-1}(+). \tag{2.78}$$

The *a priori* measurement is written as

$$\widehat{y}_k(-) = X_k^T \widehat{W}_k(-). \tag{2.79}$$

Now using Equation (2.77) and Equation (2.79), and referring Equation (2.62), the new weight estimate can be expressed as

$$\widehat{W}_k(+) = \widehat{W}_{k-1}(+) + K_k \left(d_k - X_k^T \widehat{W}_{k-1}(+)\right) \tag{2.80}$$

and from Equation (2.60) "*Kalman gain*" is given by

$$\overline{K}_k = V_{k-1}(+) X_k^T \left[X_k V_{k-1}(+) X_k^T + \xi_{min}\right]^{-1} . \tag{2.81}$$

Table 2.2: Discrete-time Kalman filter equations for ANC

State (weight) dynamic model:

$$W_k = W_{k-1}$$

Measurement model:

$$d_k = X_k^T W^* + \varepsilon_{k_{min}}$$

$$\varepsilon_{k_{min}} \sim \aleph\left(0,\, \xi_{min}\right)$$

Initial conditions:

$$E\left\langle W_0 \right\rangle = W_0$$

$$E\left\langle \left(W^* - W_0\right)\left(W^* - W_0\right)^T \right\rangle = V_0$$

Weight estimate extrapolation:

$$W_k = W_{k-1}$$

Error covariance extrapolation:

$$V_k = V_{k-1}$$

Weight estimate observational update:

$$W_k = W_{k-1} + K_k\left(d_k - X_k^T W_{k-1}\right)$$

Error covariance update:

$$V_k = \left(I - K_k X_k\right) V_{k-1}$$

Kalman gain matrix:

$$K_k = V_{k-1} X_k^T \left[X_k V_{k-1} X_k^T + \xi_{min}\right]^{-1}$$

From Equation (2.65), the error covariance updating is given by

$$V_k(+) = \left(I - K_k X_k\right) V_{k-1}(+). \tag{2.82}$$

The summary of all the equations related to the ANC using Kalman filter algorithm is given in Table 2.2. (note: As *a priori* and *a posteriori* estimate of all terms are equal so we have dropped $\hat{}$ and $(+, -)$ signs.)

2.4.1 Study of convergence of Kalman filter algorithm in ANC

The rate of convergence of the algorithm of Kalman filter can be derived [33] as follows: Multiply X_k on right side of Equation (2.81) so that it becomes

$$V_k X_k = V_{k-1} X_k - K_k X_k^T V_{k-1} X_k \tag{2.83}$$

and using Equation (2.81) and Equation (2.83) we get

$$K_k = \left(V_k X_k\right) / \xi_{min}. \tag{2.84}$$

Eliminating K_k from Equation (2.82) using Equation (2.84), we obtain

$$V_k = V_{k-1} - (V_k X_k X_k^T V_{k-1})/\xi_{min}. \tag{2.85}$$

The matrix V_k, being a error covariance matrix, is a positive definite and has an inverse. Therefore, multiplication of Equation (2.85) on the left by V_k^{-1} and on the right by V_{k-1}^{-1} leads to

$$V_k^{-1} = V_{k-1}^{-1} + X_k X_k^T/\xi_{min}. \tag{2.86}$$

Further, with initial value V_0 we can derive the following expression for weight covariance matrix

$$V_k = \xi_{min}\left(\xi_{min} V_0^{-1} + \sum_{i=1}^{k} X_i X_i^T\right)^{-1}. \tag{2.87}$$

Generally, ξ_{min} is small so the first term of Equation (2.87) can be neglected, thus Equation (2.87) becomes

$$V_k = \xi_{min}\left(\sum_{i=1}^{k} X_i X_i^T\right)^{-1}. \tag{2.88}$$

By definition the autocorrelation matrix R can be also be expressed as[2]

$$R = \frac{1}{k}\left(\sum_{i=1}^{k} X_i X_i^T\right) \quad for\, k \to \infty. \tag{2.89}$$

After about 30 or 40 iterations, it is possible to use the definition of R from Equation (2.89) to write Equation (2.88) in the following form

$$trace\,(V_k R) = (\xi_{min} N)/k. \tag{2.90}$$

If the optimal mean-square-error is known *a priori*, then we can write Equation (2.74), using Equation (2.90) in the following compact form

$$\xi_k \approx \xi_{min}\left(1 + \frac{N}{k}\right). \tag{2.91}$$

Thus, from Equation (2.91) we can conclude that the convergence in Kalman filter can theoretically be obtained within less than $2N$ iterations.

---

[2] Time average is taken since the signal X_k is assumed to be ergodic

2.4.2 Derivation of *excess-mean-square-error* and *Misadjustment*

The *excess-mean-square-error* and the *Misadjustment* for the Kalman filter algorithm can be derived in the same way as was done for the LMS algorithm in Section 2.2. For the LMS case we derived them through the covariance of weight error, while in this case we use the covariance of weight error vector which is denoted by V_k. Rewriting the expression for V_k from Equation (2.88) we get

$$V_k = \xi_{min} \left(\sum_{i=1}^{k} X_i X_i^T \right)^{-1} .$$

For large iteration, say about after $k \sim 500N$ iteration, the above equation can be written using the definition of R from Equation (2.89) as

$$V_k = \xi_{min} \frac{R^{-1}}{k}. \qquad (2.92)$$

In principle co-ordinate system [22], [25] above equation gets modified to

$$V_k' = \xi_{min} \frac{\Lambda^{-1}}{k}, \qquad (2.93)$$

where, Λ is the diagonal matrix of R, and V_k' is the transformed matrix of V_k in new co-ordinate system.

We can express the definition of *excess-mean-square-error*, i.e., Equation (2.32) in the new symbolic representations of this section to obtain

$$\chi = E\left\langle (W'^* - W_k')^T \Lambda (W'^* - W') \right\rangle . \qquad (2.94)$$

(note: primed variables are in principal co-ordinate system). It is assumed that W_k', X_k, d_k and noise are statistically stationary and zero mean signals. After the convergence of the algorithm, we can also-assume W_k and X_k to be independent [33], so Equation (2.94) can be written as

$$\chi = \sum_{n=1}^{N} \lambda_n E \left\langle (w_n'^* - w_{nk}')^T (w_n'^* - w_{nk}') \right\rangle , \qquad (2.95)$$

where, λ_n is the n^{th} diagonal element or n^{th} eigen value of Λ, $w_n'^*$ and w_{nk}' are the n^{th} element of weight vector W'^* and W_k' respectively. Now using the definition of

V_k' from Equation (2.73), we can further modify Equation (2.95) to

$$\chi = \sum_{n=1}^{N} \lambda_n v_{nk}' \tag{2.96}$$

where, v_{nk}' is the n^{th} diagonal element of V_k'. It can also be assumed that all the element of weight vector has converged approximately to its optimal value, therefore all the diagonal elements of V_k' would be approximately equal. So by using Equation (2.93) the n^{th} diagonal element of V_k' is given by

$$v_{nk}' = \xi_{min} \frac{1}{k\lambda_n}, \tag{2.97}$$

where, λ_n is the n^{th} eigen value of R. Now, using Equation (2.97), Equation (2.96) can be modified to get the following final expression for *excess-mean-square-error*,

$$\chi = \frac{\xi_{min}}{k}. \tag{2.98}$$

Misadjustment M, which is defined as $M = \chi/\xi_{min}$ can be written as

$$M = \left(\frac{1}{k}\right). \tag{2.99}$$

Thus, we observe from Equation (2.98) and Equation (2.99), that theoretically the *excess-mean-square-error* and *Misadjustment* are totally independent of the statistics of the input signals, it is also independent of the number of taps. We can approach zero *Misadjustment*, when $k \to \infty$. The theoretical value of the SNR of output signal, can also be reasoned to be equivalent to

$$SN = 10 \log \left(\frac{1}{M}\right), \tag{2.100}$$

as was pointed out in Section 2.2.4.

2.5 Review of results with both algorithm

2.5.1 Case study and general simulation idea

2.5.1.1 Cases studied for LMS algorithm based ANC with relevant theory

We studied the following cases for the LMS based ANC.

1. Effect of the signal to noise ratio SNR of the primary signal on the SNR of output signal and also its effect on the behaviour of *Misadjustment* M.
2. Effect of the number of taps, i.e., N, on M and the SNR of output signal.
3. Effect of the parameter, adaptive gain constant, i.e., μ on M and the SNR of output signal.
4. Study of the *Performance Factor* (to be defined later), i.e., PF and its variations with respect to μ.
5. Effect of the presence of several harmonics in the primary, on the SNR of output signal.
6. Performance of the system for different values of the correlation coefficient cc, between noise n_0 and n_1.

Now we describe some theoretical results related with the mentioned cases. These theoretical results are used to compare them with the measured results.

Case-(1) and Case-(2)

In Case-(1), the SNR of the primary signal is varied and the SNR of the output signal is computed. Let us call the inverse of the SNR of primary signal as noise level, l, i.e.,

$$l = \text{std. of } n_0/\text{std. of } s. \tag{2.101}$$

As we vary l, the matrix R will change and this is known for the given signal pattern, hence Equation (2.40) and Equation (2.42) is used to find theoretical results for M and SN. Similarly, for Case-(2) matrix R is known for different values of number of taps and thus theoretical SN and M can be calculated.

Case-(3)

Adaptive gain constant μ, is one of the important parameter. Equation (2.40) shows the relationship between μ and M or SN. It can also be seen from Equation (2.12) that, the time constant τ is inversely proportional to μ. So there is a trade off between number of iteration and M. Number of iteration required for the convergence of algorithm is around 9 to 10 time-constant; because of computational simplicity we have assumed it to be equal to

$$CT = 10\frac{1}{\mu\lambda_{min}} \tag{2.102}$$

where, λ_{min} is the minimum eigen value of R.

Case-(4):

If μ is chosen to be small then it requires large number of iterations for convergence, while if μ is large, though the number of iteration gets reduced but at the same time increases M. Thus, poor SNR of output signal is obtained. There is a trade-off between convergence speed and M (or steady state mean-square-error) [22]-[24]. We study this contradiction by defining a parameter "*Performance Factor*", PF. Mathematically, we define it as

$$PF = \frac{SN(\text{in}\, dB)}{CT} \tag{2.103}$$

Using Equation (2.41), Equation (2.42), and Equation (2.44) Equation (2.103) becomes

$$PF = \mu\lambda_{min} \log\left\{\frac{trace(R)}{(2-\mu trace(R))}\right\} \tag{2.104}$$

The peak value of PF can be obtained by differentiating Equation (2.104) with respect to μ and equating it to zero and then solving for μ. The value of μ where PF is maximum is the solution of

$$\log\left[\frac{2-\mu trace(R)}{\mu trace\,(R)}\right] = 1 + \ln(2) + \frac{\mu trace(R)}{(2-\mu trace(R))}. \tag{2.105}$$

Case-(5)

The theory of presence of several harmonics in the input signal can be understood better in the frequency domain or Z-transformed [37] system. Let us assume that the adaptive filter has an infinite two-sided impulse response. Then the performance surface [22] is given by

$$\xi = \phi_{dd}(0) + \sum_{l=-\infty}^{l=\infty} \sum_{m=-\infty}^{l=\infty} w_l w_m \phi_{xx}(l-m) - 2\sum_{l=-\infty}^{l=\infty} w_l \phi_{xd}(-l) \tag{2.106}$$

where, ϕ_{dd} is the autocorrelation function of primary signal, ϕ_{xx} is the autocorrelation function of reference signal, and ϕ_{dx} is the cross-correlation function between primary and reference signal. We obtain the Weiner weight vector[3], W^* by setting the derivatives of Equation (2.106) with respect to the weights to zero. We take the Z-transform of the Weiner weight [22] to get

---

[3] Here the order of weiner weight is infinitely long

$$Z\,transform[W^*] = \frac{\Phi_{xd}(z)}{\Phi_{xx}(z)} \tag{2.107}$$

where, $\Phi_{xd}(z)$ and $\Phi_{xx}(z)$ are the Z-transforms of ϕ_{xd} and ϕ_{xd} respectively.

The Z-transforms of the cross-correlation function between primary and reference signal depend only on the mutually correlated primary and reference components. If n_0 and n_1 are assumed to be highly correlated then,

$$\Phi_{xd}(z) = \Phi_{xx}(z) = \Phi_{n_0n_0}(z) \tag{2.108}$$

Hence,

$$W^*(z) = 1 \tag{2.109}$$

It is a constant, independent of the primary signal or reference signal spectrum.

Case-(6)

Effectiveness of ANC in removing the noise depends on the correlation coefficient cc between n_0 and n_1. In this case cc is varied and its effect on the system performance is studied. Referring to the block diagrams of Figure 2.1, we notice that the function of the adaptive filter is to produce output which is approximately equal to the signal n_0. Ideally, when $cc = 1$, one can achieve full noise removal, but when $cc < 1$, the amount of noise removed from the signal decreases. The amount of noise being cancelled was studied quantitatively through simulations.

2.5.1.2 Cases studied in Kalman filter based ANC

Kalman filter has two algorithmic parameters, *viz.*, initial choices of weight vector W_0 and initial value of error covariance matrix V_0. These initial choices theoretically, do not affect the performance of the system [see Equation (2.100)]. So we looked upon the other parameters and studied their effect on the performance of ANC system. We studied the following cases related to Kalman based ANC:

1. Study of the system performance, i.e., SNR of output signal and M with respect to noise level l.
2. Effect of number of taps on the SNR of output signal and M.

3. Performance of the system for different values of the correlation coefficient, cc.

From Equation (2.99) and Equation (2.100), we see that M and SN are independent of signal and system parameters. They only depend on the number of iteration.

2.5.1.3 Signal modeling

Refer to the block diagram of Figure 2.1, primary signal (d_k) is the combination of pure signal (s) and interfering noise (n_0). Reference signal (n_1) is another noise signal highly correlated with n_0. The pure signal (s) is modeled as a sinusoidal signal of frequency $2kHz$ and is sampled at $10kHz$ (which is above Nyquist rate [37]). (Note: As the final results depend on the relative ratio of the sampling frequency and the frequency of the signal, and also, we can always scale the frequency or time axis. Therefore we may choose any frequency we want and scale the axis accordingly.) The root-mean-squared value of s is $1/\sqrt{2}$. The interfering noise n_0, is taken to be white noise Gaussian signal of mean approximately equal to zero. To form reference signal n_1, another white noise Gaussian sequence is taken which is highly correlated with n_0. The mean of the reference is also taken to be equal to zero. The delay between signals n_0 and n_1 is taken to be zero.

2.5.1.4 General idea on simulations

The rate of convergence of LMS algorithm depends on the smallest eigen value of R [see Equation (2.12)], so we can write the time constant of LMS algorithm as

$$\tau^{LMS} \sim \frac{1}{\mu\lambda_{min}} \tag{2.110}$$

where, τ^{LMS} is the time constant for LMS algorithm and λ_{min} is the minimum eigen value of R. From Equation (2.91), we deduce that, for Kalman filter time constant τ^{Kal} is approximately given by

$$\tau^{Kal} \sim 2N \tag{2.111}$$

Time for convergence CT can be literally said as the time or number of iterations needed beyond which there is no significant improvement of weight vectors. We take this value for LMS algorithm to be approximately equal to $10\tau^{LMS}$ iterations and for Kalman filter it is taken approximately to be equal to $250\tau^{Kal}$ iterations.

In all simulations (otherwise stated) weight updating continues up-to $(CT-N+1)$ number of iterations. Then afterward, 750 more iterations are done with the weight fixed at last value to obtain the output signal data. This output data set is then used to calculate parameters like variance, standard deviation, SNR and Fourier transforms FFT, of the output signals. The expected values of these parameters is estimated by taking an average of 60 individual runs of program. In all cases, the weights of the adaptive filter are initially set equal to zero. The variance of noise in the primary signal is taken to be equal to the variance of reference signal.

2.5.1.5 Practical calculations of M and SNR of output signal

The most important parameter which gives us the indication of amount of noise being removed from the output is the SNR of output signal. In order to measure this quantity in output signal effectively, we follow the following procedure to calculate it.

Let the standard deviation of pure signal be *dpure* (a known quantity), and the standard deviation of output signal measured is *dop*. Then the amount of noise (i.e. standard deviation of noise) in the output signal is given by

$$dnoise = \sqrt{|dpure^2 - dop^2|} \tag{2.112}$$

where, *dnoise* is the standard deviation of the noise. Referring to the definition of *Misadjustment*, i.e. Equation (2.39), we can say that M can also be defined as

$$M = \frac{variance\,of\,noise}{variance\,of\,pure\,signal} \tag{2.113}$$

Now, using Equation (2.112) and Equation (2.113) we have

$$M = \frac{(dnoise)^2}{(dpure)^2}, \tag{2.114}$$

and

$$SN = 20\log\left(\frac{dpure}{dnoise}\right). \tag{2.115}$$

2.5.2 Results with LMS filter

Case-(1):

In this numerical experiment, we varied noise level, l from 0.1 to 2, and for each l we calculated M, FFT, SNR of output signal. Throughout this experiment adaptive

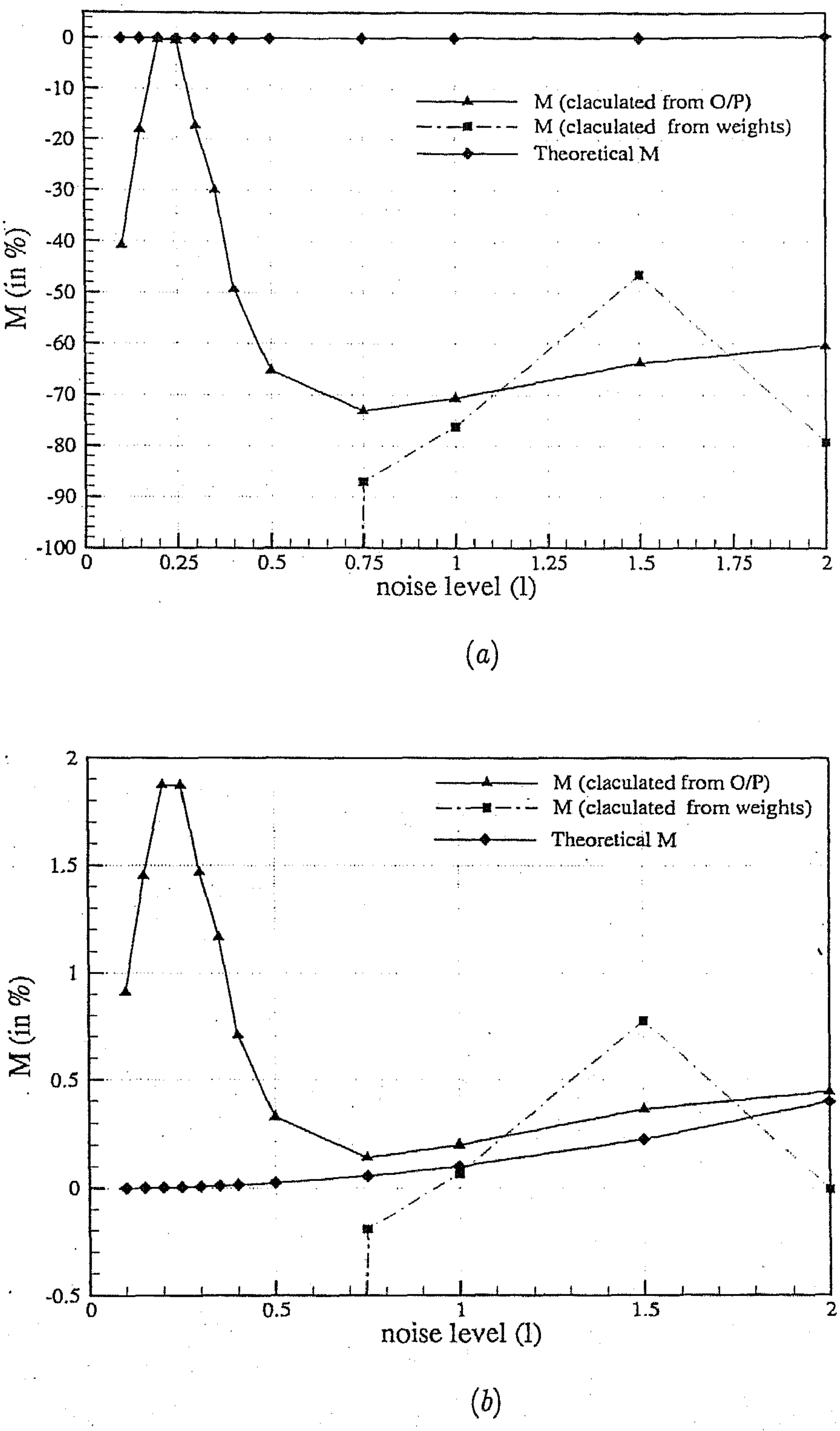

(*a*)

(*b*)

Figure 2.4: (*a*) Variation of *Misadjustment* with the noise level l ($N = 2$, $\mu = 0.002$, and $cc = 1$). (*b*) zoomed view to show discrepancy between theoretical M and practically measured M.

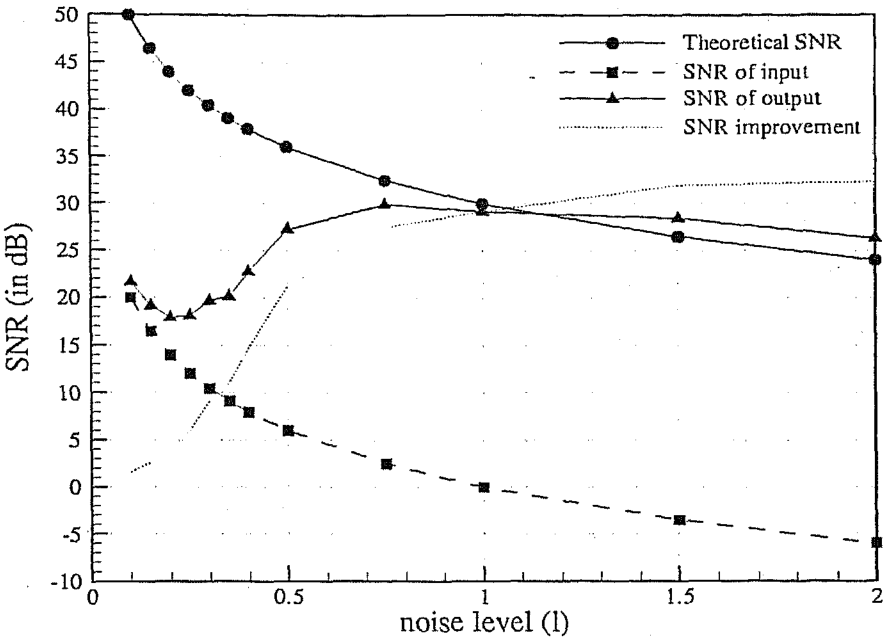

Figure 2.5: Variation of SNR of output signal with noise level l ($N = 2$, $\mu = 0.002$, and $cc = 1$).

gain constant was set at 0.002, number of taps N was set at 2, correlation coefficient cc was set at 1. We did the weight updating only up-to 9999 iterations (note: it is not the same as explained in Section 2.5.1.4). The plots in Figure 2.4 illustrates the variation of M with l. We calculated M by two different methods, one from the SNR of the output signal, i.e. from Equation (2.114), and the other from the error between weight vector with the Weiner weight vector. Theoretical curve is also plotted using Equation (2.40). The plots in Figure 2.5 show the variations of theoretical and measured curves of the SNR of output signal with l. Frequency domain plots of output signals are shown in Figure 2.6, for different noise levels.

From Figure 2.4, we observe that for $l < 0.6$ there is a huge discrepancy in the *Misadjustments* calculated by two different methods. The M calculated from the weights is very large in this range. This discrepancy is due to the fact that for small values of l, i.e, $l < 0.6$, the eigen values of matrix becomes too small, consequently CT depicted by Equation (2.102) increases by a large factor. Since, we have taken same value of adaptive gain constant and updated weight only up-to 9999 iterations, which is too less for this range. We see that both curves deviate sharply from the theoretical curve evaluated for $l < 0.6$. Because the norm of

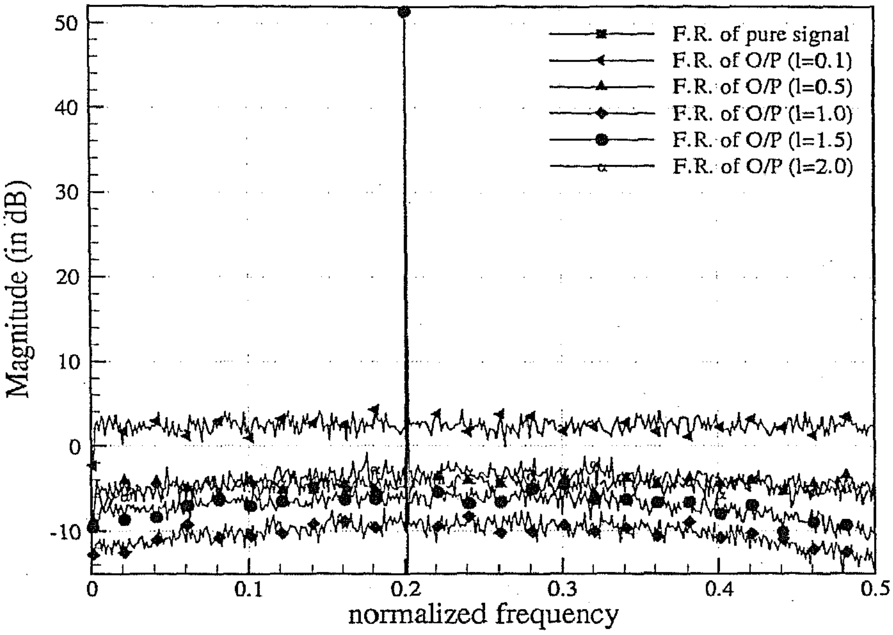

Figure 2.6: Frequency response of output signals for different values of noise level l ($N = 2$, $\mu = 0.002$, and $cc = 1$).

Weiner weight for each l is close to 1, while the actual norm of weight vector increases with l. In Figure 2.5, we can also observe the same discrepancy between theoretical SN and measured SN for small l. The curve for "*SNR improvement*" is also drawn in Figure 2.5. This curve increases with increase in l. Had the number of iteration been taken equal to CT, we would have got "*SNR improvement*" of around $30dB$ irrespective of the noise level l. The FFT of output signal is shown in Figure 2.6 for various l.

Case-(2):

In this computer experiment, N is varied from 1 to 16. In this experiment μ was set at 0.002, l at 1, and cc at 1. Figure 2.7 shows the plots of M with N. Here also, M is calculated by two methods (as in Case-(1)) and is compared with theoretical curve. We observe that M calculated from output signal increases monotonously with N in this range, while M obtained from weight vectors shows oscillating behaviour.

The plots of Figure 2.8 illustrates the variation of SNR of output with N. The theoretical plot is also drawn. We observe that, smaller the number of taps the higher is the SNR of output. There is a trade off between the convergence speed and

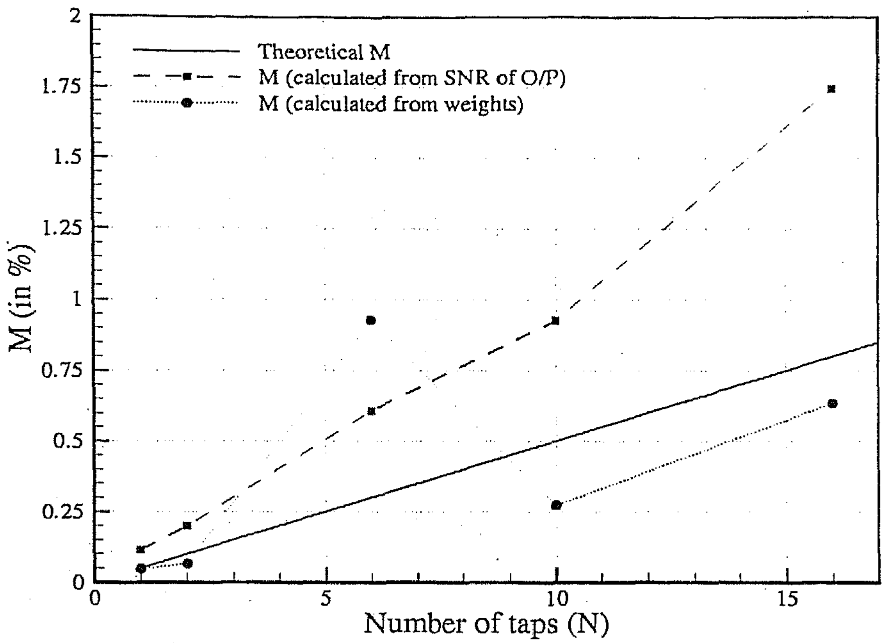

Figure 2.7: Variation of M with number of taps N ($l = 1$, $\mu = 0.002$, and $cc = 1$).

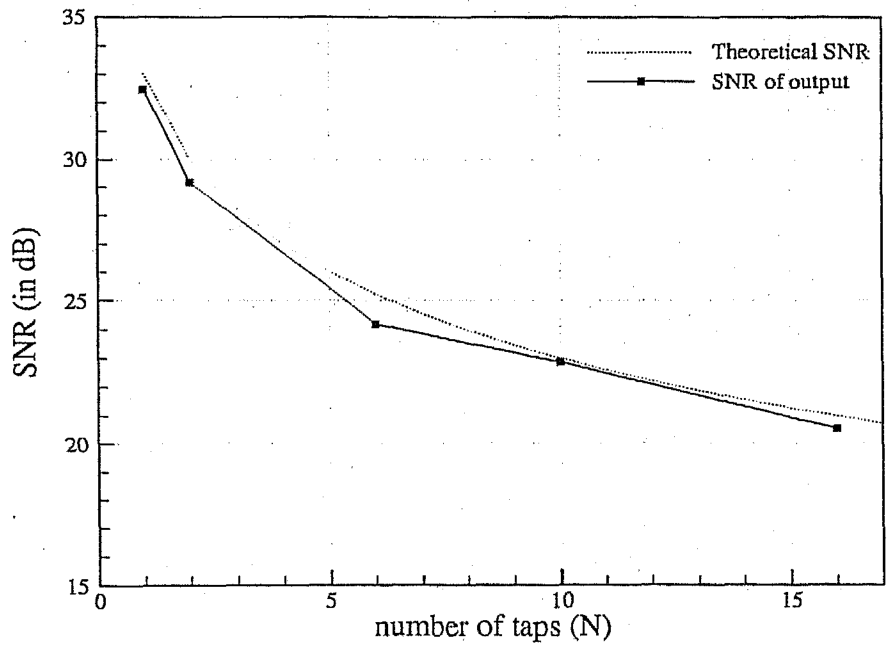

Figure 2.8: Variation of SNR of output signal with number of taps N ($l = 1$, $\mu = 0.002$, and $cc = 1$).

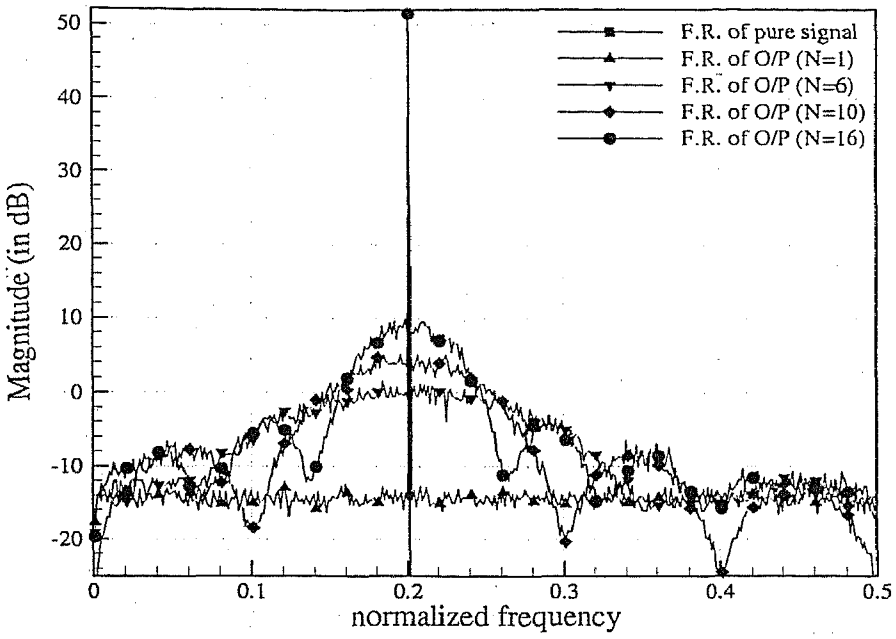

Figure 2.9: Frequency response of output signals for different number of taps N ($l = 1$, $\mu = 0.002$, and $cc = 1$).

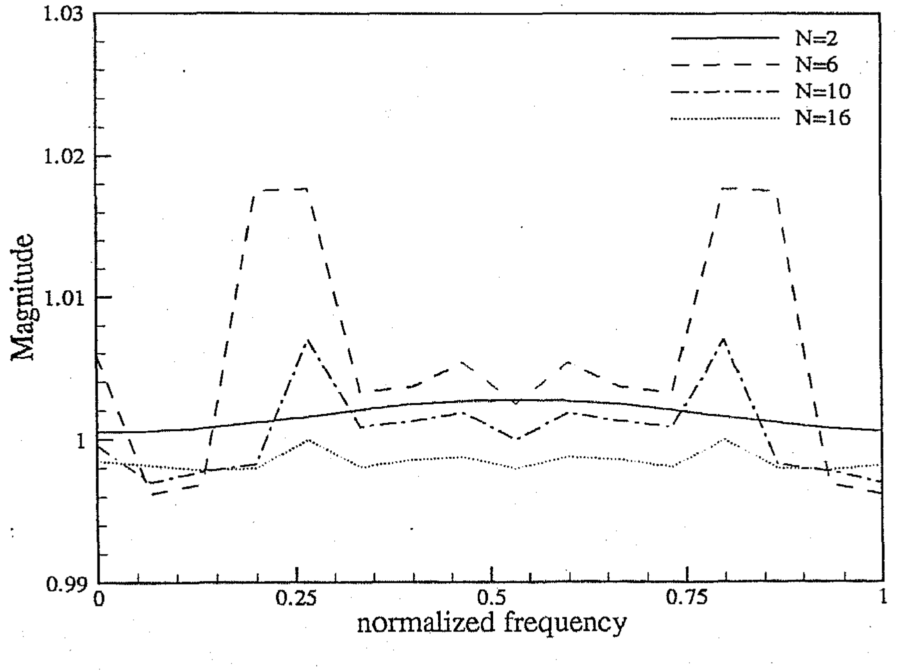

Figure 2.10: FFT of weight vectors for different filter length ($l = 1$, $\mu = 0.002$, and $cc = 1$).

Misadjustment [22]-[24] for a given filter length. Higher order filters may converge slowly and lead to higher *Misadjustment* depending on the chosen design objective. We noted two aspects related to N :

- The eigenvalue spread increases with increasing filter length. This limits the designer's freedom and cause an additional decrease in convergence speed.
- Filter length cannot be chosen arbitrary small to increase SN depicted by Equation (2.42). There must be sufficient degrees of freedom to model the unknown impulse response of the adaptive filter between the reference and the primary signal. In other words, it means that when the delay between primary and reference is large a sufficient length of adaptive filter is chosen to model the system accurately. Hence, there exists a trade-off between modeling accuracy and *Misadjustment* for long impulse responses.

Frequency response of output signal for different N is shown in Figure 2.9. For larger N, the full width half maximum ($FWHM$) of sinusoidal peak is also larger. It is because for higher order the number of side lobes in frequency response of the filter increases [37], we can see it from Figure 2.10, which shows the FFT of the weights of the adaptive filter.

Case-(3):

One of the important system parameter on which *Misadjustment* strongly depends is the adaptive gain constant μ. Figure 2.11 contains the plots of M versus μ. It can be observed from these plots that, theoretical M, M calculated from SNR of output, and also the M obtained from weights follow more or less same variations with μ.

Variations of theoretical and measured SNR of output signal with μ are illustrated in Figure 2.12. We noticed following peculiar behaviours of these curves. We observed that for μ between 0.002 and 0.3, the measured SN is higher than the theoretical value and, outside this range it is smaller. One would generally expect the theoretical value to be better than experimental results. Due to various approximations being involved in the expression of theoretical values, it comes out to be in conservative side. In the range $0.002 < \mu < 0.3$ conservation can be seen, but for $\mu > 0.3$ theoretical value is higher than measured because of the approximation of μ being small in the derivation of theoretical SN, is not valid here. In Figure 2.13, the FFT of output signals for different μ are shown.

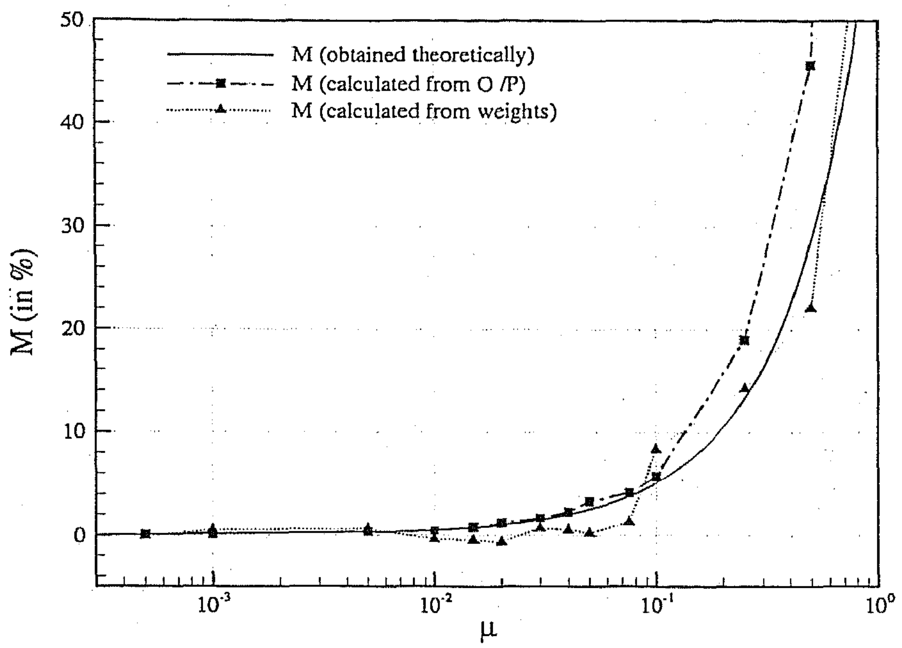

Figure 2.11: Variation of M versus the adaptive gain constant μ ($l = 1$, $N = 2$, and $cc = 1$).

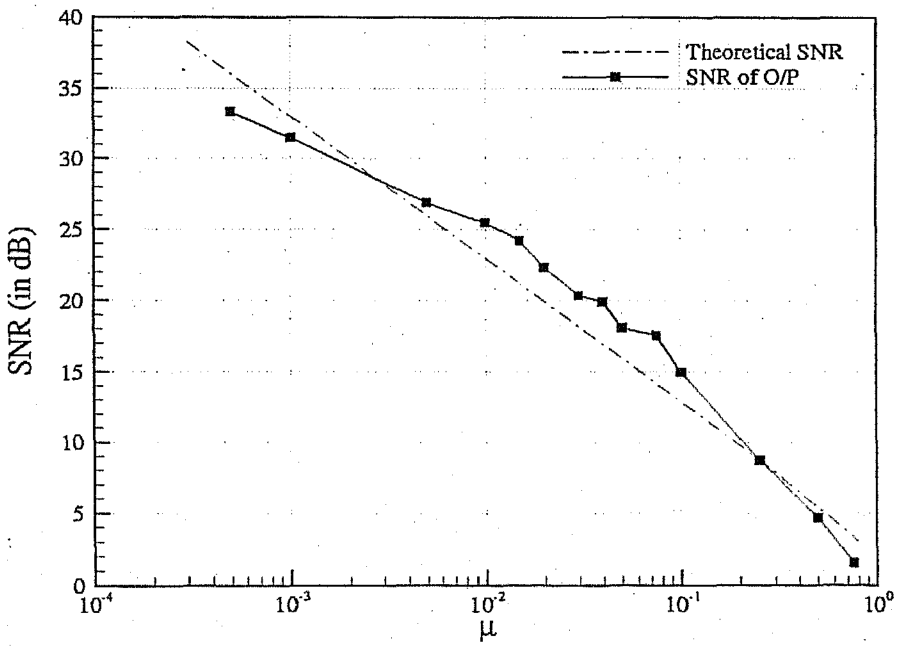

Figure 2.12: Plots showing variations of the theoretical and measured SN with μ ($l = 1$, $N = 2$, and $cc = 1$).

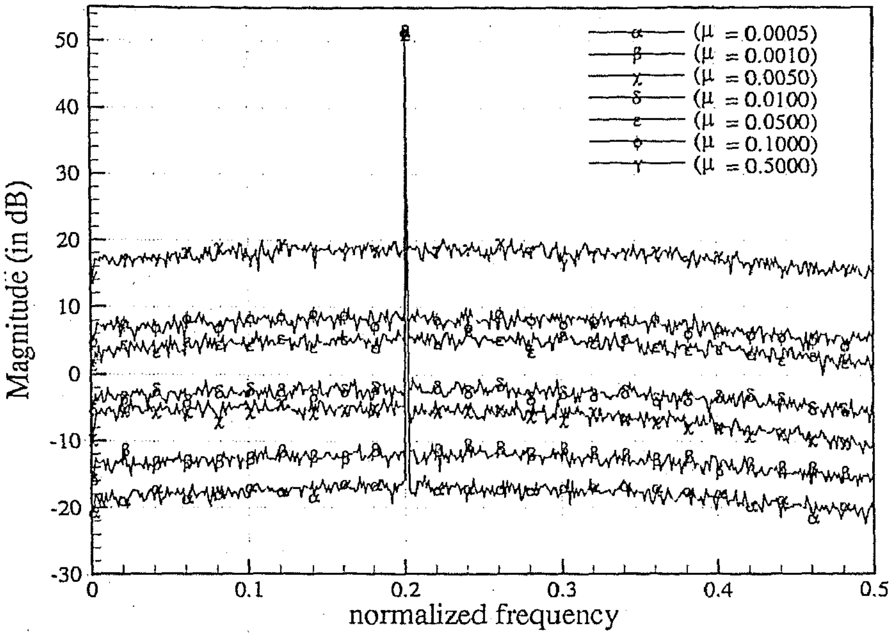

Figure 2.13: Frequency response of output signals for different μ, ($l = 1, N = 2$, and $cc = 1$).

Case-(4):

Variations of theoretical and measured PF are drawn in Figure 2.14. We observe definite peaks in these curves. Theoretical peak occurs at $\mu = 0.542$, and practical peak is at around $\mu = 0.5$. One should have high value of PF. We see that if we work at μ, where PF is maximum we can get the SNR output only up-to $7dB$ which is very low compared with smaller μ. Therefore, depending on the application one may choose higher or smaller μ. When a small μ has to be chosen then fast processors are used to reduce the computational time.

Case-(5):

From Equation (2.109) it is clear that the output signal will remain unaffected even if the pure signal may have several bands of frequencies. This fact is studied for a finite length filter. In this case we used different signal as the pure signal to the filter. We made a pure signal, by the linear combination of sinusoids of frequencies 20, 400, 600, 1000 and $2000Hz$. Number of taps was set at 2, μ at 0.002, cc at 1 and l at 1. Figure 2.15 shows the spectrum of pure signal, primary signal and output signal. Noise rejection in the output signal can be clearly observed from

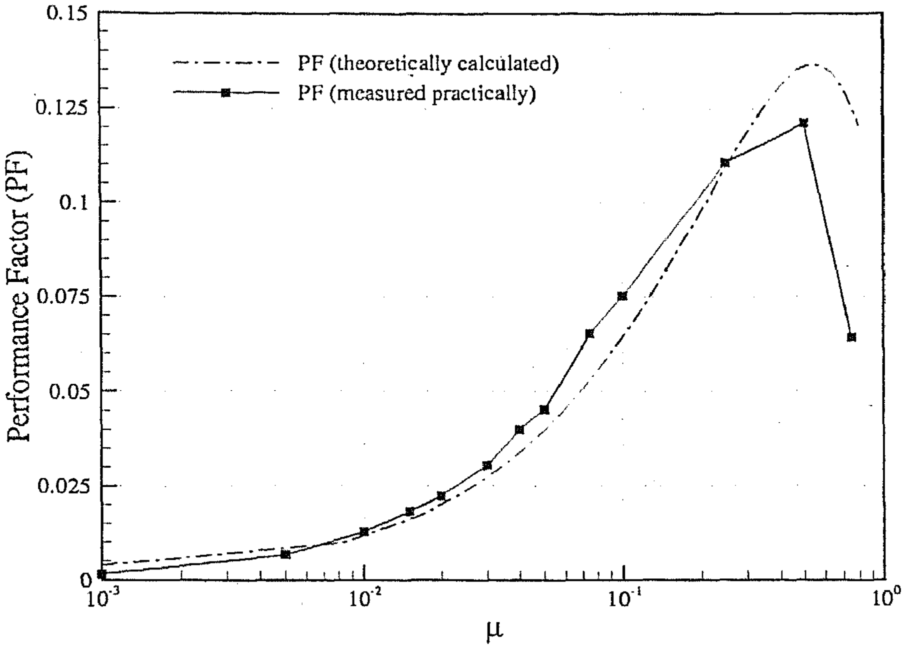

Figure 2.14: Variation of PF with μ ($l = 1$, $N = 2$, and $cc = 1$).

these plots. We found that in this case the SNR of output signal is $28.67dB$, while the SNR of output signal for the previous model of pure signal (when there was a single frequency component at $2kHz$) was $29.18dB$. Hence, we conclude that the performance of ANC is almost independent of the spectrum of the pure signal.

Case-(6):

In this simulation, we varied the cc from 1 to 0.6, and for each value of cc, we calculated M, FFT, and SNR of the output signal. Noise level l was set at 1, N at 2 and μ at 0.002. Quantitative results of the dependence between cc and M are shown in Figure 2.16. Figure 2.17 displays the variations SNR of the output signal with cc for two different filter length. We can see the spectrum of output signal in Figure 2.18 for different values of cc. From these plots we can come to following conclusions. We observe a mismatch between M calculated by the two methods in Figure 2.16. The error between Weiner weight and actual weight very small, therefore M calculated from these is very small and remains approximately constant for all values of cc. However, the SNR of output signal decreases with cc. Thus, we can say that even if the Weiner weights are considered the ANC method is not able to retain its performance for $cc < 1$. With the same noise profile, we

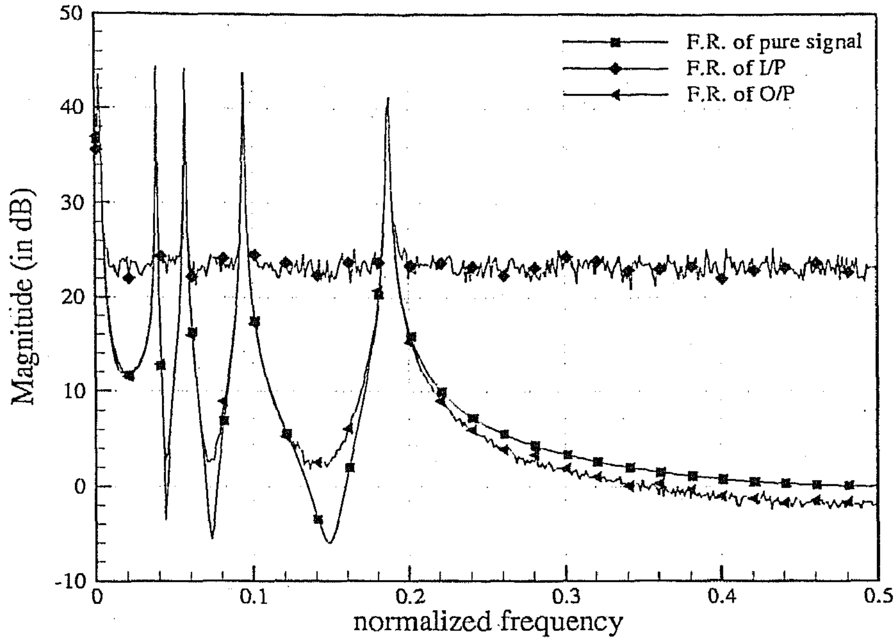

Figure 2.15: Spectrum of pure, primary and output signals ($\mu = 0.002$, $l = 1$, $N = 2$, and $cc = 1$).

also checked, if we could increase the SNR of output by increasing number of taps for $cc < 1$. And we can found that even by increasing N, the SNR of output does not improve. The SNR of output signal goes below $10dB$, even though cc is as high as 0.8. These observations can also be seen in frequency domain, through the plots of Figure 2.18.

2.5.3 Results with Kalman filter approach

In Kalman filter based ANC system, the computation of "*Kalman gain*" requires an inversion of a scalar quantity [see Equation (2.81)]. It requires a prior knowledge of the optimal mean-square-error ξ_{min}, certainly we do not know this value *a priori*. Usually, after the noise cancellation the SNR of the output is in the range of $15dB$ to $30dB$. Therefore, to compute "*Kalman gain*" one can use an estimated value of ξ_{min} in between 0.01 to 0.001. Also, this choice of ξ_{min} has no influence on the successive estimates of the tap gains [33]. In all of the simulations based on Kalman filter, we chose ξ_{min} to be equal to 0.001 and the initial covariance matrix, V_0, to be a unity matrix.

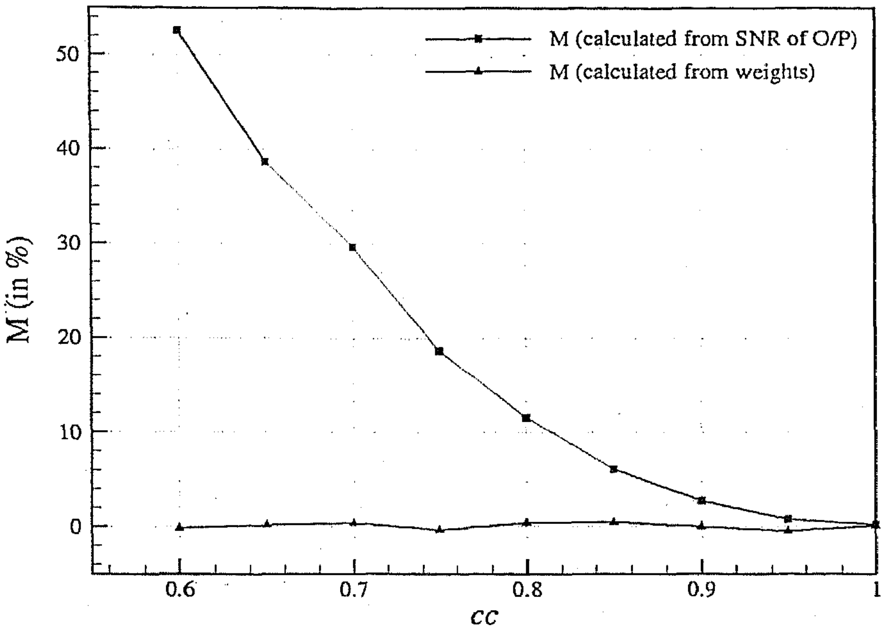

Figure 2.16: Variation of M with the correlation coefficient cc ($N = 2$, $\mu = 0.002$, and $l = 1$).

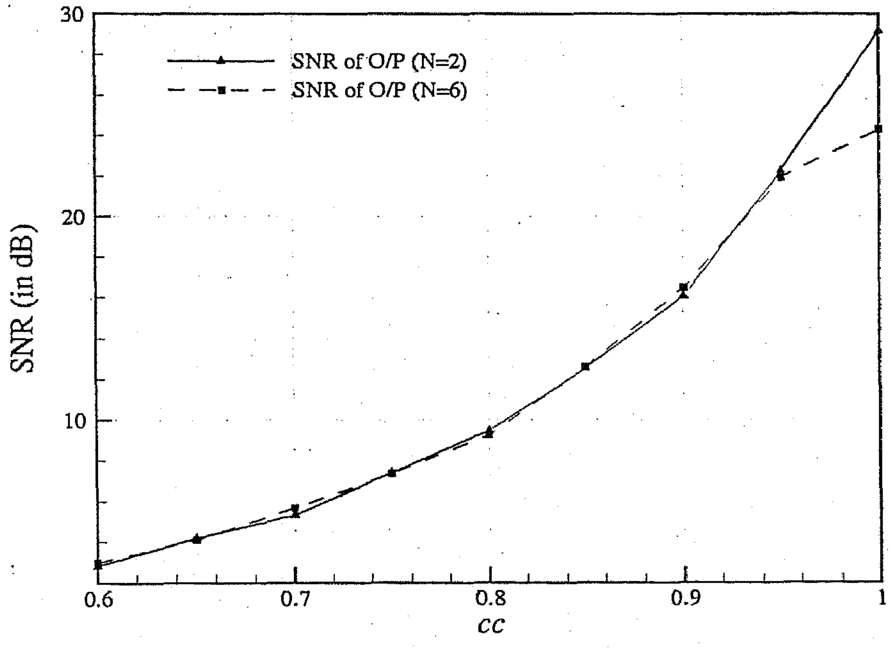

Figure 2.17: Plots showing the SNR of the output signal with cc for two different values of number of taps, $N = 2$ and 6 ($l = 1$ and $\mu = 0.002$).

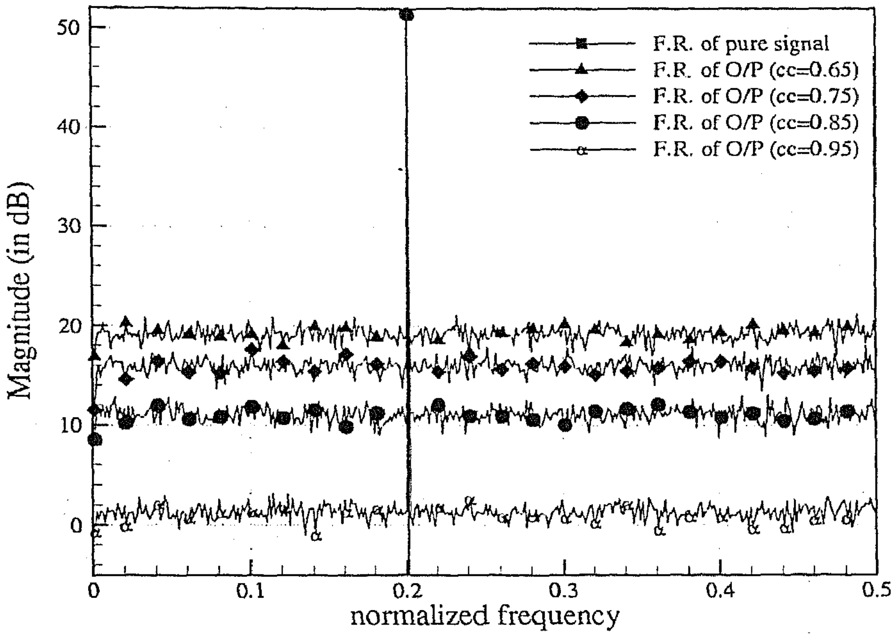

Figure 2.18: Frequency response of output signals for different cc ($l = 1$, $N = 2$, and $\mu = 0.002$).

Case (1):

In order to study the influences of noise level, l on Kalman filter based ANC, we varied l from 0.1 to 1 and for each case we calculated the M, SNR and frequency response of the output signals. We set cc at 1, and the number of taps, N was taken to be equal to 2. Figure 2.19 depicts the variations of M with l. Here also, we calculated M by two methods as mentioned in Section 2.5.2 for the case of LMS algorithm. Theoretical curve for M using Equation (2.99) is also drawn on the same figure for the comparison. The comparison of theoretical SN (from Equation (2.100)) and measured SN is done in Figure 2.20. Spectrum of the output signals for different values of l are illustrated in Figure 2.21.

We can draw following conclusions from these plots. Close match between theoretical and measured M (measured from SNR of output signal) can be observed from the plots of Figure 2.19. While M calculated by weight method toggles around the theoretical value. It is because the norm of weight vector sometimes is larger than the norm of the Weiner weight and some times smaller. It is due to the uncertainty of the noise. We can say that M is almost independent of l for $l > 0.5$. This fact is reflected in terms of the SNR of output signal in Figure 2.20,

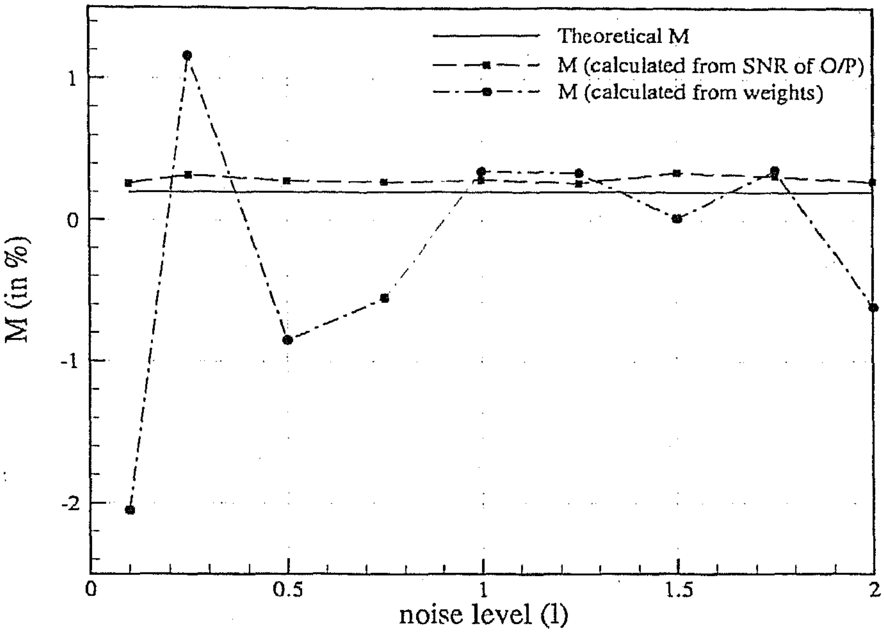

Figure 2.19: Variation of M with the noise level, l ($N = 2$ and $cc = 1$, Kalman filter).

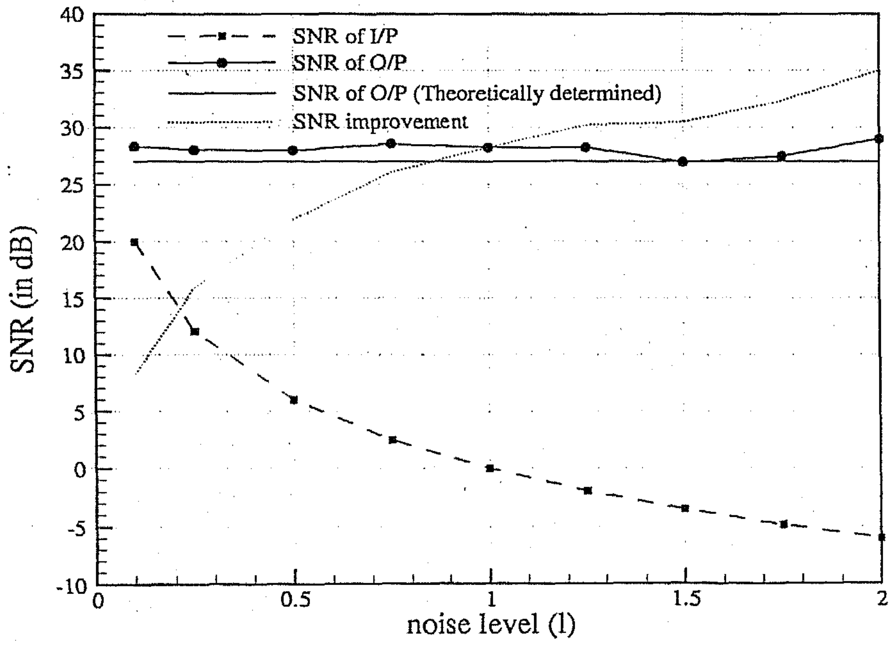

Figure 2.20: Plots showing variations of SNR of the output signal with the noise level l ($N = 2$ and $cc = 1$, Kalman filter).

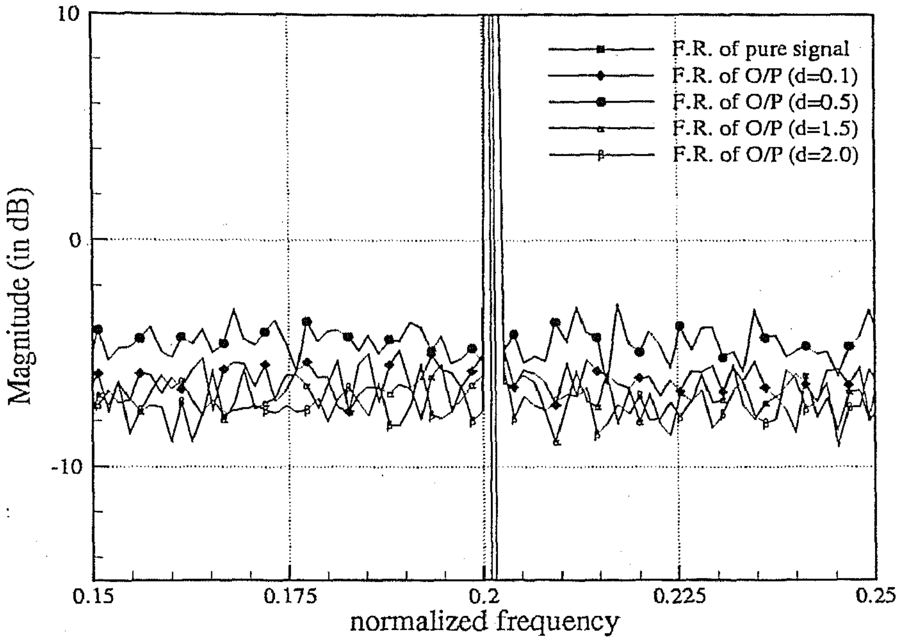

Figure 2.21: Spectrum of the output signals at different noise level l ($N = 2$ and $cc = 1$, Kalman filter).

as it remains approximately constant over the l. The curve for theoretical SN is below the measured curve. One peculiar we noticed that the "*SNR improvement*" increases with increase in l. The higher the noise in the primary signal the greater is its removal from the output. Plots of Figure 2.21 also verify some of the above observations.

Case-(2):

Behaviour of the system performance with the number of taps is examined in this case. Both l and cc were set at 1. In Figure 2.22, we have illustrated the variations of different types of M with the number of taps N. We observe that theoretical M calculated from Equation (2.100), is almost constant in this range of N. The M calculated from the SNR of output signal has a small positive slope. While the M obtained from the weight error shows an oscillating behaviour. This oscillation is because of the same reason as explained in Case-1.

Figure 2.23 brings out the variation of SNR of the output signal with N. It can seen that SN obtained from Equation (2.100) is almost independent of N. But practically, we find that it has decrement of about $5dB$ as N moves from 1, up-to

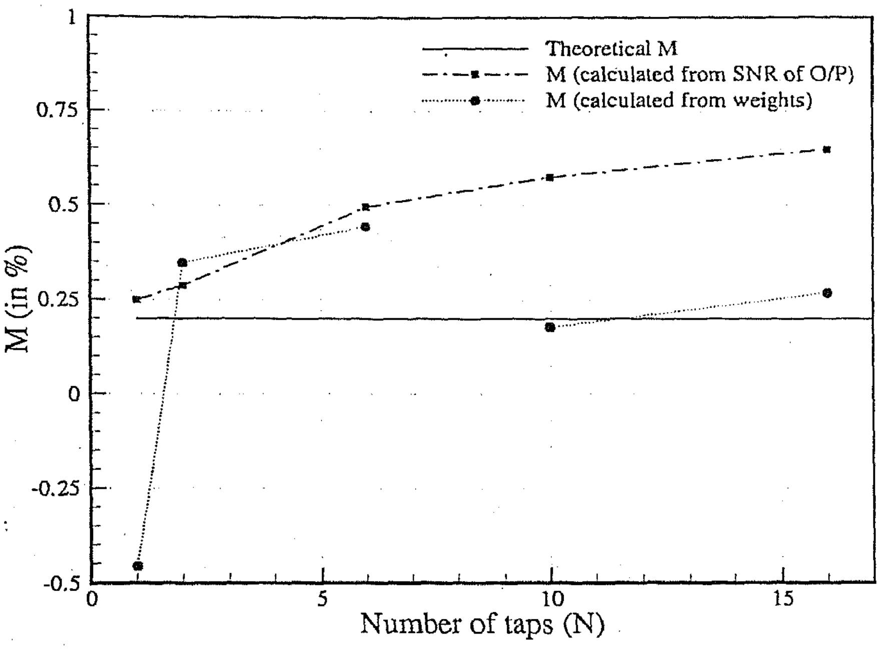

Figure 2.22: Variation of M with N ($l = 1$ and $cc = 1$, Kalman filter).

20. The theoretical value of SNR of the output signal is less than the measured value for $N < 4$ and, for $N > 4$ it behaves in the other way. The cause of this can be explained as follows: We derived Equation (2.100), by considering the CT of Kalman filter to be the same as described in Section ??, but actually for small N, the CT is even smaller than this. Hence, the SNR of output would have even more for small N, had CT been chosen smaller. Also, because the number of iteration was taken to be $(CT - N + 1)$, which comes out to be slightly more to mask the effect of N in the expression of SN [see Equation (2.100)]. The theoretical SNR of the output signal has almost no change with N, but the measured SNR of output signal decreases with about $0.1dB$ per number of taps.

Output spectrum under different N is shown in Figure 2.24. We observe that with increase of N, the $FWHM$ of the signal peaks of the spectrum increases. Because the number of side lobes [37] increases with increase in N.

Case-(3):

In this case we carried out simulations to study quantitatively, the effects of cc in system performance. The cc is varied from 1 to 0.6 with l set at 1. We did these simulations for two values of N = 2 and = 6. Figure 2.25 illustrates the

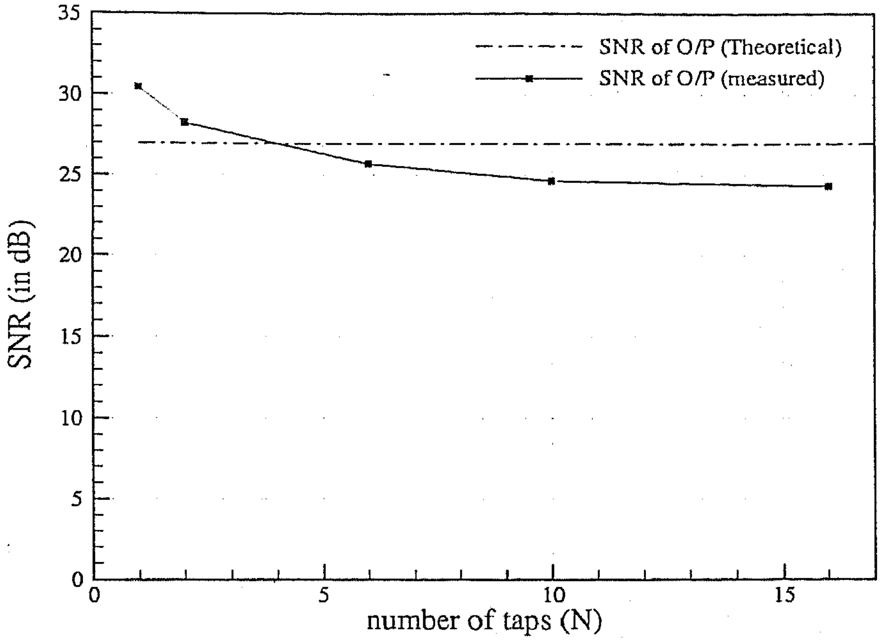

Figure 2.23: Plots showing the variations SNR of the output signal with N ($l = 1$ and $cc = 1$, Kalman filter).

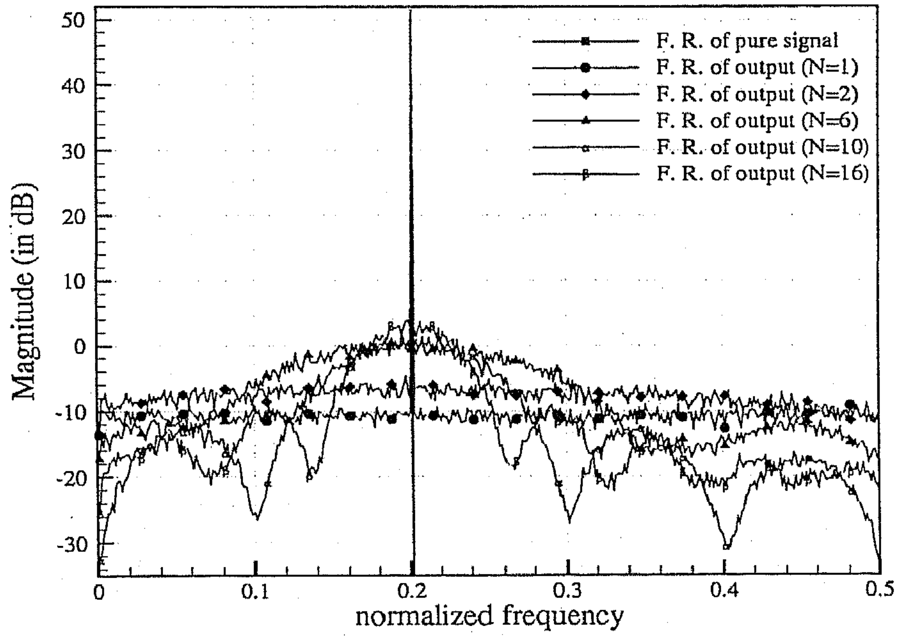

Figure 2.24: Frequency response of the output signal for different values of N ($l = 1$ and $cc = 1$, Kalman filter).

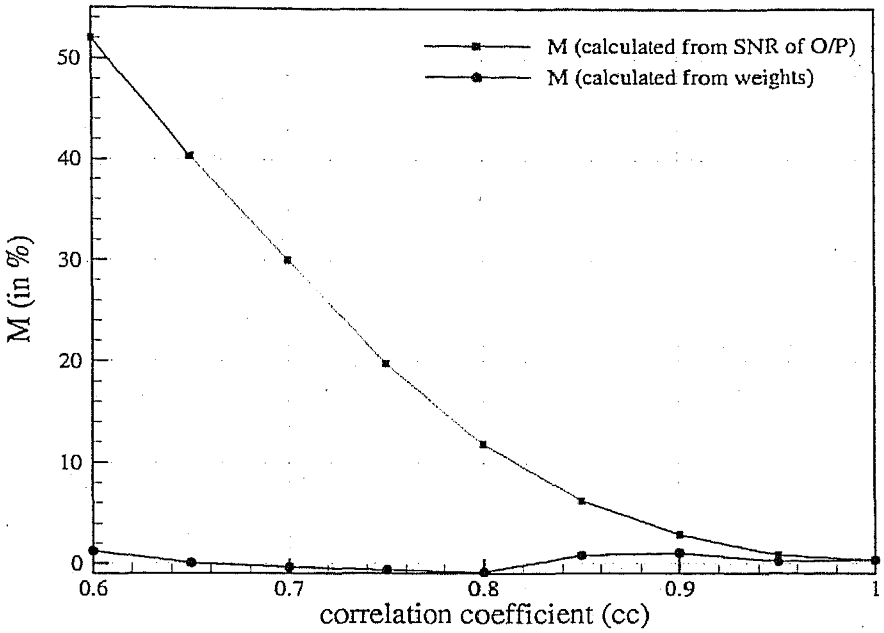

Figure 2.25: Plots of M versus cc ($l = 1$ and $N = 2$, Kalman filter).

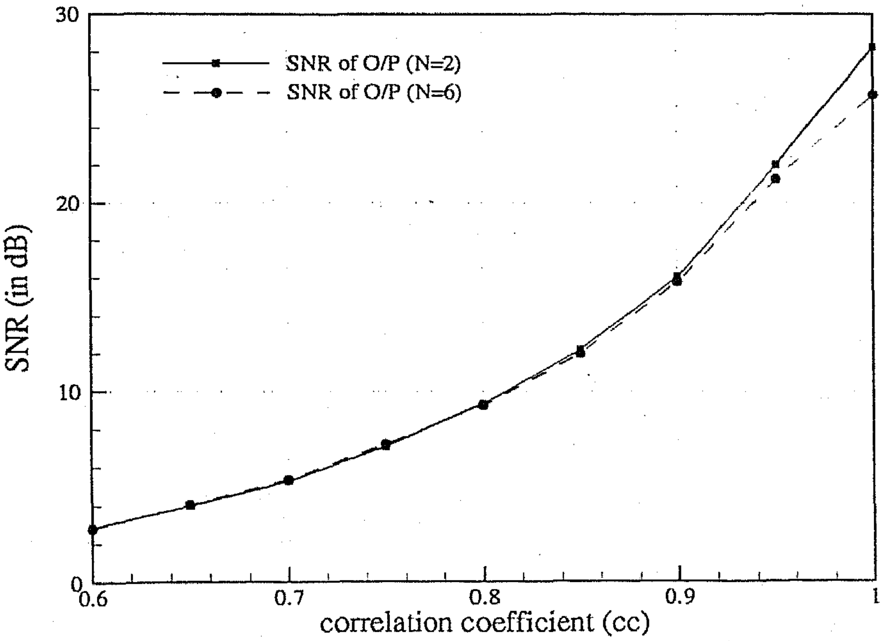

Figure 2.26: Plots of SNR of the output signal versus correlation coefficient, cc for two different values of $N = 2$ and 6 ($l = 1$, Kalman filter).

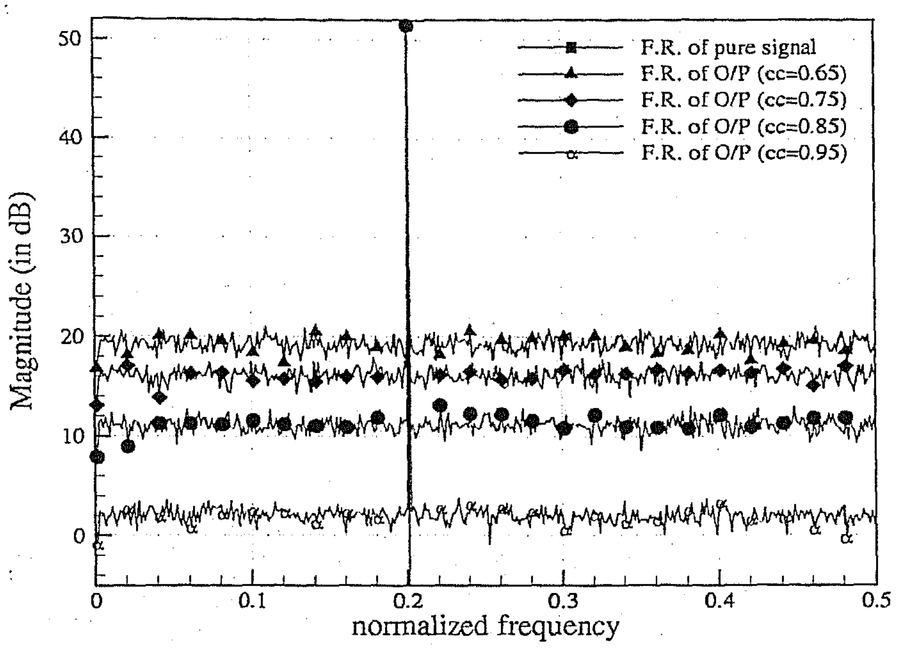

Figure 2.27: Spectrum of the output signals for various values of *cc* ($l = 1$ and $N = 2$, Kalman filter).

variations of two types of M with *cc*. There is an discrepancy between these two M. The M calculated by the weights is almost constant with *cc*, while other M calculated from the SNR of the output increases with decrease in *cc*. It shows that weight error between the actual weight and the Weiner weight is small and is approximately constant with the change in *cc*. System performance deteriorates as *cc* is decreased.

The curves of the Figure 2.26 show the variations of SNR of the output signal for $N = 2$ and 6 with *cc*. We observe that for $cc < 0.9$, the distinction between the SNR of the output signal for smaller and higher order is not clear, it means that the SNR of the output signal remains approximately independent of N for $cc < 0.9$. We also notice that when *cc* goes below 0.8 the SNR of the output signal goes below $10dB$. Spectrum of output signals for various values of *cc* is shown in Figure 2.27.

2.5.4 Comparison of results of LMS and Kalman filter

In this section, comparison of system performances with LMS and Kalman based ANC is done. The plots of Figure 2.28 illustrates the *Misadjusment M* obtained

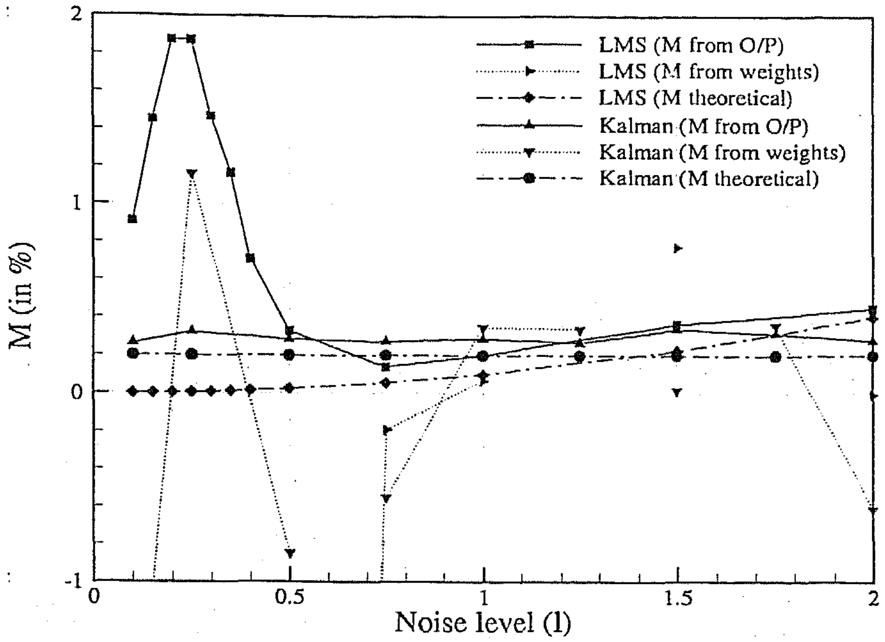

Figure 2.28: Comparison of *Misadjustment* in LMS and Kalman implementations when noise level l is varied. ($N = 2$ and $cc = 1$, in both case.)

from both Kalman and LMS methods for different values of noise level l. We observe that the *Misadjusment* calculated from output in case of Kalman filter, is quite small as compared with its counterpart in LMS for $l < 0.5$. Similar behaviour can be seen for M calculated from weights. This clearly indicates the faster convergence for Kalman filter algorithm [33]. In these simulations, the number of iteration for LMS was 9999, and for Kalman case it was only 999. Graphs of Figure 2.29 show the comparison of the behaviour of SNR of output signals for both cases with l. The output SNR in Kalman case is almost independent of the noise level. It clearly indicates the independence of Kalman filter on the eigen values of matrix R and its spread [33]. Faster convergence of Kalman filter is reflected as the higher "*SNR improvement*" compared with the LMS for $l < 0.5$. We also observe, that the theoretical output SNR in LMS is very high as compared with Kalman filter. This can be explained as follows: The term number of iterations k, in the expression of SN in Equation (2.100), bounds the theoretical value of SN. However, if, $k \to \infty$, the SN will reach to infinity. Hence, we would have obtained higher SN, if we had allowed a large value of k.

Figure 2.30 brings out the comparison of M, for LMS and Kalman filter for

पुरुषोत्तम काशीनाथ केलकर पुस्तकालय
भारतीय प्रौद्योगिकी संस्थान कानपुर
अवाप्ति क्र० A 145006

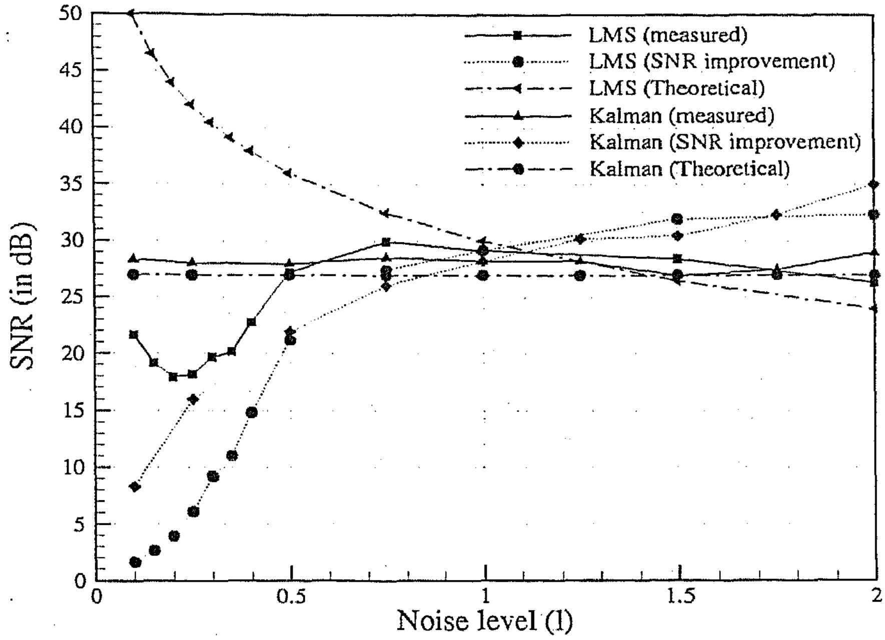

Figure 2.29: Comparison of SNR of outputs obtained from LMS and Kalman implementations of ANC when noise level l is varied ($N = 2$ and $cc = 1$, in both case).

different number of taps. For $N < 4$, it can be seen that M obtained from output SNR for LMS is less than Kalman filter case. In Figure 2.31, this behaviour is reflected in terms of SNR of the output signal. For $N < 3$, the SNR of the output signal obtained with LMS is better than Kalman. And for $N > 3$, the Kalman filter gives better results. The LMS method a noisy estimate Already mentioned in Section 2.2, that the gradient estimated by the LMS method is not accurate. If the number of taps is increased, the estimation becomes more noisy because the error from each tap adds up to increase the total effective noise in the estimation. However, in Kalman filter case, the estimation of weight is based upon the past values, so the higher is the N the better would be the estimation, consequently the better SN. Therefore, when N decreases significantly estimation of the weight in Kalman filter becomes poorer, and SNR of the output becomes less than that of the LMS.

Comparison of the variations of M with cc for both LMS and Kalman filter is shown in Figure 2.32. It is observed from this figure that the effects of cc on M in both LMS and Kalman implementations are quite similar. This can also be confirmed from Figure 2.33 which illustrates the comparison of their output SNR.

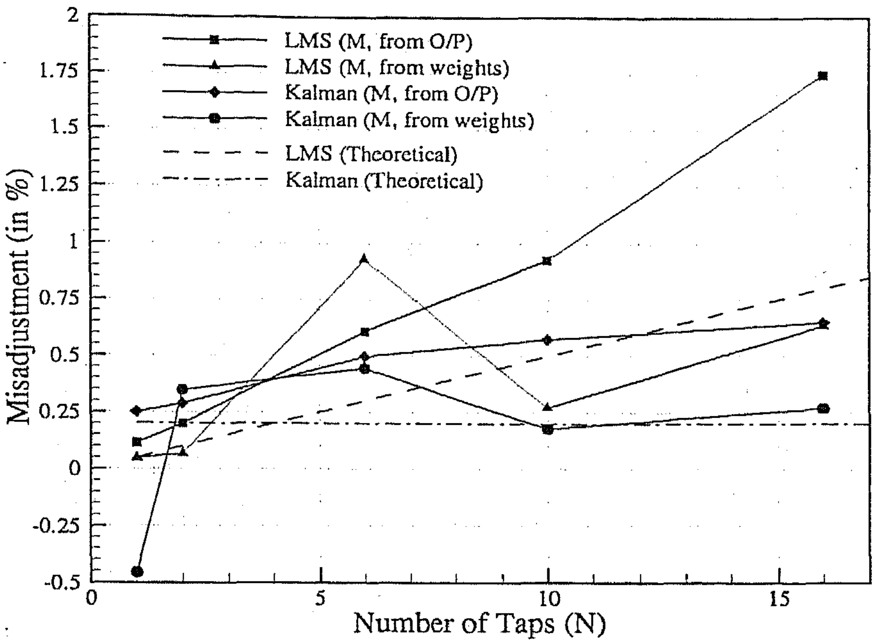

Figure 2.30: Comparison of *Misadjustment* in LMS and Kalman filter implementations when number of taps N is varied ($l = 1$ and $cc = 1$, in both case).

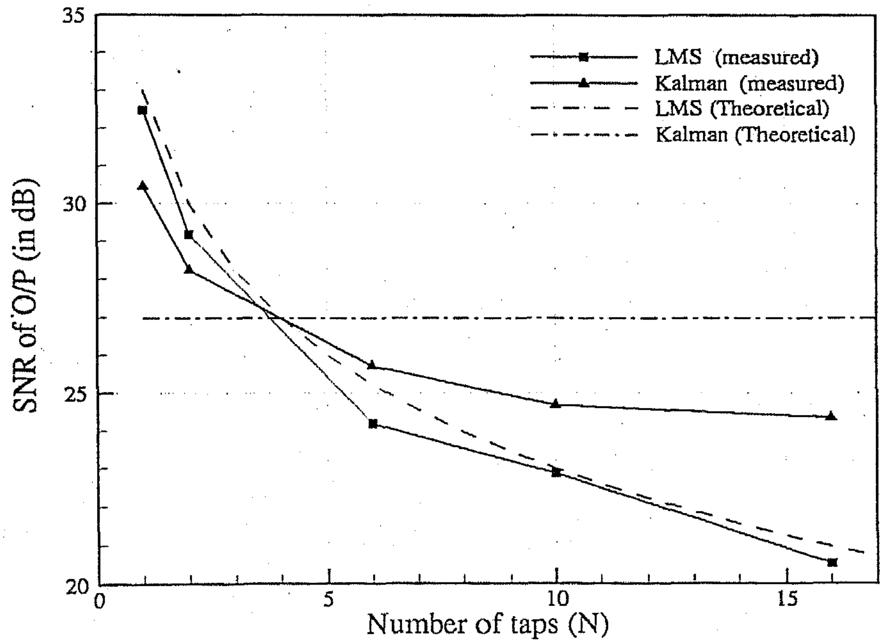

Figure 2.31: Comparison of the output SNR obtained in LMS and Kalman filter, for different number of taps ($l = 1$ and $cc = 1$, in both case).

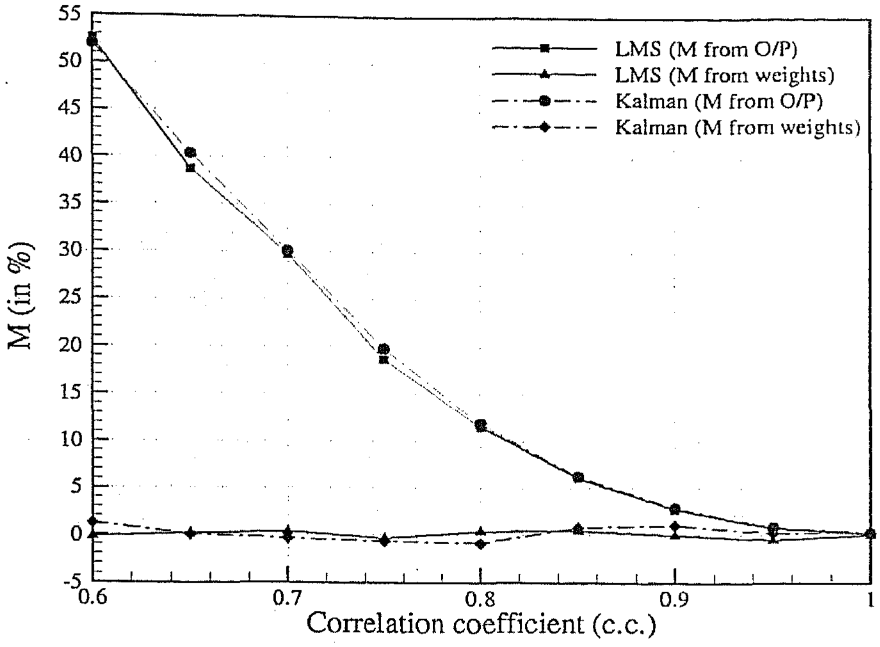

Figure 2.32: Comparison of *Misadjustment* in LMS and Kalman implementations when cc is varied ($N = 2$ and $l = 1$, in both case).

In Case-(4) of Section 2.5.2, we found that peak of the measured PF to be equal to 0.1212 and at this PF, SNR was only $4.7276dB$. In Kalman filter case, the PF can be calculated from the its definition, and we found it to be a constant equal to 0.0270. The output SNR is also constant and equal to $28.2419dB$. This observations can be stated in other language as: The CT for Kalman filter is less than ten times for that of LMS algorithm to achieve approximately same the SNR in the output signal. Kalman filter algorithm provides high speed of convergence but at the same time it involves complex computations [34]. The updating of weights are based on the *a priori* signal, so large memory is required to store these samples [34]. Whereas, the implementation of the LMS algorithm is quite simple, it requires approximately $2N+1$ multiplications and $2N+1$ additions [24] for each set of input and output samples. Apart from this LMS filter does not require *a priori* knowledge of the signal statistics, hence memory requirements are negligible compared with Kalman filter.

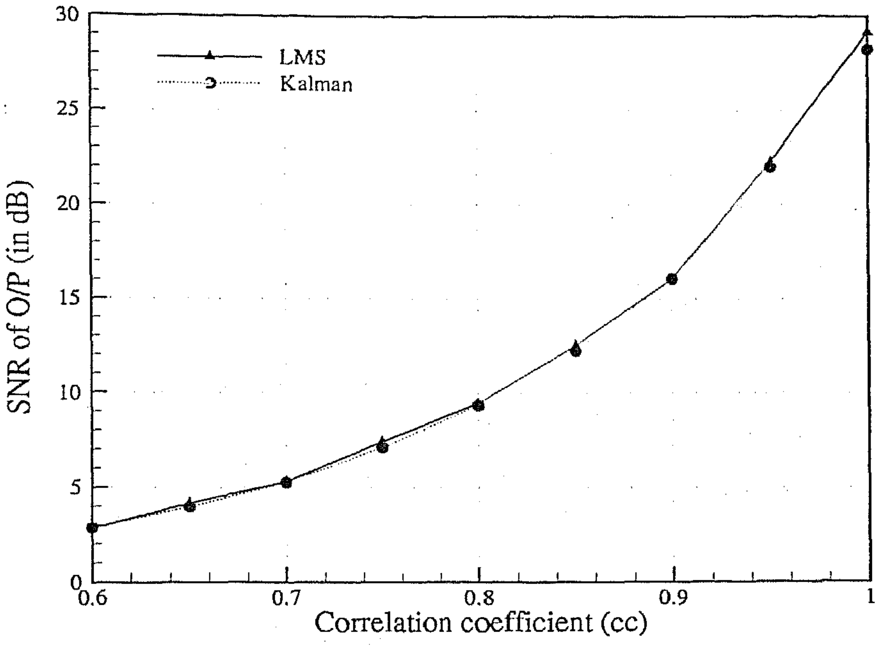

Figure 2.33: Plots showing the comparison of output SNR in LMS and Kalman filter implementations when *cc* is varied ($N = 2$ and $l = 1$, in both case).

2.5.5 Conclusions made on these results

The LMS algorithm would be the better choice where the signal is highly corrupted, or say, when SNR of primary is less than $0dB$ and output SNR of about $10dB$ is required. Under these conditions eigen values of matrix R would be large and also, output SNR required is not much, so a slightly larger value of adaptive gain constant μ would be chosen. This leads to fast convergence of LMS and also because of its simplicity it would be preferred. Whereas, the Kalman filter could be applied when SNR of primary signal is itself positive (in dB) and a high "SNR *improvement*" is required. Higher order filters are needed where the delay between primary signal and reference signal is large. We found under these conditions a Kalman filter algorithm would provide a better results in terms of noise rejection. One may employ LMS algorithm when this delay is quite small, i.e., 0 to 4 sample time.

The final parameter which decides the applicability of ANC in removing noise is the availability of reference signal highly correlated with the noise of primary signal. We found that under $0dB$(worst possible case) condition the output signal has SNR of about $3dB$ at $cc = 0.6$ and it shoots to about $30dB$ when $cc = 1$. So decision has to be made on these grounds. Where noise statistics changes rapidly or under non-stationary situations, Kalman filter would be the better choice for ANC, because of its inherent rapid convergence rate.

Chapter 3

Optical Implementation of LMS filter

Based on the Figure 2.1 and the discussions of Section 2.2, we find that the the following are the essential components needed to realize an LMS based ANC.

1. Delay line to sample the signal at sampling times.
2. Weights to modify each sampled value.
3. Adder to perform the summation of modified values (or to get vector inner product, y_k).
4. Subtracter to subtract primary signal and output of adder to generate error signal or output signal for ANC, i.e. ε_k.
5. Multiplier to perform scalar vector multiplication of μ and error signal with sampled signal, i.e. $\mu \varepsilon_k X_k$.
6. Weight modifier to update the weight vector.

Now we shall describe the substitutes of above components in electro-optic implementation of LMS algorithm for ANC.

3.1 Elements for optical realization

(1) Delay line:

The most important component of an LMS based ANC is a delay line that generates vector X_k by sampling the analog time signal x(t). In our application, the optical

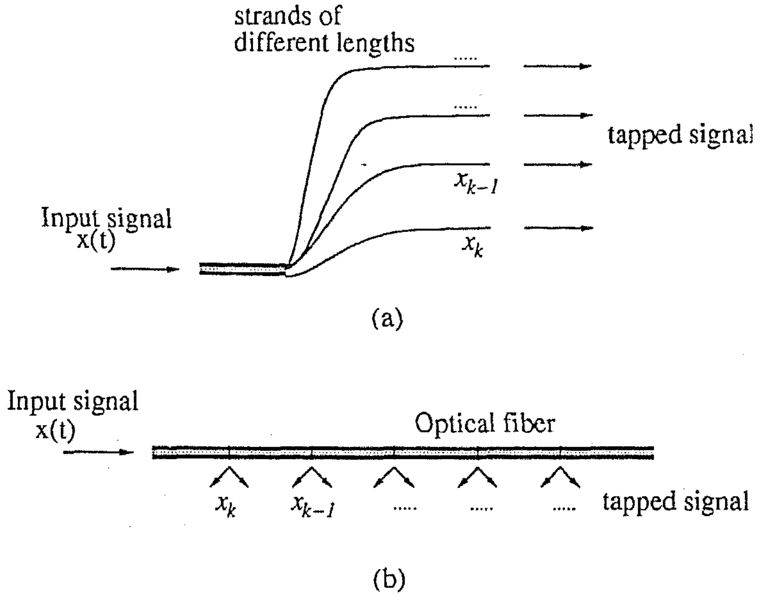

Figure 3.1: Optical fiber delay lines: (a) Fiber bundle type tapped delay line; (b) Longitudinal tapped delay line

signal is transmitted through an optical fiber and there are many techniques for creating taps on optical fibers to obtain X_k. These structures so made are known as fiber optic tapped delay lines (FOTDLs) [13], [14], [38]. The basic FOTDL consists of a fiber optic channel with taps distributed along its length. The signal x(t) is launched into one end of the channel and successively sampled at regular or irregular intervals. We can classify various techniques for making FOTDLs in two broad categories:

- Fiber bundle FOTDLs [14],[39] and
- Longitudinal FOTDLs [14], [40].

In fiber bundle FOTDLs the optical signal is launched into a bundle of fibers having different lengths, thus provide different amount of delays at the output of each strand. In longitudinal FOTDLs the taps are distributed along the length of single optical fiber carrying the signal. These two basic classes are shown in Figures 3.1(a) and (b) respectively. The longitudinal FOTDLs can be classified further into two categories, (1) collective mode and (2) individual mode, depending on how the tapped light is accessed. If the signal from each tap can be measured or modified independent of the signal from every other tap created along the fiber, we call it the individual mode FOTDL. For example, any longitudinal FOTDL with a series of polished-macrobend [38] or localized- devitrification [41] type taps, as shown in

3.1(b) is an individual mode FOTDL. In reflectively tapped [13] and recirculating [38] delay lines the tapped signal at a given instant is a combination of the signals from all taps; thus they are examples of collective mode FOTDLs. Fiber bundle FOTDLs are also individual mode as the output of each fiber strand can be accessed individually.

We can use either fiber bundle FOTDLs or individual mode longitudinal FOTDLs for realizing the delay lines. A FOTDL fabricated using laser ablative chemical etching (LACE) is found to be inexpensive technique for rapid fabrication of high quality micron scale taps on the cladding of glass or silica optical fibers [14]. In this process a CO_2 laser is used to etch a series of debris free facets into the cladding in a few microseconds. A halogen containing ambient is used in the LACE process to getter the removed material in the highly reactive environment of the thermal plasma generated at the fiber surface. The tap strengths and ratios can be precisely controlled via the laser parameters. About 30% of the output light from each tap appears as a directed optical beam whose direction and divergence angle are determined by the facet shape [14]. Another beam, diffuse in nature, appears on the side opposite the etched facet as a result of total internal reflection of a portion of the cladding field.

(2) Weight:

The other important component is the weight. We need a device that modifies the sampled data obtained from time delay line. In other words a device that changes the intensity of the light that passes through it. We use spatial light modulators (SLMs) [21] for this purpose which are high speed parallel optical vector multipliers [21]. A SLM is a device that creates some sort of modulation on the cross section of a beam of light. The modulation may be of phase, polarization and amplitude (intensity). A simple example is a transparency: after passing through a transparency, different areas in the beam's cross section have different intensities. Wide varieties of SLMs are available like: liquid crystals, electro-optic crystals, magneto-optic materials, thermoplastic, acousto-optic cell, membranes and many more. Basic underlying techniques are summarized in Table 3.1.

A generic structure of SLM is shown in Figure 3.2(a), the bias voltage V_b is shunted to the light modulating element by charges generated within the illuminated regions of the photo sensor. The resulting electric field cause the light modulating material to modify the polarization, phase, and/or amplitude (intensity) of the readout light. SLMs may be of optically addressed (or control or write) type or

modulation	*realized by*	*SLM type*
amplitude	change of transmittance	photographic film photodichroic materials
phase*	change of shape	thermoplastic micro-mechanical deformable mirror
	change of density	acousto-optic cell
polarization*	physical effects in crystals	liquid crystal electro-optic crystals magneto-optic crystals

* Phase and polarization modulations are sometimes transformed into amplitude modulation. Likewise, polarization modulation can be converted into phase modulation.

Table 3.1: Underlying techniques for spatial light modulation.

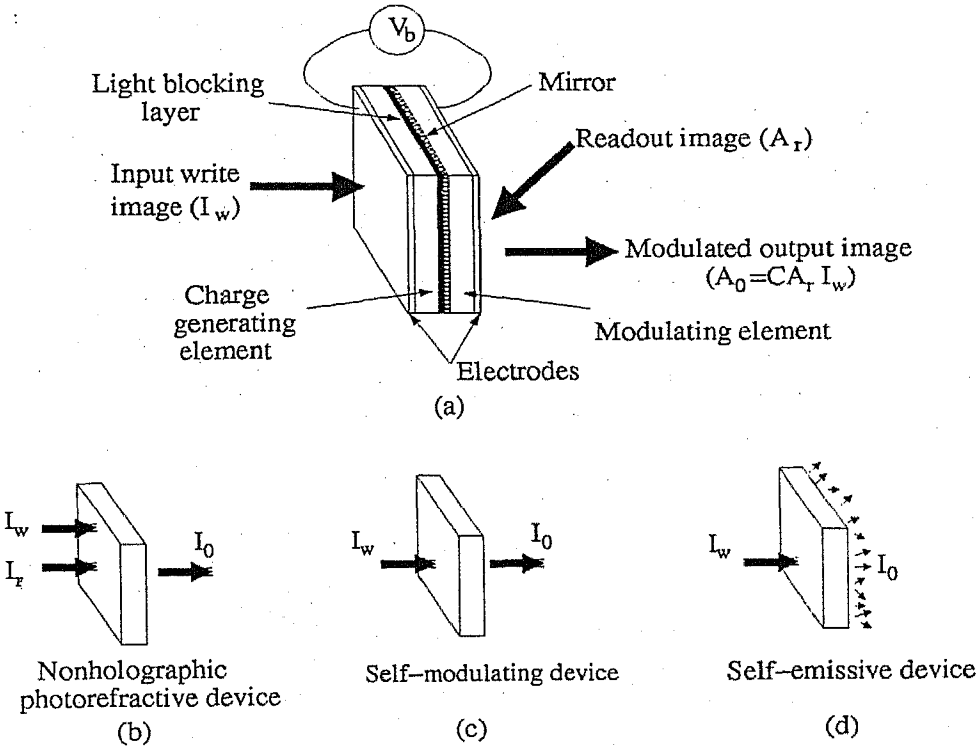

Figure 3.2: Major SLM functional structures [A indicates optical wave amplitudes and I the intensities or currents]. (a,b) Signal multiplying and amplifying type SLM; (c) Self-modulating type SLM; (d) Self-emissive type SLM.

electrically addressed type. Functionally, we further divide SLM into three basic classes: signal amplification and multiplying devices, self modulation devices, and self emissive devices. Generally the signal multiplying devices are of three-ports. In a typical amplitude-modulation application, the amplitude at each point in the readout image is multiplied by the effective transmittance of the modulating element, which is determined by the write image intensity or the electrical write signal at a corresponding point on the device. Thus the amplitude of the processed output image is essentially the product of the write image intensity, i.e., its equivalent voltage or current, and the readout image amplitude.

Self-modulating devices are generally two-port optically addressed SLMs, as shown in Figure 3.2(c). The optical properties of the modulating material are modified by the input light, which itself modified as it is transmitted through and reflected from the device to become the output image.

Self-emissive modulators generate a coherent electrical or incoherent spatial light distribution under the control of input electrical or optical information (see Figure 3.2(d)), like CRTs, platelet lasers etc.

For our application electrically addressed, signal multiplying types of SLMs are required. Transmittance of each pixel of SLM is controlled via electrical signal which corresponds to the weight vector W_k. The sampled optical signal X_k is given as the input to the corresponding pixel of a SLM to obtain the product of transmittances and corresponding input optical signal intensities. Thus, transmittances of pixel serve as the weight vector.

One can also choose MSM photo-diodes [43] or three-directional couplers [44] to implement weights. In case of MSM photo diode implementation, we use MSM photo-diodes as the different pixels of the SLM. The sensitivity of every photo diodes are varied according to the value of the weight vector. Sampled light signal from delay line is lighted on these array of photo diodes. Thus, the output of each photo-diodes (which are electrical signals) are summed to get the vector inner product of W_k^T and X_k. This scheme is shown in Figure 3.3. MSM photo-diode implementation is simpler and one can easily control the bipolar weights, but MSMs are in research phase while SLMs are commercially available and widely used for opto-electronic processing.

(3) Adder:

To perform the inner product of X_k and W_k, we need to add the signals obtained from the multiplication of weights and sampled signals. In optical domain it can

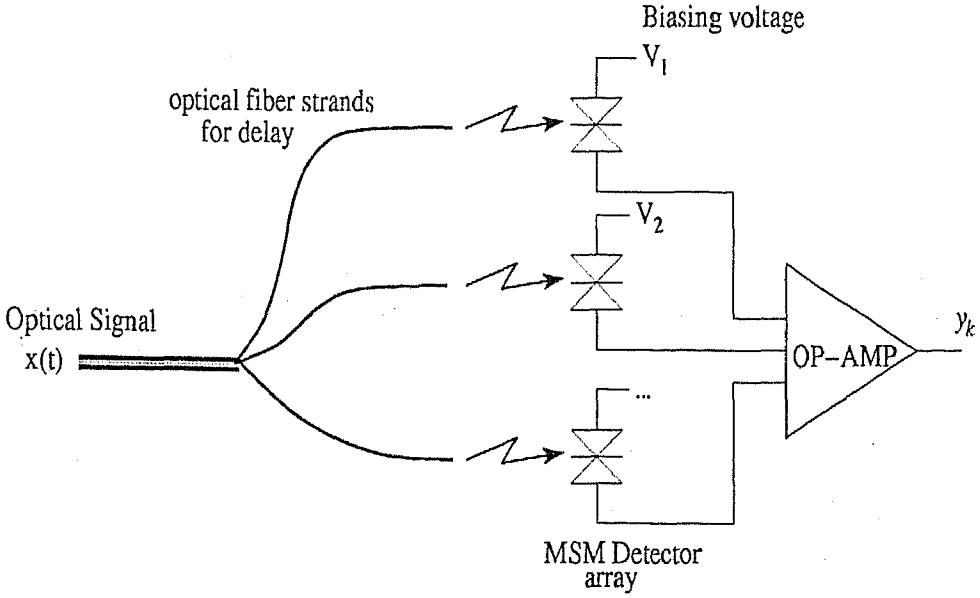

Figure 3.3: Optoelectronic transversal filter based on MSM photo-diode.

be done with the help of lens set which converge all the lights at the output of SLM at one point. Thus, at the focal point of lens we get the signal y_k, corresponding to the inner product of X_k and W_k.

(4) Subtracter:

We have to perform the subtraction of y_k from d_k to generate error signal (or output signal) for ANC. Since we are studying the incoherent light signal so subtraction is to be performed in electrical domain. A detector is placed at the focal point of the lens of the adder to convert optical signal into electrical. Now this signal is subtracted from primary signal to obtain the error signal using a high speed dedicated electronic processor.

(5) Multiplier:

The multiplication of two scalars μ and ε_k is performed by an fast electronic processor, and this product is multiplied with sampled signal X_k by using another SLM whose all pixels have same transmittances corresponding to the product $\mu\varepsilon_k$. Thus the output from the SLM corresponds to the product $\mu\varepsilon_k X_k$ as explained before.

(6) Weight updating:

From Equation (2.3), we see that weight vector is updated by adding the old weight vector with the vector obtained from multiplier, i.e., $\mu\varepsilon_k X_k$. We employ a

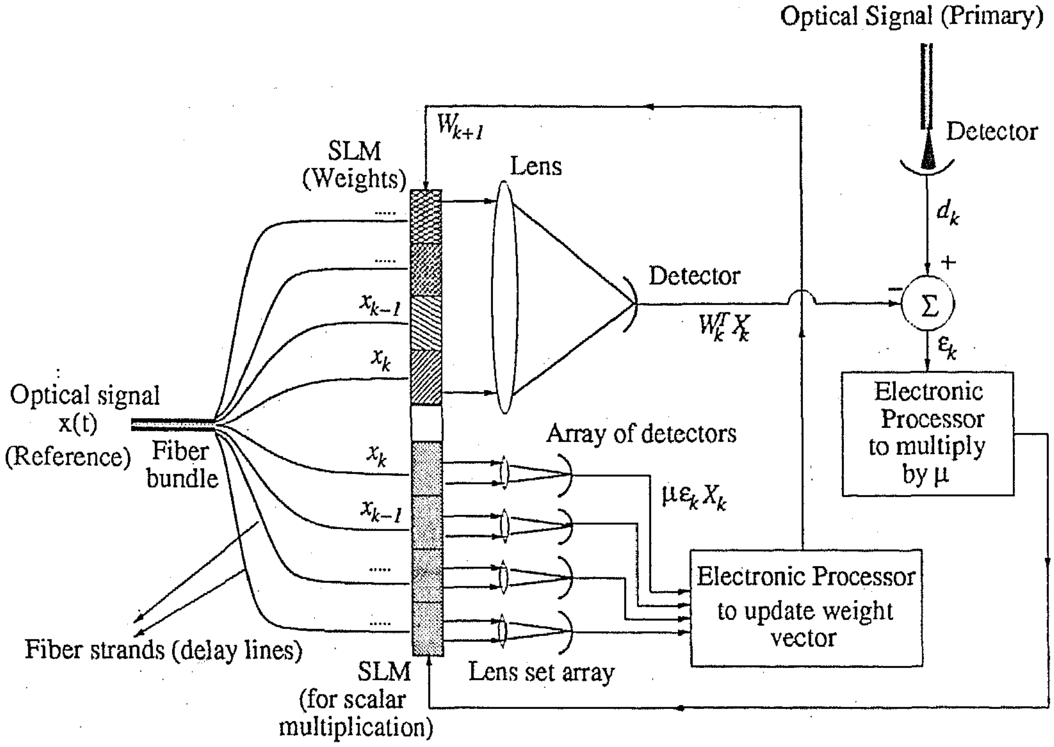

Figure 3.4: Fiber optic based ANC using fiber-bundle type FOTDL.

high speed dedicated electronic processor to execute this weight updating process. As vector $\mu\varepsilon_k X_k$ obtained at the output of SLM is optical so it is first converted to electrical signal via detectors and then fed to electronic processor. To accomplish this task an array of detectors are placed at the focal points of an array of lenses that are placed near each pixel of SLM to converge the light, thus, the output of a detector corresponds to the corresponding element of the vector $\mu\varepsilon_k X_k$. New weight vector, then serves as the control (write) signal to the weight SLM.

3.2 Optical LMS algorithm

Based on the description of Section 3.1, two types of optically implemented LMS based ANC are shown in Figure 3.4 and Figure 3.6. In Figure 3.4 we show a fiber optic ANC using a fiber bundle type FOTDL. The signal x(t) is fed to the fiber strands for obtaining delayed sampled set X_k. Since we cannot store the optical samples X_k and the two multiplications in Equation (2.1) and Equation (2.3) must be carried out separately, we need to obtain two identical samples from each tap, i.e., two identical sample vector X_k, for a truly optical realization of LMS algorithm. To solve this problem we employ a SLM having two columns of pixels placed side

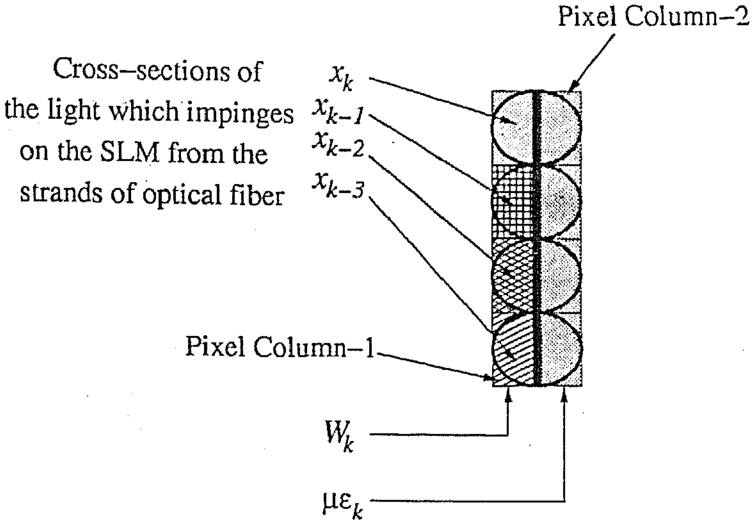
Pixel Column–2
Cross–sections of the light which impinges on the SLM from the strands of optical fiber
x_k
x_{k-1}
x_{k-2}
x_{k-3}
Pixel Column–1
W_k
$\mu\varepsilon_k$

Figure 3.5: Scheme to illustrate the arrangement of SLM in Figure 3.4.

by side, one column contains weight vector and the other contains the product $\mu\varepsilon_k$. Although in Figure 3.4 separate SLMs are shown for simplicity. The light from the fiber strands is allowed to fall on the two columns of SLM simultaneously. The scheme is shown in Figure 3.5. Thus, a single set of X_k is sufficient to carry out two multiplications. After this optical multiplications in the SLM, the light is collected using lens set and converted into corresponding electrical signals by detectors. The vector multiplications are carried out as soon as the light from the strands passes through the mask pixels and is collected by the detectors. Generally this parallel processing take place in the time $< 1ns$. Thick lines of Figure 3.4 the correspond to the optical signal path while thin line is the path of electrical signal. If, the primary is optical signal in a particular application, then it has to converted to electrical signal before the subtraction.

A fiber optic ANC employing LACE processed FOTDLs is depicted in Figure 3.6. We use directed beams from the front of the etched facets for calculating the product $W_k^T X_k$. The second set of light from the back of the facets is utilized for scalar vector product. We employ two SLM arrays to keep the optics simple. The vector multiplication are done in parallel as in the fiber-bundle based design in Figure 3.4. Thick lines of this figure shows the optical path and thin line is for electrical path. The time for one iteration of the LMS algorithm is determined by the detector time constants and the time needed in feedback process involving the calculation of new weights W_{k+1} and then writing them to the SLM mask. The implementation of fiber optic LMS algorithm is not restricted to the two types of FOTDL as described. One can easily fabricate LMS algorithm using

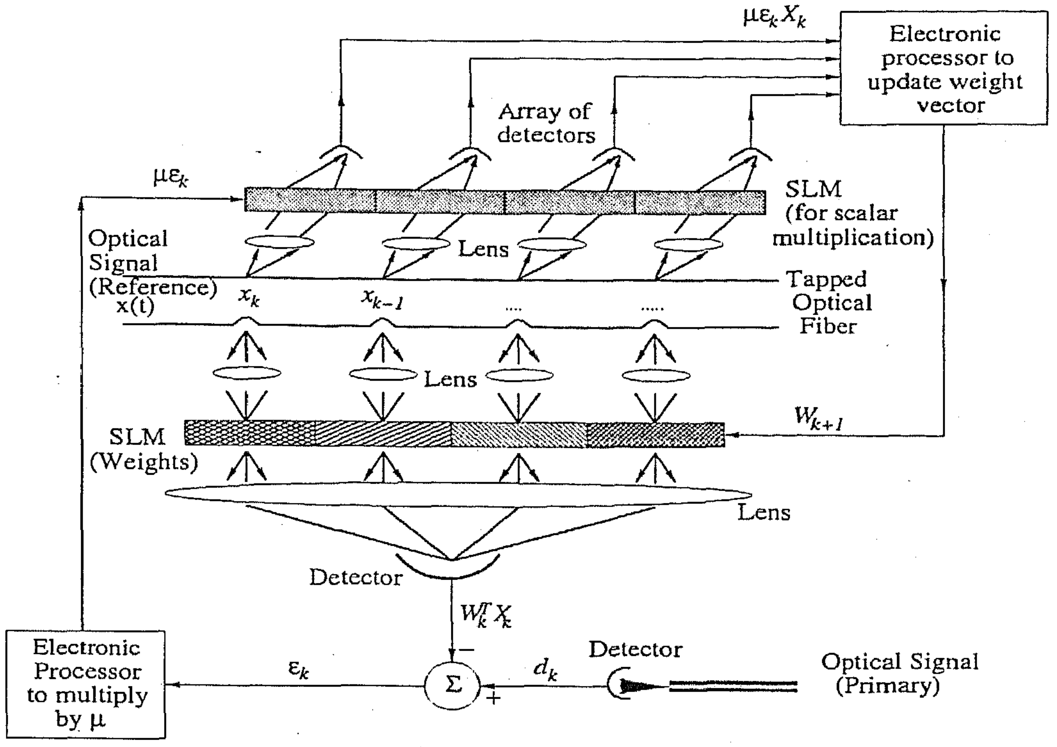

Figure 3.6: Fiber optic based ANC using a LACE processed FOTDL.

other individual mode longitudinal FOTDLs. The optical part of the optical LMS algorithm can also be realized in integrated optics.

In the above discussion on the realization of LMS algorithm for ANC using FOTDLs and SLMs we neglected the small time delay involved in the calculation of the product $W_k^T X_k$ and ε_k. This delay can be easily compensated by controlling the optical paths or the sampling times for the second version of X_k. Instead of basic LMS algorithm we can also realize block-LMS algorithm where the weights are updated after $k\,(k \neq 1)$ iteration. The block algorithm may help in matching the time for weight update with the time constant of the SLM. For the most SLMs the writing time of a pixel is of the order of $10^{-2}-10^{-6}$s [14]. This speed determines the iteration time and is suitable for most practical applications, where learning or adaptation takes place at a rate slower than that of the bandwidth of the signal. For faster iteration time, we need to use AO cells and build a coherent fiber optic system.

3.3 Handling negative values

There are cases when the weight vector, W_k or the error signal, ε_k becomes negative. Many techniques have been suggested for accommodating matrices and vectors with bipolar and complex-valued elements on an optical processor. To circumvent this problem we employ space multiplexing [45]. Each element of the vector W_k is written on two adjacent pixels of the SLM mask. The transmittance of one of the pixels is kept zero depending on whether the value of the pixel is positive or negative. The philosophy of this method is described as follows:

Let us take an example of vector inner product. Let $X = [x_1 \;\; x_2]^T$ and $W = [\; w_1 \;\; w_2]$ be the two vectors and their inner product WX has to be evaluated. Now formulate matrix

$$W_{new} = \begin{bmatrix} w_1^+ & w_2^+ & w_1^- & w_2^- \\ w_1^- & w_2^- & w_1^+ & w_2^+ \end{bmatrix}.$$

If, w_1 is positive then $w_1^+ = w_1$ and $w_1^- = 0$, otherwise, $w_1^+ = 0$ and $w_1^- = -w_1$, so with weight w_2. Similarly we can expand vector X to

$$X_{new} = \begin{bmatrix} x_1^+ \\ x_1^- \\ x_2^+ \\ x_2^- \end{bmatrix}.$$

Here also if x_1 is positive then $x_1^+ = x_1$ and $x_1^- = 0$, otherwise $x_1^+ = 0$ and $x_1^- = -x_1$, so with element x_2. Thus, we obtain matrix W_{new} and X_{new} with positive elements. Let the product $W_{new}X_{new}$ be denoted by O, it will be column vector given by

$$O = \begin{bmatrix} o_1 \\ o_2 \end{bmatrix}.$$

Having obtained this vector, we can calculate actual product of WX, which is equal to $(o_1 - o_2)$, and this subtraction is done electronically. Thus, we can solve the problem of bipolar weight. If ε_k comes out to be negative in course of iteration, it can be handled without trouble during the weight updating in the electronic processor.

The space multiplexing doubles the number of optical components. For incoherent signal and with number of taps $= N$, we need $2N \times 2$ pixels of SLM, and $2(N+1)$ elements of photo detectors for realizing both Figure 3.4 and Figure 3.6.

Chapter 4

Performance of LMS algorithm in presence of Optical Errors

In an optical implementation of LMS algorithm, both the adjustable tap weights and the various intermediate signals in the algorithm are affected by the optical errors. The perturbations from optical errors lead to deviations in the performance of the adaptive filter from the theoretically expected behavior of an ideal implementation, i.e., when optical errors are zero. In general, the presence of optical errors preclude the taps weights from reaching their optimum Weiner setting. Also, these errors may cause a large increase in the total output mean-square-error compared to the value of ideal implementation. In this section, we analyze the effects of optical errors on the performance of LMS based ANC. Throughout this section, we assume that the input data and tap weights are real valued. We used unprimed and primed symbols to represent quantities of ideal and optical implementations, respectively.

4.1 Error source identification & modeling

A schematic representation of the fiber optic LMS based ANC with dominant error sources is shown in Figure 4.1. This schematic can be used for any fiber optic LMS based ANC built with a FOTDL. We ignore all error terms higher than first order in analysis. We have also ignored the round-off error owing to electrical computation [46]. Since this error is negligible with the errors due to optical system. The results of this section is based upon [14], similar analysis can also be found in [46].

The optical setup for realizing the adaptive filter is analog, so the accuracy of the computations is affected by the error and noise sources present in the optical

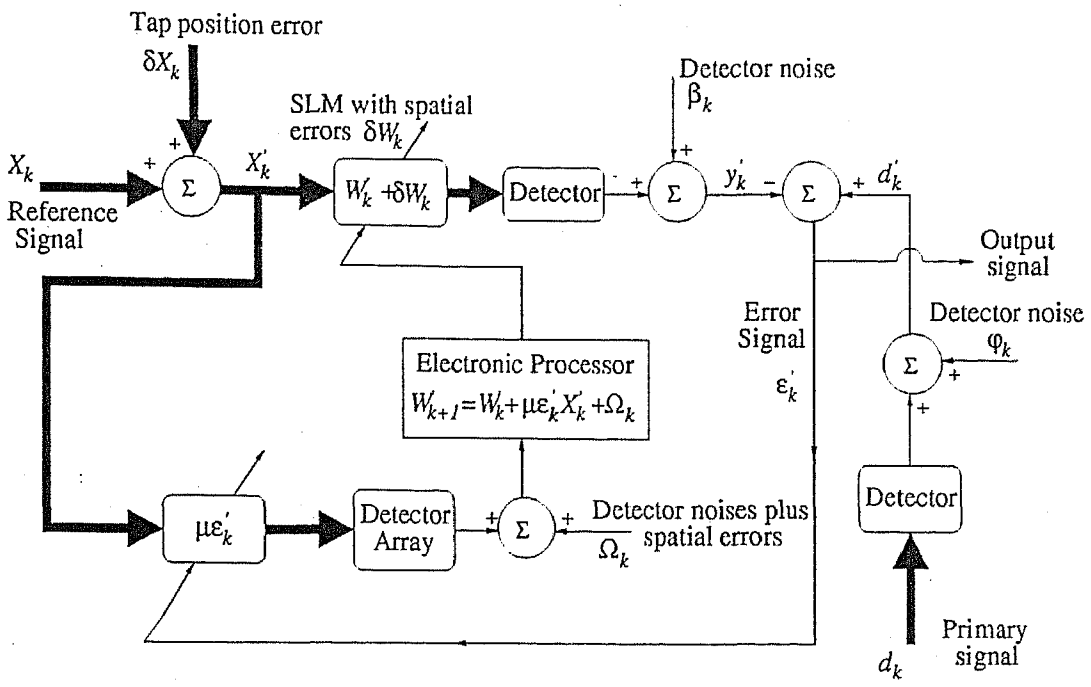

Figure 4.1: Schematic diagram of fiber optic LMS algorithm for ANC with dominant error sources.

system. Following are some dominant sources of errors present in optical system:

- Tap positioning error
- Error due to attenuation loss in optical fiber
- Spatial errors of the optical configuration
- Detector noises.

Out of these error first two are inherent to fiber optic delay lines. Tap position error comes from the mechanical tolerances involved in positioning the laser for etching taps. The error in tap positioning affects the vector X_k by changing the sampling times. Since the tap position can be controlled within few microns, we model this as an additive time varying noise [14]. The statistics of this error also depends upon the statistics of input signal. In our application, we have modeled it as a white Gaussian noise process. The other error source of error in FOTDL is the loss of power in the main fiber line because of the taps and fiber attenuation, termed the tap factor. The tap factor is modeled as a constant multiplicative factor affecting the magnitude of the elements of vector X_k. Thus we can model the vector X_k obtained from the optical delay line as

$$X'_k = F(X_k + \delta X_k), \tag{4.1}$$

where, F is a diagonal matrix with the corresponding tap factors as the diagonal elements, and δX_k is the noise vector due to tap position error. Assuming that the guided light-wave signal has a frequency $> 10MHz$, we find that the taps are distributed over a segment only a few meters in length. Hence any error in the signal owing to the dispersion [12] in the fiber is neglected.

Spatial errors arise from the quantizations and non-uniformities in: (i) the taps, (ii) transmittances of SLM pixels, and (iii) reponsivities of photodetector elements [14], [47]. These spatial error sources need not be modeled separately since they will all add linearly at the detector output. So the total spatial error is modeled as a single white noise Gaussian process. The total spatial error in the weight is represented by δW_k. The other dominant source of error is the detector noise [12]. The noises (shot and thermal noise) of detector add directly to the detected light intensities. Any phase noise in the system owing to multiple taps [22] is indistinguishable from the detector noise and is not modeled separately. The various detector noise are also modeled as different white noise Gaussian processes.

4.2 Derivation of *Excess-mean-square-error*, *Misadjustment* and SNR

Now we derive the close form expression of *Misadjustment*, M and SNR of output signal based upon the error model depicted in Figure 4.1. Since the tap factor matrix F is known and does not change with time, it is easy to to calculate the inverse matrix F^{-1}. The errors due to the tap factor can be eliminated by modifying the weights vector with a built-in weighting of F^{-1}. Thus we have neglected the errors due to the tap factor. With this modification Equation (4.1) becomes

$$X_k' = X_k + \delta X_k. \tag{4.2}$$

It can be observed from Figure 3.4 that, as the signal from the optical fiber divides into different strands its intensity goes down inversely with respect to the number of strands. Therefore the signal X_k gets down scaled. This problem can be easily handled be employing optical amplifiers [12]. Optical fiber amplifiers using erbium-doped filters [48] are now commercially available, so optical fiber amplifiers can be used before feeding the signal to the SLMs. Otherwise we can also use semi-conductor laser amplifiers [12], [48]. Optical fiber amplifiers make the system more compact than semi-conductor amplifiers. The amount down scaling can be easily found out and thus, can be corrected. By the use of optical amplifier, there arises another error term due the noise of the amplifier. This noise turned out to be additive and adds directly to X_k. Also, the tap positioning error adds directly to X_k. In our analysis, we have not modeled amplifier noise separately. Since one may treat δX_k as the summation of both amplifier noise and tap positioning error. From Figure 4.1, we see that reference signal, perturbed with the tap positioning error is fed to the SLMs. Let during the k^{th} step of iteration the actual values of the filter weights computed optoelectronically can be written as

$$W_k^{'} = W_k + \Delta W_k, \tag{4.3}$$

where, ΔW_k is the total inaccuracy in the optically computed weights at k^{th} iteration. The vector inner product computed optically is written as

$$y_k^{'} = (W_k^{'} + \delta W_k)^T X_k^{'} + \beta_k, \tag{4.4}$$

where, δW_k is the spatial error vector of same dimension as W_k, and the scalar β_k is the detector noise term. The spatial error vector δW_k adds to the vector $W_k^{'}$ when the vector is written on the SLM. Using Equation (4.2) and Equation (4.3), the optically computed output signal $y_k^{'}$ in Equation (4.4) can be written as

$$y_k^{'} = W_k^T X_k + \Delta W_k^T X_k + \delta W_k^T X_k + W_k^T \delta X_k + \beta_k. \tag{4.5}$$

The primary signal is corrupted by another detector noise signal φ_k that is generated in the detector used for its conversion to electrical signal. The noisy primary signal can be written as

$$d_k^{'} = d_k + \varphi_k. \tag{4.6}$$

Using Equation (4.5), and Equation (4.6), the total error signal is given by

$$\begin{aligned} \varepsilon_k^{'} &= d_k^{'} - y_k^{'} \\ &= \varepsilon_k - (\Delta W_k^T X_k + \delta W_k^T X_k + W_k^T \delta X_k + \beta_k - \varphi_k) \\ &= \varepsilon_k + \Delta \varepsilon_k \end{aligned} \tag{4.7}$$

where, $\varepsilon_k = d_k - W_k^T X_k$. The term ε_k is the error signal of an ideal LMS algorithm, i.e. without optical errors. The term $\Delta\varepsilon_k$ is the deviation in ε_k owing to the optical round-off errors and noises.

The elements of tap position error vector δX_k and the spatial error vector δW_k are modeled as white noise sequences that are independent of the signals and independent of each other [14]. The random processes are assumed to have Gaussian distribution with zero mean. The variance for the tap position error sequence is σ_{tap}^2, and that for the spatial errors is denoted by σ_{spa}^2. Likewise, the detector noise terms β_k and φ_k are modeled as white Gaussian noise sequences that are independent of the signals and other optical errors. The means of these sequences are zero. The variances of both detector noise is taken to be same, and it is denoted by σ_{det}^2. The values of standard deviations σ_{tap}, σ_{spa} and σ_{det} represent the RMS values of the round-off error sources in the optoelectronic system. Based on the assumption that successive reference vectors X_k are independent in time (Section 2.2) and the modeling assumptions made above, it has been shown that the terms $\Delta W_k^T X_k$, $\delta W_k^T X_k$, $W_k^T \delta X_k$, β_k and φ_k are uncorrelated with each other and that their sum in uncorrelated with ε_k [14], [46]. Thus the two terms on the right-hand side of the last line of Equation (4.7) are uncorrelated.

The total mean squared error under optical errors is given by

$$\begin{aligned} \xi_k' &= E\left\langle \varepsilon_k'^2 \right\rangle \\ &= E\left\langle \varepsilon_k^2 \right\rangle \quad + \quad E\left\langle \Delta\varepsilon_k^2 \right\rangle \end{aligned} \tag{4.8}$$

since $\Delta\varepsilon_k$ has zero mean. The value of the first term of Equation (4.8) is the same as ξ_{total} derived in Section 2.2, i.e. Equation (2.38). Now the goal of the rest of the section is to derive $E\left\langle \Delta\varepsilon_k^2 \right\rangle$ based upon [14], [46]. We note that the individual components of $\Delta\varepsilon_k$ (from Equation (4.7)) are uncorrelated with each other. Thus the mean squared value of $\Delta\varepsilon_k$ is equal to

$$\begin{aligned} E\left\langle \Delta\varepsilon_k^2 \right\rangle \;=\; & E\left\langle \left(\Delta W_k^T X_k\right)^2 \right\rangle + E\left\langle \left(\delta W_k^T X_k\right)^2 \right\rangle \\ & + E\left\langle \left(W_k^T \delta X_k\right)^2 \right\rangle + E\left\langle (\beta_k)^2 \right\rangle + E\left\langle (\varphi_k)^2 \right\rangle \end{aligned} \tag{4.9}$$

In the steady state, the contribution of tap position error to the total mean square error is given by

$$\begin{aligned} E\left\langle \left(W_k^T \delta X_k\right)^2 \right\rangle &= E\left\langle W_k^T W_k \right\rangle \sigma_{tap}^2 \\ &= \left(\|W^*\|^2 + \tfrac{\mu \xi_{min} N}{2} \right) \sigma_{tap}^2 \end{aligned} \tag{4.10}$$

where, $\|W^*\|^2$ is the square of the norm of the Weiner vector. Similarly, the contribution of the spatial errors in the inner product computation is given by

$$\begin{aligned} E\left\langle\left(\delta W_k^T X_k\right)^2\right\rangle &= trace\left[E\left\langle\delta W_k \delta W_k^T\right\rangle R\right] \\ &= \sigma_{spa}^2 trace\left[R\right] \end{aligned} . \tag{4.11}$$

The last two terms of Equation (4.9) are equal, i.e.

$$E\left\langle(\beta_k)^2\right\rangle = E\left\langle(\varphi_k)^2\right\rangle = \sigma_{det}^2. \tag{4.12}$$

From the schematic representation of Figure 4.1, we notice that during the scalar vector multiplication of $\mu\varepsilon_k'$ and X_k', additional error, Ω_k is generated because of the spatial errors and detector noises. We call this error as multiplication error; it can be regarded as the summation of both detector and spatial errors. In the present analysis for the sake of simplicity we have modeled multiplication noise separately as the white noise Gaussian sequence of zero mean and a variance of σ_{mul}^2. Now the optical version of the weight update equation can be written as

$$\begin{aligned} W_{k+1}' &= W_k' + \mu\varepsilon_k' X_k' + \Omega_k \\ &= W_k' + \mu\varepsilon_k X_k + \mu\Delta\varepsilon_k X_k + \mu\varepsilon_k \delta X_k + \Omega_k \end{aligned} \tag{4.13}$$

Combining the results from Equation (2.3), Equation (4.3), Equation (4.7), and Equation (4.13), we obtain

$$\Delta W_{k+1} = A_k \Delta W_k + B_k \tag{4.14}$$

where,

$$A_k = I - \mu X_k X_k^T, \tag{4.15}$$

$$B_k = -\mu X_k \delta W_k^T X_k - \mu X_k W_k^T \delta X_k - \mu X_k \beta_k + \mu X_k \varphi_k + \mu\varepsilon_k \delta X_k + \Omega_k. \tag{4.16}$$

For simplicity, we assume that the algorithm starts with $W_0 = 0$ and $\Delta W_0 = 0$. Taking the expected value of ΔW_{k+1} in Equation (4.14) to get the following recursive equation

$$T_{k+1} = E\left\langle A_k T_k A_k\right\rangle + C_k, \tag{4.17}$$

where, T_k and C_k are $N \times N$ matrix equal to $E\left\langle\Delta W_k \Delta W_k^T\right\rangle$ and $E\left\langle B_k B_k^T\right\rangle$ respectively. Using Equation (4.15), Equation (4.17) can be modified to

$$T_{k+1} = T_k - \mu(RT_k + T_k R) + \mu^2 E\left\langle X_k X_k^T T_k X_k X_k^T\right\rangle + C_k. \tag{4.18}$$

We assume $T_0 = 0$ [14]. In practice μ is small, i.e., $\mu \ll 2/trace[R]$ and also the error matrix T_k becomes small for large iteration. The contribution from the term weighted by μ^2 in Equation (4.18) is small compared with the other terms and is neglected. In the steady state, when $T_{k+1} = T_k$, Equation (4.18) simplifies to

$$\mu(RT_k + T_kR) - C_k = 0. \tag{4.19}$$

Calculating the trace of both sides of Equation (4.19), we obtain a scalar equation

$$trace[RT_k] = \frac{trace[C_k]}{2\mu}. \tag{4.20}$$

From Equation (4.16), we have at steady state [14], [46]

$$\begin{aligned} C_k = E\left\langle B_k B_k^T \right\rangle &= \mu^2 E\left\langle X_k X_k^T X_k X_k^T \right\rangle \sigma_{spa}^2 + \mu^2 \sigma_{pos}^2 \left\|W^*\right\|^2 R \\ &= +2\mu^2\sigma_{det}^2 + (\mu^2 \xi_{min} \sigma_{pos}^2 + \sigma_{mul}^2) I. \end{aligned} \tag{4.21}$$

The first term on the right-hand side of Equation (4.21) involves fourth-order moments of sample vectors of the reference signal. It is a common practice to assume the elements of the sample vector to be jointly Gaussian, so that fourth-order moments can be expressed in terms of the known second-order moments. In the incoherent optical system described here, the signal in the optical fiber is always positive. Thus we assume the elements of the reference vector to be nonzero mean Gaussian, i.e.,

$$X_k = J_k + DL, \tag{4.22}$$

where the elements of J_k are zero-mean Gaussian signal with variance σ_j^2, D is the DC (positive) value, and L is a column vector with every elements equal to 1. We can also express the correlation matrix R for above signal X_k as

$$R = E\left\langle X_k X_k^T \right\rangle = R_j + D^2 L L^T, \tag{4.23}$$

where, R_j is the correlation matrix of signal J_k, it is given by $R_j = E\left\langle J_k J_k^T \right\rangle$. The value of D is taken to be large compared to the standard deviation of the Gaussian process. The fourth-order moments of X_k are derived in [46]. Using the results of [46], Equation (4.9)-Equation (4.12), Equation (4.20), and Equation (4.21), we can express the total steady state mean-square-error as

$$\begin{aligned}\xi'_{total} = \; & \xi_{min} + \mu\xi_{min}\textstyle\sum_{n=1}^{N}\frac{\lambda_n}{(2-\mu\lambda_n)} + \left(1 + \mu trace[R]/2\right)\sigma_{det}^2 + N\sigma_{mul}^2/2\mu \\ & + \left(\mu\left\|W^*\right\|^2 trace[R] + 2\mu N\xi_{min} + 2\left\|W^*\right\|^2\right)\sigma_{tap}^2/2 \\ & + \left(\mu trace[R^2] + \mu trace^2[R]/2 - \mu N^2 D^4 + trace[R]\right)\sigma_{spa}^2. \end{aligned} \tag{4.24}$$

We notice from the bock diagram of Figure 2.1, that in ANC the output signal ε_k, is obtained when filter output signal y_k is subtracted from the primary signal d_k. In the process of subtraction the DC value of signal y_k is also gets subtracted from the DC value of d_k. Thus, the output signal will have the residual DC value equal to $(D_x - D_d)$, where D_x and D_d are the DC values of the signals X_k and d_k respectively. The first term is the error due to the LMS algorithm. This error appears at the output of the ANC system. Therefore, from the above reasoning, we conclude that for ANC applications, the first term of Equation (4.24) holds true, if we use a modified matrix in place of R. The modified matrix can be calculated from Equation (4.23) by replacing D by $(D_x - D_d)$. The other terms of Equation (4.24) arise due to the internal optical errors. So the R present in the other terms need not be modified.

Equation (4.24) delineates the total mean-square-error in optical realization of LMS based ANC. The first term of Equation (4.24) is the inherent mean-square-error owing to the algorithm itself, second term is the mean-square-error owing to the detector noise, third term is the mean-square-error because of the multiplication error, the fourth term is due to the position error in the taps and the final term appears due to the spatial errors in the system. The total *Misadjustment* under optical realization can be calculated from Equation (4.24), and is written as

$$M' = \frac{\left(\xi'_{total} - \xi_{min}\right)}{\xi_{min}}. \tag{4.25}$$

The theoretical value of SNR of output signal under optical implementation SN', is given by

$$SN' = 10\log\left(\frac{1}{M'}\right). \tag{4.26}$$

4.3 Performance optimization

In the case of ideal LMS based ANC, i.e., without optical errors, the SNR of output signal increases monotonically with the decrease in the adaptive gain, μ, albeit with slower convergence [see Section 2.5.2]. But in the presence of optical errors/noise this is only true up-to when the noise effects become more significant. The important point that emerges from Equation (4.24) is that the mean-square-error due to multiplication error is inversely proportional to μ [14]. One other interesting observation is that the contribution from each optical error is weighted by a factor proportional to μ. For example, in Equation (4.24) the contribution from the detector noise in the inner product $W_k^T X_k$ calculation is weighted by $(2+\mu trace[R])$. Thus, by the proper adjustment of the parameter μ, we can control the weighting factors such that the overall contribution of each optical error source to total mean-square-error is minimal. Based on these insights we can formulate guidelines for the realization of fiber optic LMS algorithm based ANC.

The expression of SN' in Equation (4.26) can be solved for the optimal adaptive gain constant, i.e., μ, that maximizes the SNR of the output signal or in other sense minimizes the total steady state mean-square-error. Normally, μ is the parameter over which the designer has the most control. We find the optimal value of μ by solving $\partial\xi_{total}/\partial\mu = 0$ and selecting the real root in convergence range of μ [see Equation (2.14)] as the optimum value, μ_{opt}. Using Equation (4.24), the partial derivative with respective to μ is found to have this form

$$\partial\xi_{total}/\partial\mu = c_4\mu^4 + c_3\mu^3 + c_2\mu^2 + c_1\mu + c_0 = 0, \tag{4.27}$$

where, c_0, c_1, c_2, c_3 and c_4 are the coefficients involved with other parameters of Equation (4.24), after deriving $\partial\xi_{total}/\partial\mu$. Generally the other parameters are known to us, so all the coefficients of Equation (4.27) can be evaluated and thus can be solved to get μ_{opt}. The selection of μ in the vicinity of μ_{opt} allows us to reduce the effects of optical errors/noise, thereby improving the SN'.

Chapter 5

Optical realization of Kalman filter

Before discussing the optical realization of Kalman filter let us first review the basic elements and operations of optical linear algebra processors (OLAPs). OLAPs utilizes the real time and parallel processing features of optical systems to carry out the linear algebraic operations like: matrix-vector multiplication, matrix-matrix multiplication, matrix inversion, triple matrix product, direct and indirect solutions of systems of linear algebraic equations [49]. Most of the operations mentioned above are based upon acousto-optic(AO) transducers (or modulators). The AO cell uses an iterative algorithms to carry out the optical computing. These architectures are also known as optical systolic array processors. AO cells are the key elements in such systems. In next section we describe the basic operations of AO cells which are used in optical computations.

5.1 Acousto-optic Systems

Acousto-optic transducers are the special materials where the interaction between light waves and acoustic waves take place. Generally speaking, acoustic waves are waves of deformation in a material medium. When an acoustic wave exits in a medium, a snapshot of the medium will reveal a regular spatial variations in its density. Because of the high speed of light compared with the speed of acoustic waves, a light wave passing through the medium will "*see*" just a such snapshot. In other words, from the light's point of view, the medium has the characteristics of a phase grating. The interaction between the light and this grating, known as *Brillouin scattering* causes various effects of deflection, modulation, and frequency shifting of the light. The exact interaction depends on the relative angle between the light waves and acoustic waves. We discuss only the interaction when the

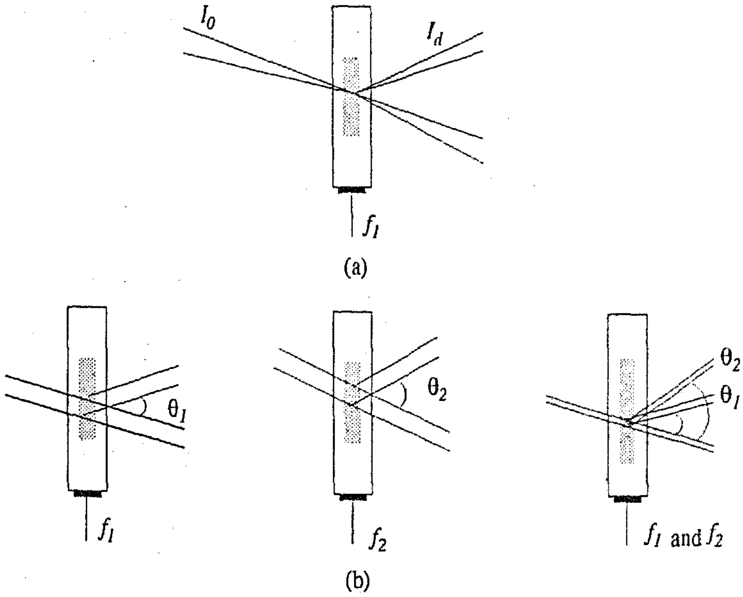

Figure 5.1: Bragg cell used as (a) light-beam modulator and (b) light-beam deflector. Input beam enter from the left at angle satisfying condition for Bragg diffraction.

direction of light wave satisfies Bragg diffraction condition, as, this interaction is useful for the AO based algebraic processors. AO cells using Bragg diffraction principle are also termed as AO Bragg cells. The AO Bragg cell can either modulate the intensity of a beam of light or deflect a beam of light in different directions.

The operation of an AO Bragg cell to modulate a light beam is illustrated in Figure 5.1(a). A piezoelectric transducer launches an acoustic wave into an optically transparent block of material. The wave traveling with the velocity of sound through the medium induces a periodic compression of the medium. This results in a periodic spatial variation of refractive index of the medium and this variation moves along the cell. It behaves like a moving phase grating. Thus the AO cell can be used to diffract an incident beam of light. The light that is reflected from this grating interferes. Constructive interference occurs only if the light impinges on the surface at *Bragg angle*, defined by

$$\theta = \arcsin \frac{\lambda}{2\Upsilon},$$

where, λ is the wavelength of the light and Υ is the wavelength of the acoustic wave, and it is also the separation between the grating surfaces. The intensity of the diffracted beam I_d is given by $I_d = \eta I_0$, where I_0 is the intensity of the incident beam and η is the diffraction efficiency of the grating. Electronic circuits can be

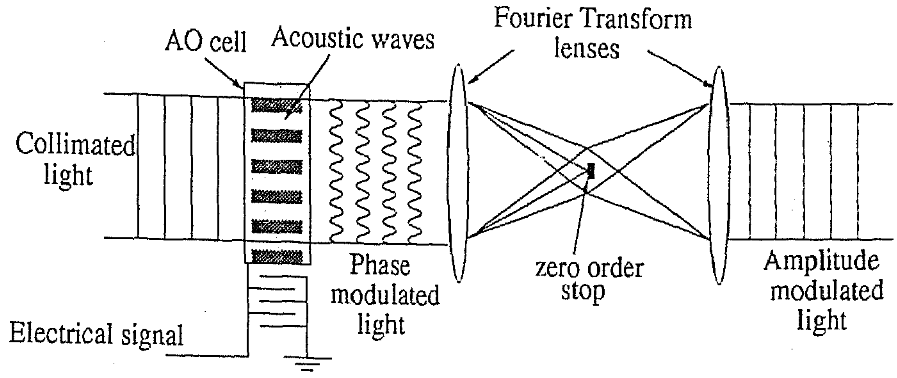

Figure 5.2: Schematic diagram shows the use of AO Bragg cell to produce amplitude modulated light.

designed such that the diffraction efficiency is proportional to the amplitude of the signal input to the cell driver. This scheme is shown in Figure 5.2. The electrical signal produces an acoustic wave in the piezoelectric material which is its own replica. Therefore light passing through medium will become phase modulated. After filtering out the zero-frequency bias we get an amplitude modulated beam. This filtering is performed by Fourier-transforming lens set. An AO Bragg cell operates such that only a single diffraction component is produced.

An AO Bragg cell to deflect a light beam is illustrated in Figure 5.1(b). It operates on the principle that the sine of the angle of diffraction is proportional to the temporal frequency of the acoustic wave in the cell. One can thus choose the direction of the diffracted beam by choosing the frequency of the driving signal. Depending on the cell type, the frequency is typically in $20MHz - 2GHz$ range, with diffraction angle ranging up to 10°. As suggested in Figure 5.1(b), if n sinusoidal signals of different frequencies are simultaneously input to the cell, n diffracted beams result, each propagating in a different direction. The amplitudes of the different sinusoids determine the amount of light sent in the different directions. To avoid nonlinear interactions that result in additional diffraction components, the Bragg cell must be operated at relatively low diffraction efficiencies if multiple grating frequencies are present.

The Bragg cell with multiple input and output beams are shown in Figure 5.3. Each beam can be modulated, deflected, or both, by the grating segments in different regions of the Bragg cell. Further more, each input beam can be produced by its own individual source-either an LED or a laser diode or signal from optical fiber. Since the intensity of a beam leaving the Bragg cell is determined by the product of the input beam intensity with the grating segment diffraction efficiency, it is possi-

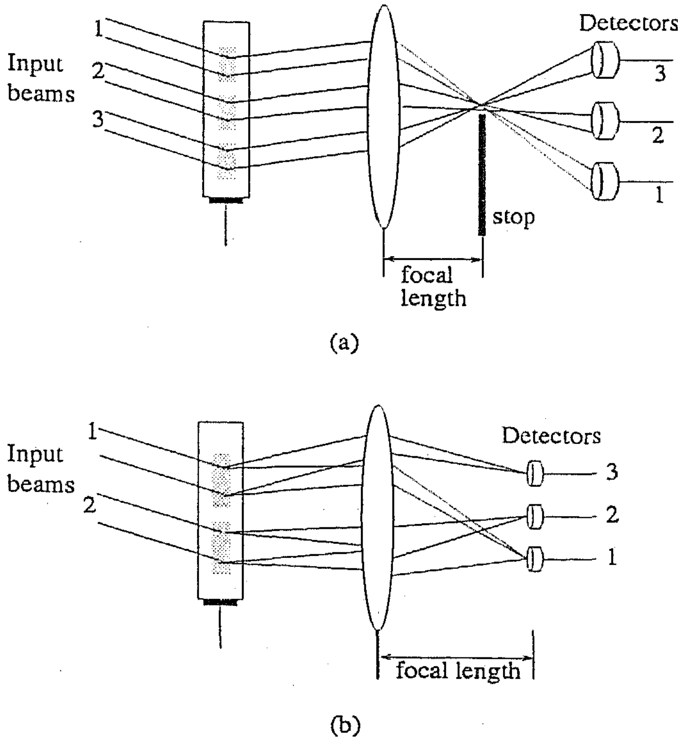

Figure 5.3: Multiple input-output beam (a) modulation and (b) deflection. Optical stop in (a) prevents undiffracted light from reaching image plane.

ble to perform analog multiplications. Successive multiplications can be performed as quickly as the source intensity can be changed, and, with multiple input beams, many multiplication can be performed simultaneously. The information input to the Bragg cell is in a natural pipeline, and as the grating segments move toward different beam positions, additional multiplication can be performed. The parallel processing and pipeline characteristics of the Bragg cell methods are illustrative of the powers of optics in such a structured computations. Figure 5.3(a) shows a multiple input-output beam modulator. In this case, the Bragg cell is imaged onto an array of detectors such that each modulated beam illuminates a different detector. The imaging system contains a stop in the back focal plane of the lens that blocks all light not diffracted by the acoustic grating segments. Figure 5.3(b) shows a multiple input-output beam deflector, where light from a given input beam can be sent simultaneously to any subset of the detectors in the back focal plane of the lens. The deflected beams can be controlled individually in intensity.

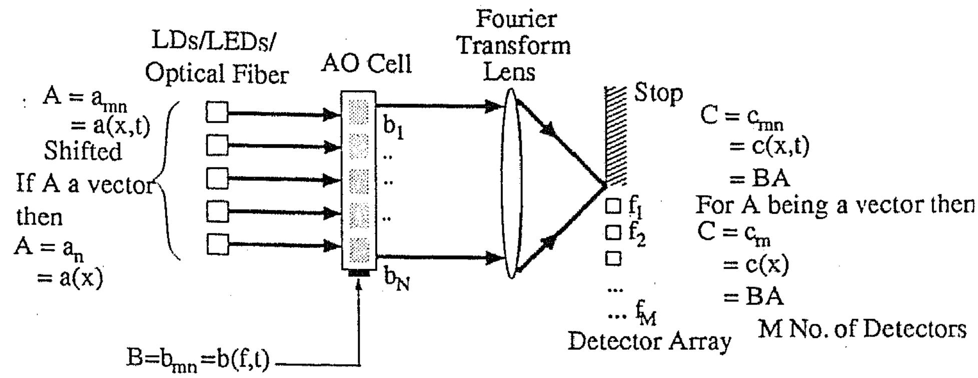

Figure 5.4: Basic space-, time-, and frequency-multiplexed optical systolic matrix-vector or matrix-matrix processor system.

5.2 Basic algebraic calculations using AO cell

A plethora of optical linear algebra processor architectures using AO Bragg cell have been described [45], [49], [50]. In this section we shall demonstrate in brief the basic architectures to evaluate some basic algebraic calculations.

5.2.1 Matrix-vector multiplication

Based upon the characteristics of deflection and modulation of an AO cell, we now show how it an be utilized for an efficient matrix-vector multiplication. Out of many architectures we choose frequency-multiplexed optical systolic array processor architecture [45] for our purpose since these architectures unitizes the maximum of frequency-bandwidth and time-bandwidth products available with the AO devices. This system for matrix-vector multiplication is shown if Figure 5.4. Suppose a matrix B has to be multiplied with a vector A to obtain vector C, i.e.,

$$\begin{bmatrix} b_{11} & .. & .. & b_{1N} \\ . & .. & .. & . \\ . & .. & .. & . \\ b_{M1} & ... & .. & b_{MN} \end{bmatrix} \begin{bmatrix} a_1 \\ . \\ . \\ a_N \end{bmatrix} = \begin{bmatrix} c_1 \\ . \\ . \\ c_M \end{bmatrix}. \tag{5.1}$$

We first partition matrix B into column vectors b_n and write Equation (5.1) as

$$\begin{bmatrix} b_1 & ... & b_n & ... & b_N \end{bmatrix} A = C. \tag{5.2}$$

Input vector A is space multiplexed and is fed as an optical signal either from a laser diode, LEDs or from optical fibers. Each b_n is time multiplexed and its M

elements are frequency multiplexed and this is input to the AO cell as electrical signals. Specifically, b_1 is the AO cell input at acoustic transit bit time T_B [51] (with the elements of b_1 frequency-multiplexed, b_2 is the AO cell input at time $2T_B$, etc.). In this system after NT_B time intervals, i.e., after all the b_n's are fed serially, the contents of the AO cell are as shown in Figure 5.4. At this time the vector A is fed from a optical source. This NT_B time has enabled the AO cell to convert the time- and frequency- multiplexed representation of the matrix B into the indicated frequency- and space-multiplexed arrangement shown. When the optical source is pulsed on, the full matrix-vector product in Equation (5.1) or Equation (5.2) is generated parallel in one bit time. The product is collected by an array of detectors.

5.2.2 Matrix-matrix multiplication

The concept of matrix-vector multiplication described above can be extended to carry on matrix-matrix multiplication. The concept is shown is Figure 5.4. Here, the vector A has become a matrix so it is space- and time-multiplexed as $a_{nm} = a(x,t)$. For a 3 order matrices, the matrix-matrix product can be realized as

$$\begin{array}{cc} & \xrightarrow{\text{Space/Time}} n \\ \text{Frequency}\Big\downarrow m & \begin{bmatrix} b_{11} & b_{12} & b_{13} \\ b_{21} & b_{22} & b_{23} \\ b_{31} & b_{32} & b_{33} \end{bmatrix} \end{array} \cdot \begin{array}{cc} & \xrightarrow{\text{Time}} m \\ \text{Space}\Big\downarrow n & \begin{bmatrix} a_{11} & a_{12} & a_{13} \\ a_{21} & a_{22} & a_{23} \\ a_{31} & a_{32} & a_{33} \end{bmatrix} \end{array} = \begin{array}{cc} & \xrightarrow{\text{Time}} m \\ \text{Space}\Big\downarrow m & \begin{bmatrix} c_{11} & c_{12} & c_{13} \\ c_{21} & c_{22} & c_{23} \\ c_{31} & c_{32} & c_{33} \end{bmatrix} \end{array}.$$

The elements of a column of output matrix C is obtained in space as in the case of matrix-vector system and consecutive columns are obtained in time. So matrix C is both space- and time-multiplexed. Pipelining of data can be found in [45]. The delay or dead time in product of $(M \times N)$ matrix with $(N \times M)$ matrix is found to be $(N-1)T_B$.

5.2.3 Vector outer product

Vector outer product multiplier uses a totally different configuration [21], [52]. The outer product of two vectors $A = [a_1 \ldots a_N]$ and $B = [b_1 \ldots b_M]$ is written as

$$C = A^T B = \begin{bmatrix} a_1b_1 & a_1b_2 & \ldots & a_1b_M \\ a_2b_1 & a_2b_2 & \ldots & a_2b_M \\ . & & & \\ . & & & \\ a_Nb_1 & a_Nb_2 & \ldots & a_Nb_M \end{bmatrix}.$$

This product can be obtained by using the configuration of Figure 5.5. Vector A

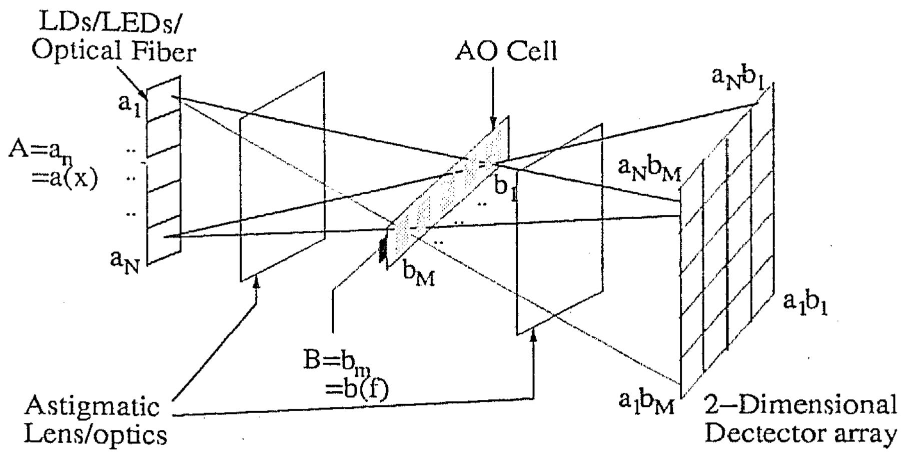

Figure 5.5: A schematic diagram of an optical processor for calculating outer product between a column and a row vector.

is treated as an array of optical source and vector B is fed to an AO modulator . Both optical source and AO cell are placed orthogonal to each other. An Astigmatic lens spreads the light from the array of the source onto the every part of the AO cell. This results in the multiplication of every element of A with every element of B. Since, this result in the 2-dimensional format, hence an array of 2-dimensional detectors are placed after another set of astigmatic lens to obtain the product.

5.3 Optical Kalman filter

From Section 2.4 and specifically from Table 2.2, we observe that for implementing a Kalman filter for an ANC it requires complex computations as compared to the LMS algorithm. Error covariance update equation requires calculation of a vector outer product a subtraction and matrix-matrix product while the calculation of *Kalman gain* needs a matrix-vector product, a vector inner product, a adder, a inversion of a scalar quantity and scalar vector multiplication. A Kalman filter algorithm is known for its faster convergence [33], if it is implemented digitally a lot of time is wasted in the calculations just mentioned. While, if these calculations are performed optically we can reduce its computation time, hence an effective faster convergence is obtained. A SLM based optical processor could have been used for parallel processing but owing to its large refresh time the effective convergence time of the system would be more. Hence we use AO based optical processor to carry out the calculations needed in the Kalman filter based ANC. Although with AO cells the processing takes place serially but because of its fastness the effective convergence time in it is less, when compared with the SLM based processors. In opto-electronic version of a Kalman filter most of these calculations are performed optically.

Figure 5.6, illustrates a possible optical implementation of Kalman filter for ANC utilizing AO cells for optical computations. Four set of the sampled reference signal X_k is required according to the Kalman filter algorithm (see Table 2.2); one set is used for the calculation of y_k, two sets are for the calculation of *Kalman gain*, K_k and one for updating the error covariance matrix, V_k. Since the covariance matrix V_k is coming out to be symmetric, hence the elemental values of the products $V_{k-1}X_k$ and $X_k^T V_{k-1}$ will be the same. So to reduce the amount of computations we use the transpose of result of the product $V_{k-1}X_k$ obtained during the calculation of *Kalman gain* matrix in the equation for error covariance matrix updating. Now, effectively we have reduced the number of sets of X_k to three. We observe that one sampled set of X_k is used for the calculation of vector inner product involving weight vector, one is used for matrix vector multiplication of V_{k-1} and X_k, and the last one is again used to calculate vector inner product of X_k and $V_{k-1}X_k$. To make the optical system more compact a single AO cell having three channels is used for the calculations involving with sampled reference signal X_k. We use bundle type FOTDL to produce X_k and the signal from only one such set of fiber strands are fanout over the three channels of AO cell as illustrated in Figure 5.7, to carry out the three computations involving with X_k simultaneously. Although in Figure 5.6, we have shown these calculations separately for the sake of clarity.

Now we spend some time on a detail description of Figure 5.6. The weight vector modulate the carrier signal and it is fed to the channel-1 of AO cell-1, this signal modulates the cell and this modulated AO cell interact with optical signal X_k. The inner product of these two signals, i.e., y_k is obtained by collecting the optical signal to a point using lens set where a detector is placed. This electrical signal is subtracted from primary signal electronically to generate output/error signal; i.e., ε_k. If primary signal happens to be an optical signal then it needs to be converted to an electrical by another detector. The error covariances matrix is time- and frequency multiplexed and fed to the channel-2 of the AO cell-1. Upon the interaction of X_k on this channel the matrix-vector product of V_{k-1} and X_k is obtained as depicted in Figure 5.4. This matrix-vector product has to be used twice one for calculation of vector inner product with X_k and other for the updating of V_{k-1}. The error covariance update equation in Table 2.2 can be modified as

$$V_k = V_{k-1} - K_k X_k^T V_{k-1} \tag{5.3}$$

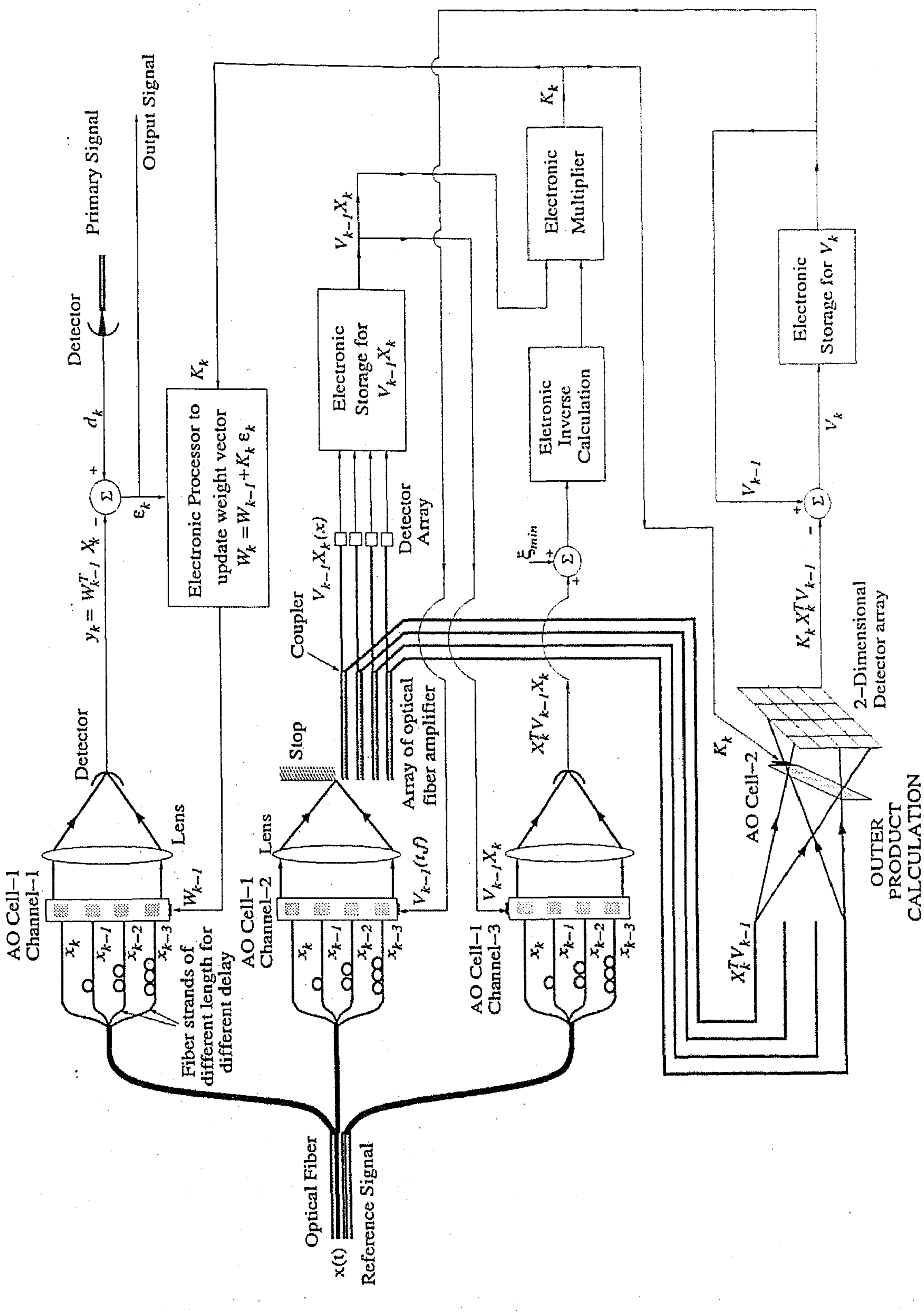

Figure 5.6: Optical Implementation of a Kalman filter for ANC using fiber bundle FOTDL and AO Bragg cells. (Thick lines are for the optical signal while thin line shows the electrical path.)

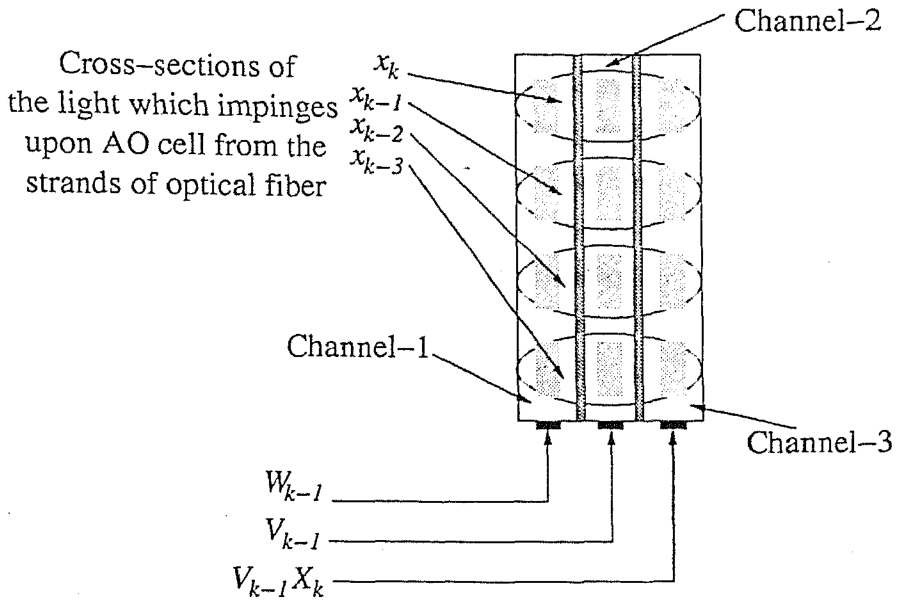

Figure 5.7: Scheme to illustrate the optical computations of three quantity simultaneously using a 3-channel AO cell.

since, we have already mentioned that $X_k^T V_{k-1} = (V_{k-1}X_k)^T$, so Equation (5.3) becomes,

$$V_k = V_{k-1} - K_k(V_{k-1}X_k)^T \tag{5.4}$$

We see that Equation (5.4) involves a vector outer product. Our system would be more fast if we could directly feed the signal corresponding to the product $V_{k-1}X_k$ as an optical signal to evaluate the outer product of involved in Equation (5.4). This helps us in eliminating the need of an intermediate electro-optical converter. In order to meet this requirement, we put in place of the array of detectors which are configured to receive the matrix-vector product of V_{k-1} and X_k, an array of optical fiber amplifiers. Thus, the product $V_{k-1}X_k$, gets launched into the optical fiber amplifier as an optical signal. A coupler is used to divide this signal into two parts. The fiber optic amplifier amplifies it by a factor of 2 to account for the loss of its intensity due to the division in two paths. One part is send for the calculation of outer product with K_k, while the second part is fed to an array of detectors. This detector array converts the optical signal into electrical signal which is equivalent to $V_{k-1}X_k$. The signal $V_{k-1}X_k$ signal after being modulated on a carrier is fed to the channel-3 of AO cell-1. The modulated AO cell interacts with the optical signal X_k, and we get the inner product of $V_{k-1}X_k$ and X_k with the help of lens set and a detector as shown in Figure 5.6. The inner product so obtained is now added electronically with ξ_{min}, and then its inverse is calculated. This result is multiplied electronically with $V_{k-1}X_k$ to obtain *Kalman gain*, K_k. The signals K_k and ε_k are then used to update the weight vector W_k in an electronic processor. The thick lines in Figure 5.6 correspond to the paths of the optical signals and the thin lines correspond to the electrical signals. The error covariance matrix is updated by first calculating the outer products of $V_{k-1}X_k$ and K_k and then subtracting this result electronically with the previous error covariance matrix. To calculate the outer product we use another AO cell, i.e., AO cell-2. The signal K_k is fed to the AO cell-2. The optical signal corresponding to $V_{k-1}X_k$ in the optical fiber amplifiers is lighted on the cell in the same manner shown in Figure 5.5, to obtain the vector outer product of K_k and $V_{k-1}X_k$. The outer product is detected by using a 2-dimensional array of detectors. Finally the outer product is subtracted from V_{k-1} to get new value of error covariance matrix, i.e., V_k. Thus the algorithm of Kalman filter for an ANC is accomplished.

Chapter 6

Optical Error and Noise Modeling in Kalman Filter algorithm

The optical computations are affected by the optical round off-errors and noise. In Kalman based ANC it prevent the weights from reaching the optimum Wiener solution, W^*owing the errors in weights (AO modulator) itself, and also because of the errors involved in the computations of other parameters which update the weights. In this section we detail the types of optical errors and noise possible in the optical implementation of Kalman filter for the ANC system mentioned in Section 5, and derive model for noise- and error- sources. From Figure 5.6, we notice that all the optical computations are based upon the AO cells, so first we look upon the errors of an AO cell based optical matrix-vector multiplier [47] and having studied this, error models for other computations can easily be reduced.

6.1 Error source modeling of AO cell

Referring Figure 5.4, a matrix-vector multiplier consists of a linear array of inputs point modulators (in our case fiber strands), an AO cell, and a detector array. In the present modeling, we neglect the errors originated from the associated optics, i.e., we assume ideal lenses, no dispersion, and no cross-talks. Errors in a matrix-vector multiplier can be divided into three planes: (1) Input Plane Errors, (2) AO Cell Plane Errors, and (3) Detector Plane Errors. The major input plane errors include the tap positioning error (already discussed in Section 4) and the interconnection error between the input plane and the AO cell, i.e., error in positioning the fiber strands at proper place. Acoustic attenuation of the signal produces a deterministic taper $\exp(-\alpha l)$ across the length l of the AO cell, where α is the attenuation constant of the AO cell material used. We assume that α is small and non-dispersive. This attenuation lead to the spatial error in the AO cell plane. Spatial errors also arise in the AO cell owing to the imperfections in the AO material and because of the amplifier error, i.e., error in representing a quantity in a AO cell. Variations in the frequency response $H(f)$ of the AO cell also lead to produce errors in computations. Detector plane error include the time-varying detector noise, dark current variations in different detectors, and the spatial errors due to the variations in the spatial response of the individual output detectors, i.e., error in positioning of the detector array. All spatial errors mentioned are correctable and can be reduced to low residual levels by adjusting the input signal to AO cell or by use of a correction mask in front of the AO cell (Mask can correct the α error only at one frequency.). All the spatial errors in the AO cell can be mapped into spatial input-plane errors and its frequency dependent error can be mapped to the detector plane errors (since the FT lens converts frequency in the AO plane into position in the detector plane).

Table 6.1, summarizes the notation used and the various input, AO, and detector plane errors. If a 2×2 matrix A is fed to the AO cell and a 2×1 vector X is input from the optical fiber. The errors in the matrix-vector product of $AX = B$ produced is described as [47]

$$\begin{bmatrix} b_1' \\ b_2' \end{bmatrix} = \begin{bmatrix} 1+\delta_1^{(3)} & 0 \\ 0 & 1+\delta_2^{(3)} \end{bmatrix} \begin{bmatrix} H(f_1) & 0 \\ 0 & H(f_2) \end{bmatrix} \begin{bmatrix} a_{11} & a_{12} \\ a_{21} & a_{22} \end{bmatrix} \begin{bmatrix} 1+\Psi_2 & 0 \\ 0 & 1+\Psi_1 \end{bmatrix} \begin{bmatrix} \exp(-\alpha l_2) & 0 \\ 0 & \exp(-\alpha l_1) \end{bmatrix} \begin{bmatrix} x_1+\delta x_1 \\ x_2+\delta x_2 \end{bmatrix} + \begin{bmatrix} d_1 \\ d_2 \end{bmatrix} + \begin{bmatrix} n_1(t) \\ n_2(t) \end{bmatrix}. \tag{6.1}$$

here, all the spatial errors (subscript i) are combined into a single variable Ψ_i, given as

$$\Psi_i = \delta_i^{(1)} + \delta^{(2)} + \delta_i^{(2)}, \tag{6.2}$$

and primes over $b's$ is the observed values under optical calculations (lower case a, x, and b represent the elements of A, X, and B respectively). Based upon the origin of error sources we can write Equation (6.1) as

$$\begin{aligned}\begin{bmatrix} B' \\ observed \end{bmatrix} = \begin{bmatrix} Detector\,Spatial \\ Response\,Variations \end{bmatrix} \begin{bmatrix} AO\,frequency \\ Response\,Variations \end{bmatrix} \begin{bmatrix} A,\,Exact \\ Matrix \end{bmatrix} \\ \begin{bmatrix} Input\,Spatial \\ Response\,Variations \end{bmatrix} \begin{bmatrix} Acoustic \\ Attenuation \end{bmatrix} \begin{bmatrix} X,\,Exact \\ +tap\,error \end{bmatrix} + \\ \begin{bmatrix} Detector \\ Dark\,Current \end{bmatrix} + \begin{bmatrix} Detector \\ Noise \end{bmatrix}.\end{aligned} \tag{6.3}$$

We combine all the multiplicative errors by multiplying all of them, and add all the additive errors, thus we reduce Equation (6.3) to

$$\begin{aligned}\begin{bmatrix} B' \\ observed \end{bmatrix} = \begin{bmatrix} Total\,multipli- \\ cative\,errors \end{bmatrix} \begin{bmatrix} A,\,Exact \\ Matrix \end{bmatrix} \begin{bmatrix} X,\,Exact \\ vector \end{bmatrix} \\ + \begin{bmatrix} Total\,additive \\ error \end{bmatrix}.\end{aligned} \tag{6.4}$$

As mentioned earlier, that the spatial errors are fixed for a particular system and hence can be reduced to small residual levels by correction. The detector dark current noise can also be reduced by appropriate post-processing. Time-varying detector noise remains as the major non-correctable error source. Similarly, the acoustic attenuation and transfer function errors are deterministic and can be reduced to a small value. Thus, after correction we can write the residual acoustic error as $1 + \delta AA^{(2)}$ and transfer function error as $1 + \delta TF$. Therefore, B' can be written as

$$B' = A(I + \delta Mul)X + \delta Add \tag{6.5}$$

where, δMul is the equivalent matrix of the combined effects of total residual spatial error, attenuation error and transfer function error. (The term $(I + \delta Mul)$ is the total residual multiplicative error.). The term δAdd is the vector of total residual additive error.

6.2 Error source modeling of optical Kalman filter

Based upon the concept of error and noise sources of Section 6.1, we have drawn the schematic presentation of the dominant error sources, which occur in the optical realization of Kalman filter based ANC in Figure 6.1. We have considered only the first order noise and also neglected the round-off errors due to the electronic com-

Error Source	*Notation*
Spatial errors	Subscript i
Frequency errors	Subscript j
Input plane errors	Superscript 1
AO cell errors	Superscript 2
Detector-plane errors	Superscript 3
Input Plane Errors	*Notation*
Defect in tap-positioning	$\delta X^{(1)}$
Coupling (spatial)	$1+\delta_i^{(1)}$
AO Cell Plane Errors	*Notation*
Amplifier errors	$1+\delta^{(2)}$
Spatial response	$1+\delta_i^{(2)}$
AO transfer function	$H(f_j)$
Acoustic attenuation	$\exp(-\alpha l_i)$
Detector Plane Errors	*Notation*
Spatial response	$1+\delta_j^{(3)}$
Dark current	d_j
Time-varying noise	$n_j(t)$

Table 6.1: Error source model for matrix vector multiplier.

putations owing to their small magnitudes. Variables are primed to represent the quantity in optical implementation. There are two vector inner products involved in the algorithm, these products can be seen as one special case of matrix-vector multiplication, i.e., when a vector is fed to the AO cell and a single detector is placed in the detector plane. Therefore, in the optical computation of these products we have only one error present at the detector plane, i.e., time varying detector noise.The other error sources remains the same as for the case of matrix-vector.

We have already mentioned in Section 5, the use of the optical fiber amplifiers to extract the product $V_{k-1}X_k$ as an optical signal. This fiber introduces amplifier noise, δOFA in the signal. We assume amplifier noise to be additive. In the optical computation of matrix-vector, i.e., $V_{k-1}X_k$, all the light is directed to the detectors using optical fibers, so we neglect the errors due to the dark current variations. Also, the error due to the detector-spatial response variations becomes the error due to the optical fiber spatial response variations. This optical signal is free from the detector noise when coupled out and used for the vector outer product with K_k in AO cell-2 as depicted in Figure 6.1. Also, it can be assumed that there is no tap-positioning error in this signal. (Since we assume all optical fiber amplifiers are approximately of the same length.) Other errors in the vector outer product calculation are same as in the case of matrix-vector product. We have neglected the errors which comes into the picture due to the use of coupler, as it can be modeled along-with amplifier noise δOFA.

In our simulations, the tap-positioning error is modeled as white noise zero-mean Gaussian sequence with variance of σ_{tap}^2 (same as in Section 4). It is observed that the tap error after getting multiplied with some constant becomes a part of total residual additive error (see Equation (6.1), Equation (6.3) and Equation (6.5)). Power loss in the fiber strands and intensity reduction due to division of signal into several strands is compensated using optical laser amplifiers or optical fiber amplifiers. The noise introduced by laser/fiber amplifier is not modeled separately as it can be regarded as some part of the tap-positioning error (same as in Section 4). The time varying detector noise is also modeled as zero-mean Gaussian process of variance equal to σ_{det}^2. Similarly, the optical fiber amplifier noise δOFA is modeled as zero-mean Gaussian process with variance of σ_{ofa}^2. The errors due to tap positioning, noise of the optical amplifier and the noise of the detector are time varying, i.e., at each iteration new sequence is considered. The remaining errors, i.e., coupling error $\delta_i^{(1)}$, error in representing a particular quantity in AO cell (amplifier errors) $\delta^{(2)}$, error due to spatial response of AO cell $\delta_i^{(2)}$, error due to AO transfer function $H(f_j)$, acoustic attenuation error $\exp(-\alpha l_i)$, error due to spatial response of detector/optical fiber amplifier $\delta_j^{(3)}$, and error due to dark current variations (if exist) d_j, are time-independent; hence they do not change with iteration. After the correction of time-independent errors, we model the residual errors as white noise Gaussian sequences with zero-mean and variances equal to σ_{coup}^2, σ_{amp}^2, σ_{AOspa}^2, σ_{AOfreq}^2, $\sigma_{AOatten}^2$, σ_{DFspa}^2, and σ_{dark}^2 respectively. (Note: After correction, $H(f_j)$ and $\exp(-\alpha l_i)$ becomes $1 + \delta TF$ and $1 + \delta AA$ respectively, also σ_{AOfreq}^2 and $\sigma_{AOatten}^2$ are the variances of δTF and δAA respectively, not of $H(f_j)$ and $\exp(-\alpha l_i)$). The matrices corresponding to these errors remain constant throughout the simulation. All the noise sequences are assumed to be independent of the signal and with each other.

The elemental values of the error covariance matrix, *Kalman gain* vector, and other products generated from these two comes out to be very small, of the order of 10^{-5}. If these signals are sent without modifying then it will be effectively killed by the optical errors/noise of the system; that are generally of the order of 10^{-3}. Hence an electronic up-scalar, shown in Figure 6.1, is used. It is needed only for the first iteration. A electronic down-scalar is also used to revert back to the original values of K_k, which is used in weight updating. Unlike in LMS case, here the closed form expression of signal to noise ratio of output signal is very difficult to derive. So a quantitative analysis of optical noise/errors will be done in Section 7.3.

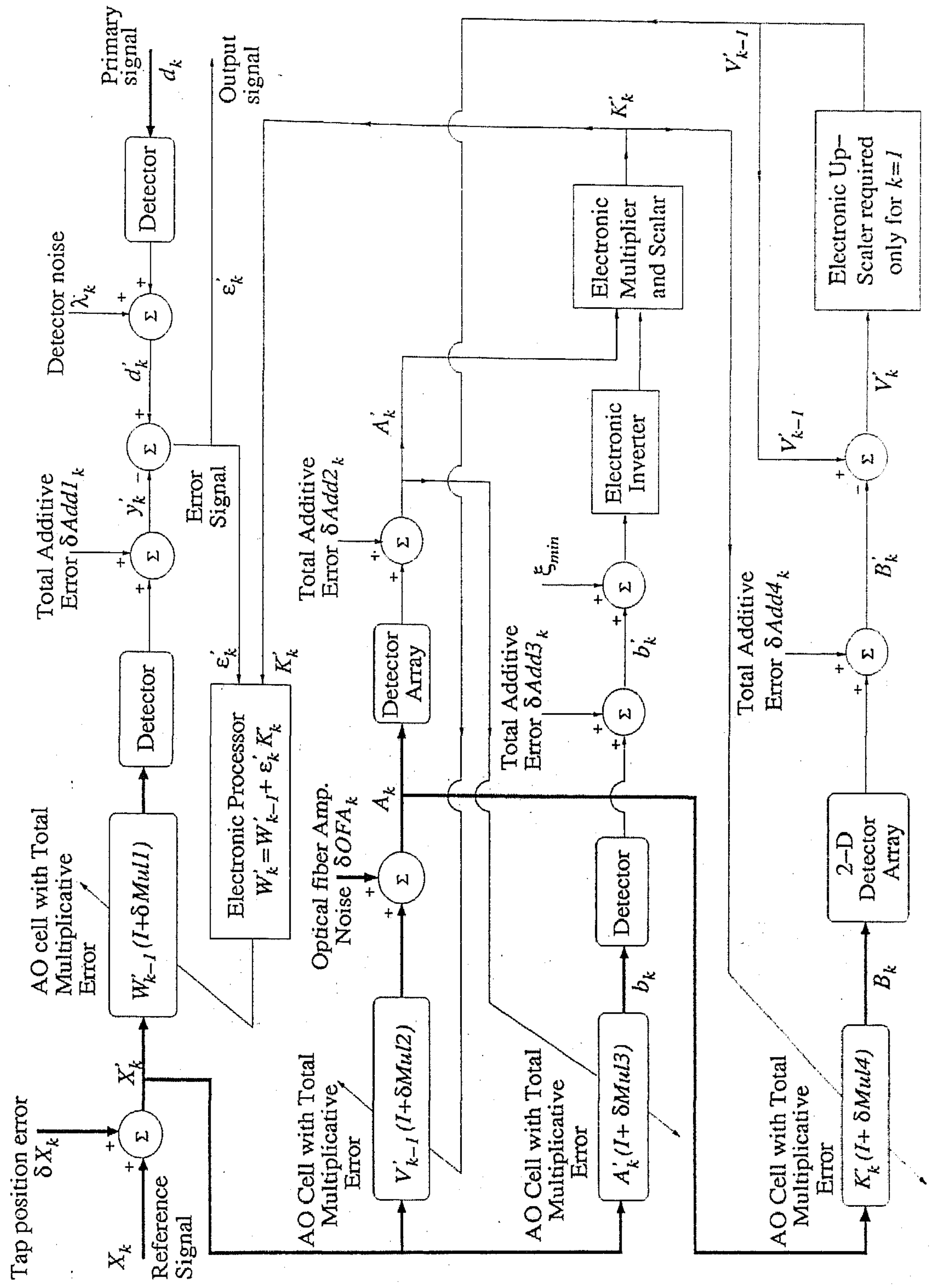
Tap position error
δX_k
X_k
Reference Signal
X'_k
AO cell with Total Multiplicative Error
$W'_{k-1}(I+\delta Mul1)$
Detector
Total Additive Error $\delta Add1_k$
y'_k
Error Signal
d'_k
Detector noise
λ_k
Detector
Primary signal
d_k
Output signal
ε'_k
Electronic Processor
$W'_k = W'_{k-1} + \varepsilon'_k K_k$
K'_k
AO Cell with Total Multiplicative Error
$V'_{k-1}(I+\delta Mul2)$
Optical fiber Amp. Noise δOFA_k
A_k
Detector Array
Total Additive Error $\delta Add2_k$
A'_k
AO Cell with Total Multiplicative Error
$A'_k(I+\delta Mul3)$
b_k
Detector
Total Additive Error $\delta Add3_k$
b'_k
ξ_{min}
Electronic Inverter
Electronic Multiplier and Scalar
AO Cell with Total Multiplicative Error
$K'_k(I+\delta Mul4)$
B_k
2-D Detector Array
Total Additive Error $\delta Add4_k$
B'_k
V'_{k-1}
V'_k
Electronic Up-Scaler required only for $k=1$
Σ
+
-

Figure 6.1: Schematic diagram of error model with dominant error sources in realizing optical Kalman filter based ANC.

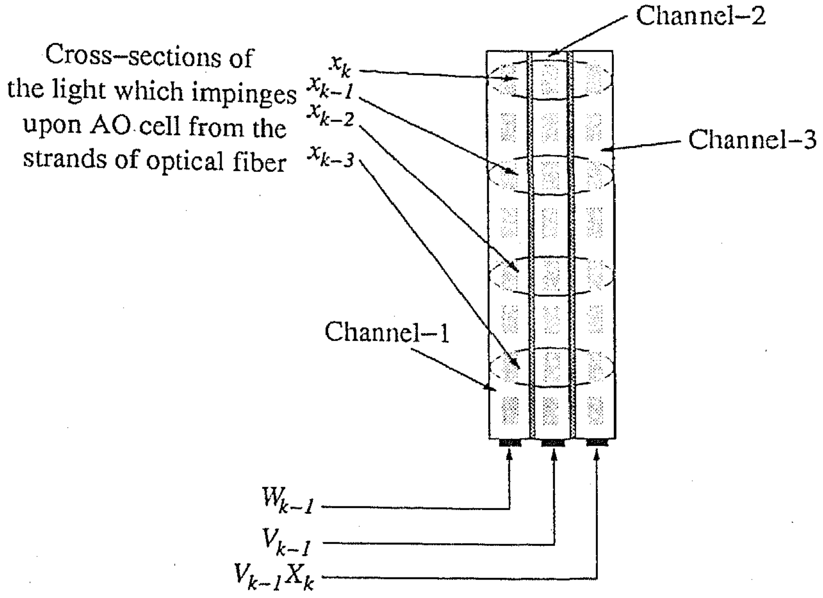
Channel–2
Cross–sections of the light which impinges upon AO cell from the strands of optical fiber
x_k
x_{k-1}
x_{k-2}
x_{k-3}
Channel–3
Channel–1
W_{k-1}
V_{k-1}
$V_{k-1}X_k$

Figure 6.2: Positions of elements of X_k while handling bipolar data. Only alternate positions of the AO cell is illuminated by the signal.

In our application, the vector X_k always remains positive, while the other quantity may become negative in the course of iteration, so to handle them we need to adopt the procedure as described in [45] or Section 3. To handle bipolar values we need the same number of AO cell mentioned earlier, since the modified matrices can be accommodated by doubling the amount of frequency- and time-multiplexes. While there is an increase in the number of other elements of, i.e., detectors, fiber amplifiers, couplers and frequencies, in fact they are doubled. Since X_k is always positive, so we do not need to multiplex or relocate their positions, as they automatically fixed at alternate positions of the elements of the AO cell because of the doubling of the data in the AO channel. This concept is shown in Figure 6.2.

Chapter 7

Simulation and results

7.1 Signal modeling

We have shown the optical realization of both LMS and Kalman filter algorithm based ANC system. The performance of the system depends on the amount of optical error or noises present in the optical components. In order to study the effects of these errors/noise, we apply some specific primary and reference signals to the optical systems and study the SNR of output signal.

The signals which were used in Section 2.5, were modified to meet the requirements in optical domain. In optical domain, the primary and reference signals should be positive valued and thus have positive mean. We modeled pure signal (s) in the same way as in Section 2.5. The noise signals n_0 and n_1 were taken to be white noise Gaussian processes with means of 4.5. Few samples of the primary or reference which comes out to be negative were discarded.

We also notice that the presence of optical errors do not affect the convergence characteristics of LMS or Kalman filter algorithms, because the term $\Delta\varepsilon = (\varepsilon_k^{'} - \varepsilon_k)$ has a approximately zero mean for all k [14]. Hence, we considered the same number of iterations as was mentioned in Section 2.5. For all simulations of this section, we took SNR of primary signal to be equal to $0dB$. Bipolar data generated in course of time were handled as described in the earlier chapters. Remaining methods in simulation remained the same as of the Section 2.5.

7.2 Results of LMS implementation

To know how a optical ANC system behaves under different levels of optical noise/errors and under different system parameters, we vary these noise/errors

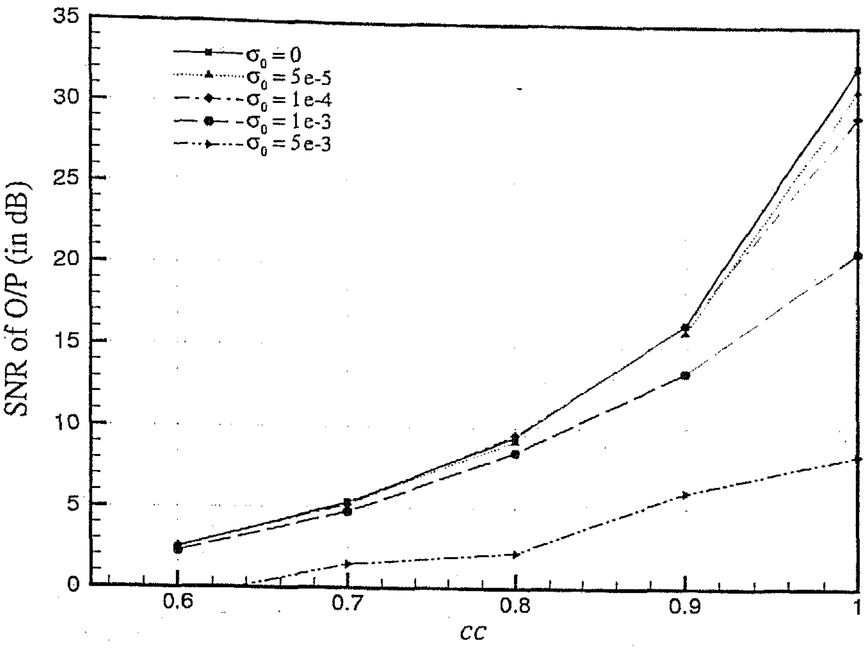

Figure 7.1: Variation of SNR of output signal with *cc* for different levels of optical errors (number of taps=2 and $\mu = 0.002$).

or parameters and study their effects in noise removal. The performance of ANC based technique of noise reduction is highly dependent on correlation coefficient between noise n_0 and n_1. Performance of optical ANC is studied for various values of correlation coefficient. In Section 4.3, we noticed the presence of optimum value of adaptive gain constants μ_{opt}. To illustrate this μ_{opt}, we study the behavior of SNR of output with μ at different optical noise/errors values. Similarly, we also study the same behavior at different number of taps, i.e., for different number of taps the performance of the ANC is studied with adaptive gain constant μ. Finally we attempt to study the relative dominance of different types of optical errors/noise.

Case-1

In this case, we varied the correlation coefficient between n_0 and n_1, i.e., *cc* and measured the output SNR at various levels of optical error/noise. The adaptive gain constant μ was set at 0.002 and the number of taps used was 2. For simplicity, all the error and noise sources were set equal such that $\sigma_{tap} = \sigma_{spa} = \sigma_{det} = \frac{\sigma_{mul}}{\sqrt{2}} = \sigma_0$. Here, the multiplication error is chosen so because its sequence is nothing but the summation of spatial and detector error sequences as shown in Figure 4.1.

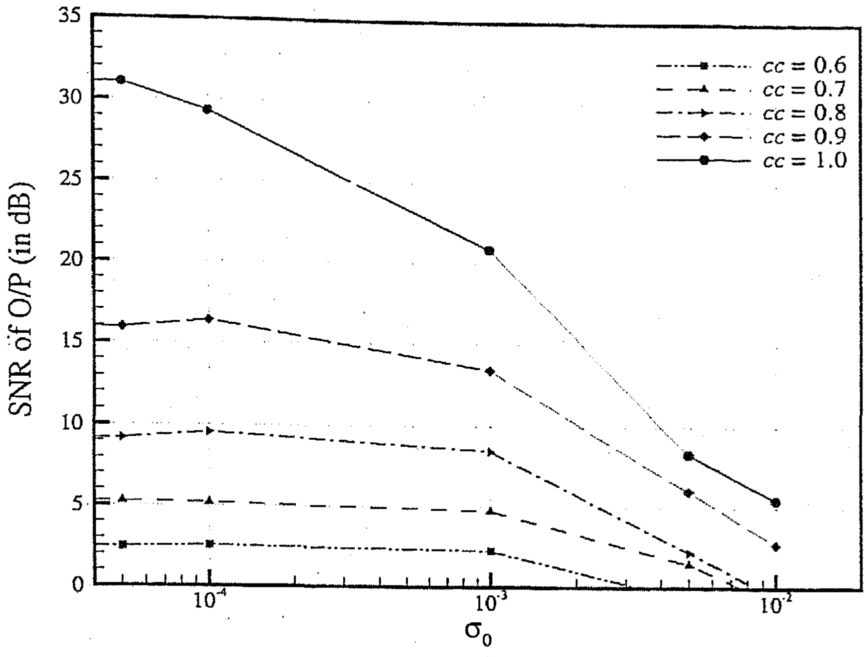

Figure 7.2: Variation of SNR of output signal with optical error σ_0 for different values of *cc* (number of taps=2 and $\mu = 0.002$).

Figure 7.1, and Figure 7.2 are the results of our simulation for this case. From Figure 7.1, we see decrement in SNR of output signal with the decrease of *cc* as expected. With the increase in the optical errors the curve shifts downward. At lower *cc*, the distinction between different levels of optical error present in the system reduces. Curves of Figure 7.2 show the variation of SNR of output with the optical error at different values of *cc*. One important observation is made from these plots that for $cc < 1$, the SNR of output is nearly unaffected by the presence of optical errors of the order as high as 10^{-3}.

Case-2

In this case, we investigated the theoretical results of Equation (4.26) with simulation and illustrate some of the design trade-offs in building fiber optic adaptive filter. Quantitative results of the dependence between SNR and μ obtained from the simulations are depicted in Figure 7.3 The results were calculated for different levels of optical errors in a two-tap filter and *cc* was set at 1. Theoretical plots obtained from Equation (4.26) are also superimposed on the same figure for comparison. An interesting characteristic of the plots in Figure 7.3 is the existence of

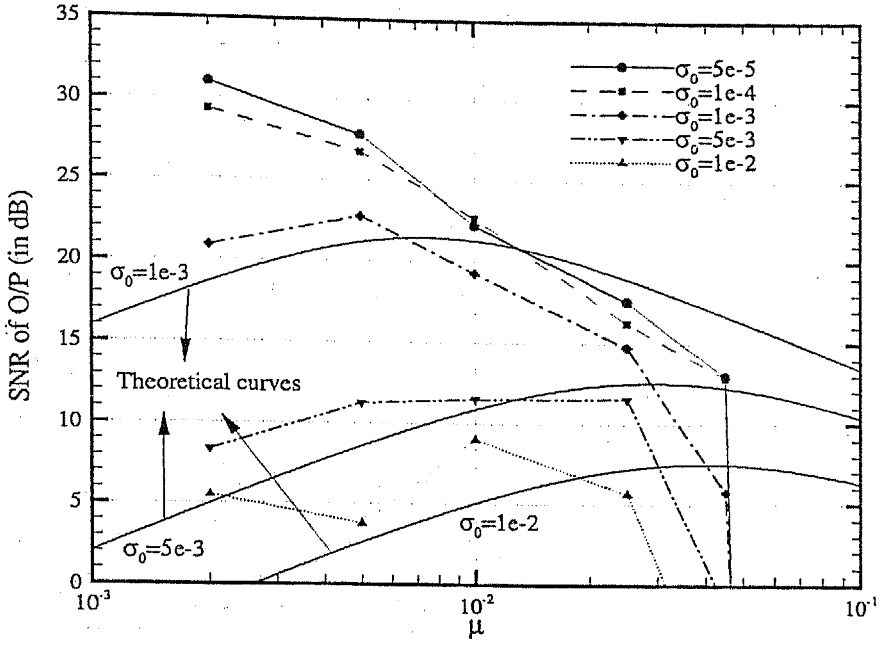

Figure 7.3: Variation of SNR of output signal with adaptive gain μ for different levels of optical errors (number of taps, N=2 and $cc = 1$).

optimum value of adaptive gain constant, μ_{opt}, for which the SNR is maximum. In ideal implementation ($\sigma_0 = 0$) there is no such optimum μ (refer Section 2.5.2), but in presence of optical error, the optimum value does come in the picture, it can be seen that μ_{opt} exist at around 10^{-2}, 2×10^{-2} and 5×10^{-3} for the optical errors $\sigma_0 = 10^{-2}$, 5×10^{-3} and 10^{-3} respectively. Optimum values exist for other values of optical error levels which lie beyond the range of μ that has been shown in Figure 7.3. We also notice that the plots are nearly flat in the vicinity μ_{opt}. This feature implies that the optimum value of μ need not be very accurate. Thus, the selection of μ in the vicinity of μ_{opt} allows us reduce the effects of optical errors/noise, thereby improving the output SNR. SNR at μ_{opt} is maximum, if μ is increased beyond μ_{opt}, the SNR tend to decrease and as it approaches $2/\lambda_{max}$, the SNR decreases very rapidly owing to the inception of instability in the LMS algorithm. The SNR of output signal tends to decrease if μ is decreased below μ_{opt}. This shows that the SNR of output signal is inversely proportional to μ. Physically, if μ is small enough, most of the time weights are not updated (i.e., a change in weights is negligible compared to noise terms), and the adaptation of the filter virtually stops. This early termination of the adaptation due to optical errors may

optical error (σ_0)	μ_{opt} Simulated	μ_{opt} Theoretical	SNR of O/P Simulated	SNR of O/P Theoretical
10^{-3}	0.005	0.0075	22.783	21.494
5×10^{-3}	0.025	0.0295	11.587	12.591
10^{-2}	0.01	0.0395	9.016	7.523

Table 7.1: Comparison of theoretical and simulated values of μ_{opt} at different levels of optical error.

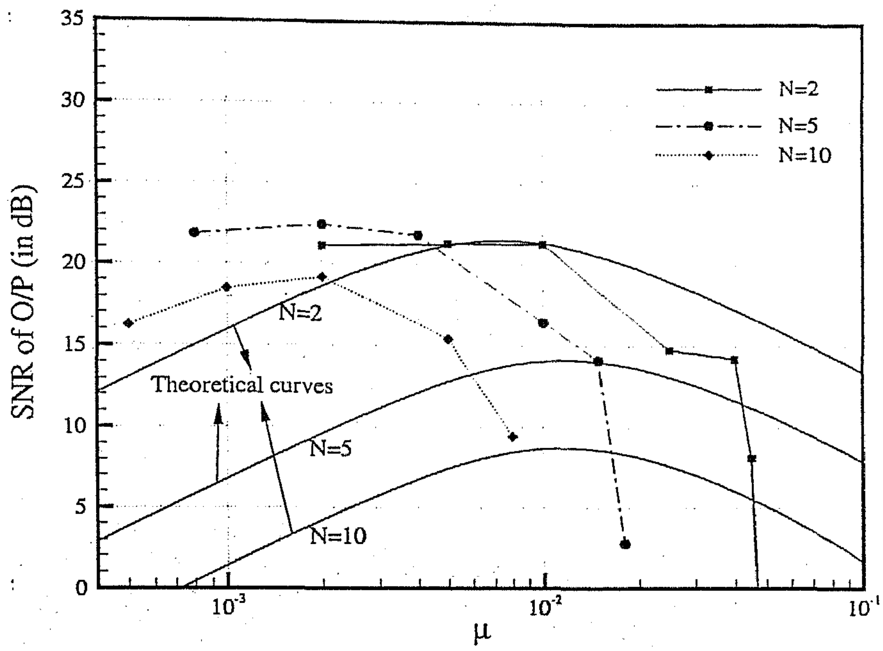

Figure 7.4: Variation of SNR of output signal with adaptive gain μ for different number of taps ($\sigma_0 = 10^{-3}$ and $cc = 1$).

result in a output SNR significantly smaller than the SNR of ideal implementation. Theoretical curves follows approximately the same behavior as the simulated curves for $\mu < \mu_{opt}$. Theoretical and simulated values of μ_{opt} under different optical error levels alongwith its SNR are depicted in Table 7.1.

Case-3

In Case-2, we studied the SNR of output signal vs. μ plots at different optical noise level, in this case we studied the same variations but at different number of taps. Results obtained from the simulation are drawn in Figure 7.4. The optical error σ_0 was set at 10^{-3} and cc was set to 1. These plots show similar characteristics as of

Number of taps (N)	μ_{opt} Simulated	μ_{opt} Theoretical	SNR of O/P Simulated	SNR of O/P Theoretical
2	0.005	0.0075	21.291	21.494
5	0.002	0.0118	22.438	14.136
10	0.002	0.0116	19.181	8.715

Table 7.2: Comparison of theoretical and simulated values of μ_{opt} for different number of taps.

Figure 7.3. We notice that with the increase in number of taps, the SNR of output decreases as expected (see Section 2.5.2). Like Case-2, the optimum value μ_{opt} can be observed in these plots. Theoretical plots obtained from Equation (4.26) are also drawn for the sake of comparison. It can be seen that lower limit of μ in theoretical curve is less than the simulated values. Practically, with the increase of N, the maximum eigen value of matrix R increases, hence the upper limit of μ decreases [see Equation (2.14)]. Comparison is made in Table (7.2) between the theoretical and simulated values of μ_{opt} for different N.

Case-4

In Section (4), we considered four types of optical errors/noise, i.e., σ_{spa}, σ_{det}, σ_{tap} and σ_{mul}. It was pointed out earlier that $\sigma^2_{mul} = \sigma^2_{spa} + \sigma^2_{det}$. Now, basically we are left with three types of errors, *viz.* σ_{spa}, σ_{det}, and σ_{tap}. It will be explained later that practically, the tap position error is quite small compared to detector or spatial errors. The aim of the simulations in this case is to figure out the relative effects of spatial errors and detector noise in the SNR of output signal. In these simulations tap error, σ_{tap} was fixed at one constant value equal to 10^{-5}, μ at 0.002, cc at 1 and number of taps, N at 2. Then the simulation was done for different values of spatial errors and detector noise. Figure 7.5 illustrates the variations of SNR of output signal with detector noise at different levels of spatial error. Similarly, Figure 7.6, gives an insight into the curves of SNR *vs.* spatial error at different levels of detector noise. It is obvious that SNR of output decreases with the increase of either of optical error. Apart from it, we discern that the impact of spatial errors in decreasing the SNR of output is more prominent than the detector noise. For example, follow the curves with σ_{spa} and σ_{det}= 5×10^{-3} in Figure 7.5 and Figure 7.6 respectively, we observe that the first curve is lower than the second curve up to σ_{det} and σ_{spa}= 10^{-3} , in Figure 7.5 and Figure 7.6 respectively, and after this value the second curve steeps downward sharply. It means that when σ_{spa} was 5×10^{-3} the SNR of first curve is lower than when σ_{det} was 5×10^{-3} of the second curve,

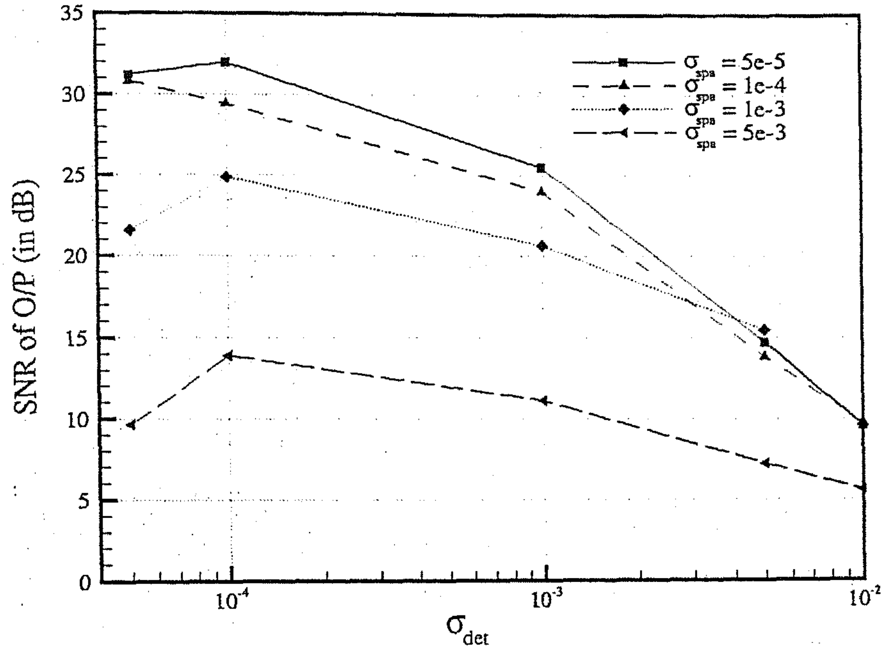

Figure 7.5: Variation of SNR of output signal with detector noise σ_{det}, at different values of spatial error σ_{spa} (Number of taps, $N = 2$, adaptive gain constant $\mu = 0.002$, $cc = 1$, and $\sigma_{tap} = 10^{-5}$).

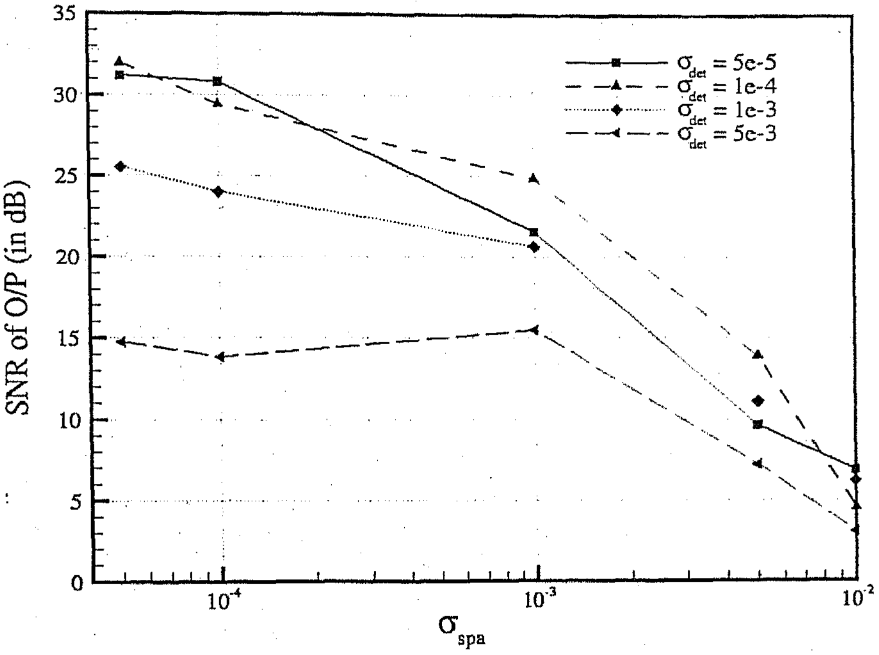

Figure 7.6: Variation of SNR of output signal with spatial error σ_{spa}, at different values of detector noise σ_{det} (Number of taps, $N = 2$, adaptive gain constant $\mu = 0.002$, $cc = 1$, and $\sigma_{tap} = 10^{-5}$).

i.e., spatial errors deteriorate the output signal more than the detector noise. Also, the first curve dips slowly even when detector noise is high and second curve dips sharply in high spatial error zone which show the less dependence of detector noise on system output than spatial error.

From the theoretical analysis and numerical simulations, we have observed that the optical errors involved in the weight update process are the dominant sources, i.e., the terms involving σ_{spa} and σ_{mul} in Equation (4.24) are the dominant components. Thus, to decrease the effects of optical errors on the performance of LMS based optical ANC, the designer should try to reduce the σ_{spa} and σ_{mul} levels and operate the system with μ in the vicinity of μ_{opt}.

7.3 Results of Kalman filter implementation

In optical Kalman filter based ANC, we study the behavior of SNR of output with respect to the correlation coefficient *cc*. We also figure out the effects of number of taps in the SNR of output signal. Finally, we study the relative dominance of different types of optical errors/noise in the output performances.

Optical realization of Kalman filter for ANC requires many optical components. The total amount of errors/noise introduced by the optical components will also be high. Thorough numerical analysis under various optical error/noise level is needed to check the feasibility and viability of our optical system of Kalman filter. In this section, we present the results of numerical analysis done through computer simulations. Section 6 discusses about ten different types of error/noise which originates in the optical Kalman filter. Let us rewrite them here for simplicity: (1) Tap error σ_{tap}, (2) Detector noise σ_{det}, (3) Error in presenting a quantity in AO cell (amplifier noise) σ_{spa}, (4) Optical fiber noise σ_{ofa}, (5) Coupling error σ_{coup}, (6) AO spatial error σ_{AOspa}, (7) AO transfer function error σ_{AOfreq}, (8) AO attenuation error $\sigma_{AOatten}$, (9) Detector or optical fiber amplifier spatial error σ_{DFspa}, and (10) Dark current error σ_{dark}. All the residual errors involved in the computations with AO cell can be categorized into multiplicative and additive errors as explained in Section 6. Thus, σ_{tap}, σ_{det}, σ_{ofa}, and σ_{dark} falls under additive errors and σ_{spa}, σ_{coup}, σ_{AOspa}, σ_{AOfreq}, $\sigma_{AOatten}$, and σ_{DFspa} are treated as multiplicative error. Also, the errors σ_{tap}, σ_{det}, and σ_{ofa} are time varying, while remaining errors are fixed.

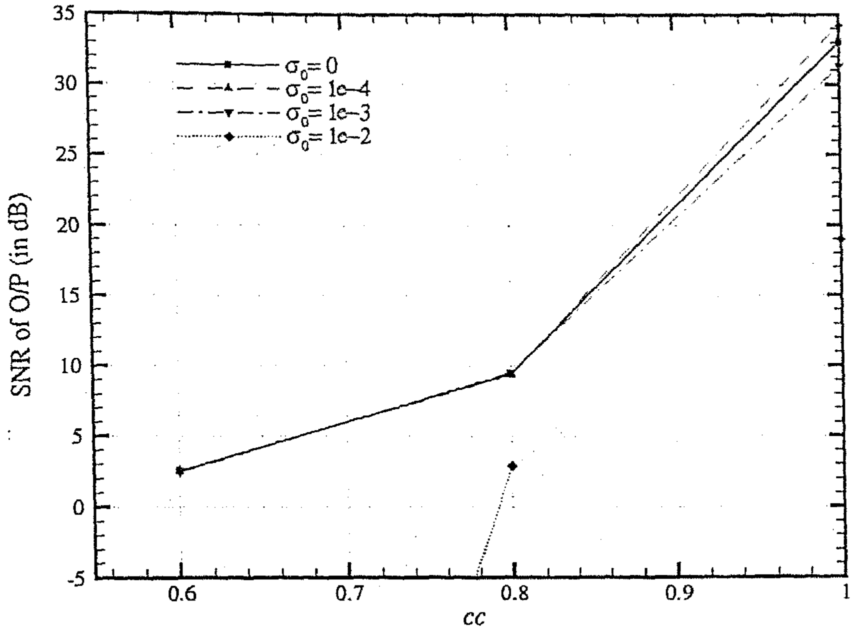

Figure 7.7: Variation of SNR of output signal with correlation coefficient *cc*, at different levels of optical error σ_0 (Number of taps, $N = 2$, Kalman filter).

Case-1

In this case, we treated the standard deviations of all the optical errors to be same, and equal to σ_0. The correlation coefficient, *cc* was varied and the SNR of output signal was measured at different optical σ_0. Simulations were done for number of taps equal to 2. Figure 7.7 depicts the variation of SNR of output with *cc* for different levels of σ_0 and Figure 7.8 shows the variation of SNR of output with σ_0 at different values of *cc*. From the plots of these figures we draw some important conclusions that optical Kalman filter based ANC technique removes noise from the signal well, even when the optical error is of the order 10^{-2}, the performance deteriorates when optical error crosses this limit. As pointed out earlier (in Section 2.5.2, and Section 2.5.3) that the ANC technique is highly dependent upon *cc*. When *cc* is reduced from 1 to 0.9, there is a decrease of about $10dB$ in the SNR of output at $\sigma_0 = 10^{-3}$.

Case-2

Dependence of SNR of output signal with number of taps at different optical error level is studied through the simulated results in this case. *cc* was set at 1 in these

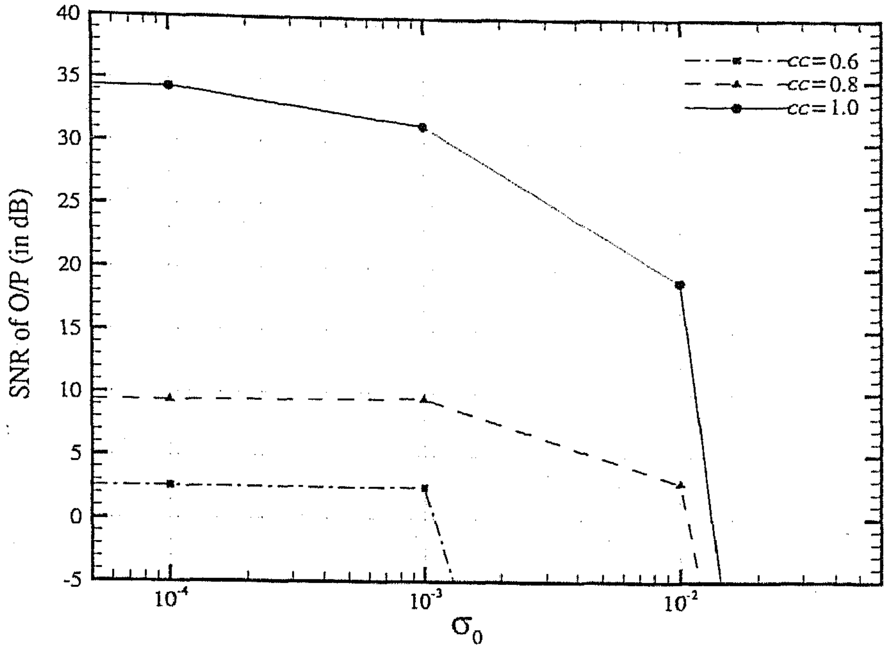

Figure 7.8: Variation of SNR of output signal with optical error σ_0, for different values of correlation coefficient cc (Number of taps, $N = 2$, Kalman filter).

simulations. Curves showing the variations of SNR of output with N at different levels of optical error σ_0 is drawn in Figure 7.9. Under ideal implementation, i.e., $\sigma_0 = 0$, the SNR is almost constant with number of taps (refer Section 2.5.3), it is also obvious from Equation (2.99); but under optical implementation with the inception of optical errors, the SNR of output starts decreasing almost linearly with the number of taps. The reason of this fact can be explained as follows: Kalman filter algorithm requires the computations of many multiplications involving matrices or vectors. Elements of the matrices or vectors are represented on AO cells with embedded optical errors. Thus, if the number of elements increases, i.e., N increases, then the total errors accompanied with them also increase, thereby system errors increase and result in the reduction of SNR of output signal. It can also be observed from the same figure that the declination of the curve increases with increase in the optical error.

Case-3

We set cc at 1 and simulations were done to figure out the relation between SNR of the output and optical error σ_0 for different number of taps. Basically, Case-3

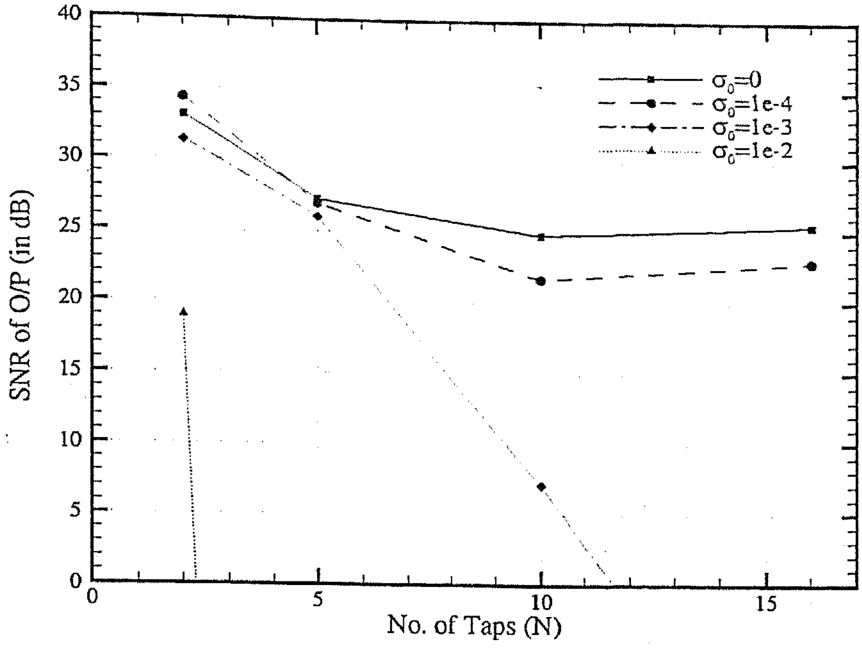

Figure 7.9: Variation of SNR of output signal with number of taps N, at various levels of optical error σ_0 ($cc = 1$, Kalman filter).

is same as Case-2 only the axes are interchanged. Figure 7.10 depicts the curves which show the mentioned variations. Here also, it can be noticed the curves of higher order filters are below the lower ones. When number of taps is 2, the effects of optical errors become significant after $\sigma_0 > 10^{-3}$. While for $N = 16$, the optical errors $\sigma_0 > 10^{-4}$ cause the SNR of output to decline sharply. Thus we can say, with the increase of the filter order in the ANC system, the maximum allowable optical errors of the system decrease.

Case-4

We have mentioned at the start of this section about ten different types of errors/noise in optical realization of Kalman filter, which can be grouped under additive error and multiplicative error. Let us treat the standard deviations of all additive errors to be equal to σ_a, and similarly, the standard deviations of all multiplicative errors to be equal to σ_m. Number of taps was set at 2 and cc at 1. Then simulations were done for different values of σ_a and σ_m, the results obtained from simulations are shown in the forms of plots of Figure 7.11 and Figure 7.12. Plots of Figure 7.11 illustrate the variations of SNR of output signal with additive

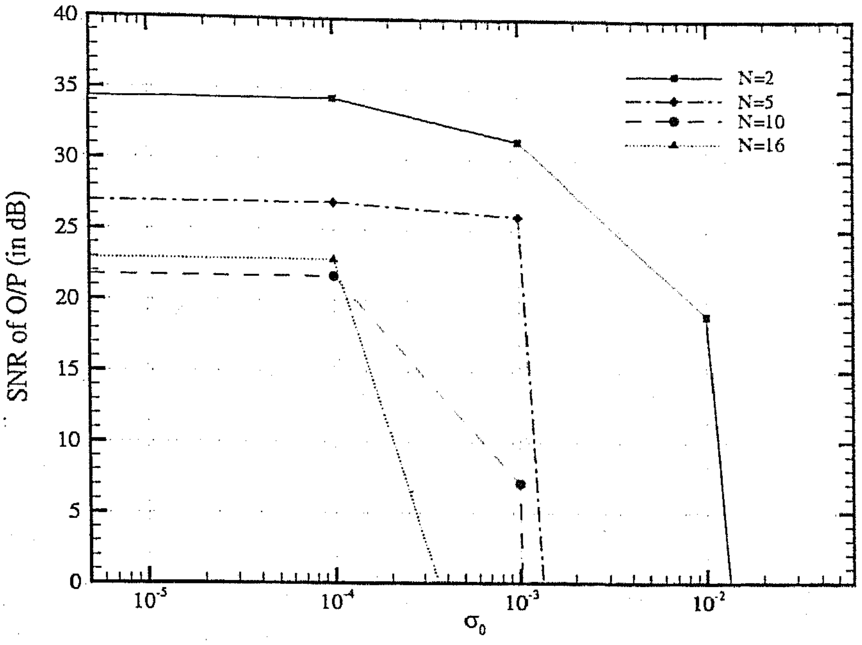

Figure 7.10: Variation of SNR of output signal with optical error σ_0 for different values of number of taps N ($cc = 1$, Kalman filter).

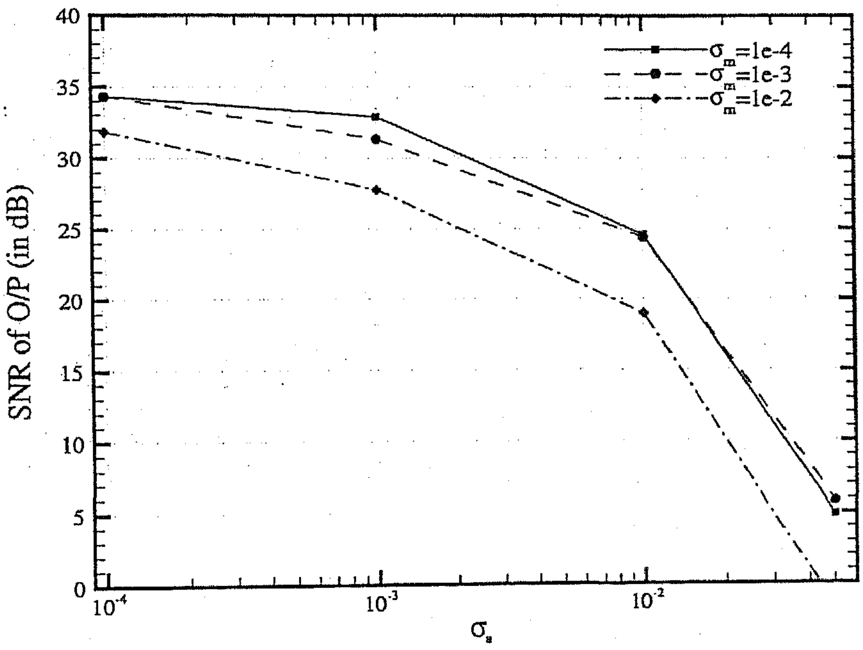

Figure 7.11: Variation of SNR of output signal with additive error, σ_a for different levels of multiplicative error σ_m ($cc = 1$, $N = 2$, Kalman filter).

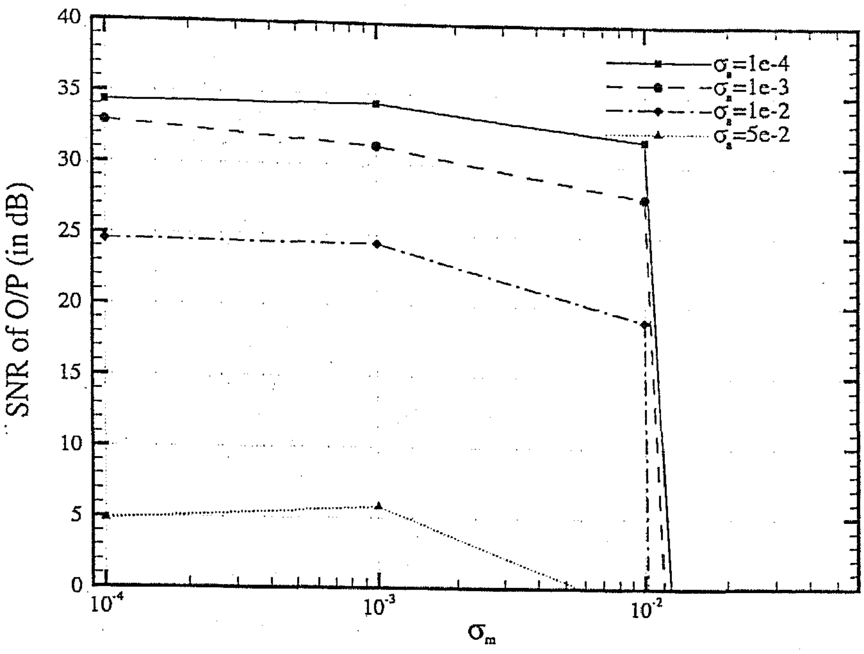

Figure 7.12: Variation of SNR of output signal with multiplicative error, σ_m for different levels of additive error σ_a ($cc = 1$, $N = 2$, Kalman filter).

error σ_a, at various values of multiplicative error σ_m, while Figure 7.12 shows the SNR of output *vs.* σ_m plots at various values on σ_a. From these plots, similar kind of characteristic can be observed between σ_a and σ_m as was between σ_{det} and σ_{slm} respectively, in optical LMS implementation. We noticed the effects of multiplicative errors in the reduction of SNR of output is more decisive than additive errors. Steep fall of curves after $\sigma_m > 10^{-2}$ in Figure 7.12 confirms this fact. Hence, the designer should be more concerned to reduce the level of multiplicative errors in the optical configuration of optical Kalman filter. One more observation can be derived at by observing these plots that, if we allow the upper limit of optical errors to be of the order of 10^{-2}, i.e., σ_a, $\sigma_m \leq 10^{-2}$, the optical Kalman filter gives SNR of output $\leq 7dB$ as compared with the ideal implementation ($\sigma_a = \sigma_m = 0$). This values can be treated as the upper limits of the optical errors.

Chapter 8

General discussion on optical system

The aim of this section is to provide some general features of optical systems and some current researches/technologies which prompted us for the current thesis.

8.1 Merits and limitations of optical system

An optical system can be divided into two parts:

- The optical communication system
- Carrying out a sort of computation with or utilizing optical signal and associated components.

The most remarkable feature of the optical system (part one), which has been luring researchers for long time is its available bandwidth or the amount of data that can be transmitted. Striking feature of second part is the enormous speed of computation (in SLM structure the computation occurs with the speed of light, i.e., within$< 1ns$). In the present thesis, we basically dealt with the optical system of second part. Now we present some other salient features of the second part.

Apart from the speed, the inherent parallelism of optics is other prominent feature. Unlike electronic signal processing systems, which have one (temporal) degree of freedom, typical optical processors have two (spatial) degree of freedom. Utilizing this feature, the speed of computation on huge data can further be increased. As image is itself an optical signal, so certain image processing functions may be carried out by specific optical systems in it, with no need of sampling, quantization, and such. This results in faster and better resolution outputs than their electronic counterparts. Immunity to electromagnetic interference is other important aspect of optical processors.

Optical processors based on SLM although seems very powerful but lack of availability fast, high resolution SLMs is the major obstacle that has prevented many optical computing systems from reaching reality. Particularly its writing time is the major concern. Large writing time reduces the throughput of the system. For most SLMs the writing time of a pixel is of the order of $10^{-2} - 10^{-6}s$ [14]. AO cell is a good choice in place of SLMs. AO cells are simpler, faster, and have better operating characteristics, but architectures of AO cells are not completely parallel. Hence, parallelism of optics cannot be fully utilized. Apart from it, AO cell requires bulky driving circuitry. Another limitation in AO cell is its available time-bandwidth product, TB [50]. It limits the maximum number of elements that can be represented in AO cell or in other words restrict the array size of matrix or vector that has to be handled. Crossing this limit, results in crosstalk [50] between different elements. Thereby degrade the result. Typically, TB lies between 200 and 2000. To circumvent this problem, multiple AO cells can be used.

The other important thing to point out is the dynamic range of optical systems [21]. The range of possible values, as well as how fine its division is, are limited by various properties of the optical system like, energy of light source, efficiency of modulators, and performance of photodetectors etc. Typical optical systems have dynamic range of few hundreds, which implies that when data values are represented by analog intensities the obtainable accuracy is roughly equivalent to that of 8-bit binary numbers. To obtain the digital accuracy optical signal is made binary. Many optical system architectures have been proposed to get the digital accuracy [53]-[55] at the same time, it increases the complexities of optical processor.

Now we discuss about typical error/noise levels of optical components we have used. In fabrication of tapped optical delay lines, the positional accuracy of the taps can be maintained within $10\mu m$. Hence, the error in sampling time is [14], [15] of the order of 10^{-4}. Therefore, the additive noise due to tap positioning error is of the order of 10^{-4}. In implementing the weight vector with the SLM, an error of less than 5% is expected. So, the RMS values of the spatial errors should be between 10^{-3} and 10^{-2}. Similarly, the RMS value in the detector noise will be in the range of 10^{-3} and 10^{-2} [14], [15]. In AO cell structure after correcting all the correctable errors, one can still expect an error of the order of 10^{-3}.

8.2 Current technology

A very high cost of optical components has prevented the wide spread use of optical processors and limited it for specific applications. On the other hand electronic processors are very easy to fabricate using VLSI technologies, thus electronic processor chips are cheap. While fabrication and assembling the optical components require time which increases its cost. Efforts are being made to micro-integrate and miniaturize the optical components to obtain reasonably compact and robust optical processors compatible with the existing electronic VLSI technology. M. Gruber *et al.* in their paper [56] has demonstrated a planar-integrated optical vector-matrix multiplier. This multiplier is based on planar-integrated free-space optics [57], [58] which means that the optical system is folded into a transparent substrate so that all functional components such as lenses or diffraction gratings are located at the surfaces. In this way the optical system can be fabricated as a whole with planar lithographic techniques. Opto-electronic circuits that acts as signal sources, modulators, or detectors can be bonded onto the optical substrate. This technique promises to integrate various optical components to miniaturize and make it robust, therefore we are hopeful that further research on it would be able to make optical processors commercial. Also, with the improvement in the technology of SLMs, writing speeds in nanoseconds are expected in future. This will make optical processors more viable.

Chapter 9

Summary and Conclusions

9.1 Main contributions

We have discussed the electro-optic implementation of ANC based on LMS and Kalman filter algorithms. Their performance analysis was done under optical errors/noise and also under different algorithm parameters through the computer simulations. The theoretical equation obtained for *excess-mean-square-error* was modified with respect to the ANC. Guidelines on finding acceptable upper limits on standard deviations of errors/noise present in various optical devices were determined. These guidelines are helpful for the engineers involved in the design and fabrication of high performance optical processors for noise cancellation in optical signals. We also compared the ANC method with respect to both LMS and Kalman filter algorithms. Effects of various parameters such as adaptive gain constant and initial number of taps, on performance of ANC were studied.

9.2 Conclusions

The research carried out for this thesis reviewed the concepts of ANC method using LMS and Kalman filter algorithms and showed that it is possible to realize these algorithms on optical processors.

From the analysis of results, it is found that if the standard deviation of optical errors/noise $< 10^{-3}$, the output SNR obtained from the optical realization of LMS algorithm for ANC and that from an electronic realization of the same algorithm is comparable. Also, if the adaptive gain constant μ, is chosen approximately equal to μ_{opt}, the effects of optical errors/noise on the output of the optical realization of ANC can be reduced further. The designer should give more emphasis to reduce the spatial errors of the SLMs. With the increase of number of taps the performance deteriorates, hence attempts should be made to use as few number of taps as possible. The time delay between primary and reference should be calculated *a priori,* this helps in choosing minimum number of taps.

Similarly, for the model of optical Kalman filter, the RMS values of optical errors/noise should be controlled to be less than 10^{-3}, the output SNR is almost same to that obtained from an electronic realization. Despite the increase of optical components in the realization of Kalman filter, this algorithm is more resistant to the errors/noise, if the the intermediate signal values are suitably modified. The designer should make attempts to reduce the RMS value of the residual multiplicative errors (fixed errors) of the system below 10^{-2}. If this limit is not maintained the performance of the optical realization of Kalman filter deteriorates. Hence, the fixed errors of the system should be calculated precisely and a proper correction should be made. On the other hand, the ANC works even if the RMS values of the additive errors/noise are of the order of 10^{-1}. In Kalman filter case also, the number of taps should be taken as small as possible. We also observe that the Kalman filter is more prone to deteriorate than the LMS filter with the increase of number of taps in presence of optical errors/noise.

Final parameter that decides the applicability of an ANC for removing noise of the system is the correlation coefficient *cc.* Decrease in its value, causes the output SNR to decrease. Hence ANC is applied where *cc* is close to 1. Under this condition it gives output SNR, which is very difficult to obtain by direct filtering method.

Despite the hardware errors and noise in the optical realizations of ANC, it seems to be promising for the signals in the bandwidth $> 100MHz$. With the advancement of technology it is possible to miniaturize and integrate the various optical components. We are hopeful that the optical processors can be made more commercial in future. Also, with the improvement in the technology of SLMs, their writing speeds in nanoseconds are expected in future. This will make optical processors more viable.

9.3 Future work

The optical implementations of LMS and Kalman filter algorithms discussed in this thesis do not restrict their applications only to ANC, but can be extended to other problems. Some of the earlier works on optical Kalman filter are described in [59]-[62]. It can be applied to the problems of adaptive phased array radar processing [63], optimal control, and state estimation. There is a wide scope of using it in many applications; particularly in optical communication systems, where optical signals from optical fiber can directly be processed without converting it to electrical signals. By following the approach in this thesis one can also implement some other algorithms electro-optically.

Important aspect that we did not cover is the timing analysis of the optical implementations, i.e., the actual time taken for a single iteration or actual time for the convergence of algorithms. This analysis will show the advantages of optical processors in realizing complex signal processing algorithms. One can also analyze the system by taking other errors into consideration, which we had neglected. As a future research, these areas can be explored.

Bibliography

[1] B. Widrow et al., "Adaptive noise canceling: Principles and applications," *Proc. IEEE*, vol. 63, pp. 1692-1716, Dec. 1975.

[2] M.R. Sambur, "Adaptive noise cancelling for speech signals," *IEEE Trans. on Acoust. Speech Signal Proc.*, vol. ASSP-26, no.5, pp. 419-423, 1978.

[3] G. S. Kang, and L. J. Fransen, "Experimentation with an adaptive noise cancellation filter," *IEEE Trans. Circuits Syst.*, vol. CAS-34, pp. 753-758, 1987.

[4] D. Chazan, Y. Medan, U. Shvadron, "Noise cancellation for hearing aids," *IEEE Trans. on Acoust. Speech Signal Proc.*, vol. ASSP-36, pp. 1697-1705, 1988.

[5] M. M. Sondhi, "An adaptive echo canceller," *Bell syst. Tech. J.*, vol. 46, pp. 497-511, 1967.

[6] P. W. Howells, "*Intermediate Frequency Sidelobe Canceller*," U. S. Patent3,202,990, August 24, 1965.

[7] B. Widrow, *et al.*, "Adaptive antenna systems," *Proc. IEEE*, vol. 55, pp. 2143-2159, 1967.

[8] N. Srinivasa, K.R. Ramakrishanan, K. Rajgopal, "Adaptive noise cancelling in computed tomography," *IEEE Cnf., Engg. of Comp.-Based Medical Syst., Proc. of Symp. on the,* pp. 65-68, 1988.

[9] M. Afzal, R. Polikar, L.Upda, S. Upda, "Adaptive noise cancellation schemes for magnetic flux leakage signals obtained from gas pipeline inspection," *ASSP, Proc., IEEE Int. Cnf.*, vol. 6, pp. 3389-3392, 2001.

[10] G. Placzek, J. W. Lane, Jr., G. Coutu, "Application of noise-cancelling methods to ground-penetrating radar data," *Int. Cnf. on S.P. Appl. and Tech.,Boston, Mass. oct 7-8, Proc.: San Francisco, Miller Freeman Inc.*, pp. 958-962, 1996.

[11] C. L. Bhat, *et al.*, "Ground-based detection of cosmic gamma-ray bursts through atmospheric scintillation technique-A feasibility study," *Bull. Astr. Soc. India*, vol. 27, pp. 323-326, 1999.

[12] W. B. Jones, Jr., *Introduction to Optical Fiber Communications Systems*, Holt, Rinehart and Winston, New York, NY, 1988.

[13] H. Taylor, "Application of Guided-Wave Optics in Signal Processing and Sensing," *Proc. IEEE,* vol. 75, pp. 1524-1535, 1987. Also see C. T. Chang, J. A. Cassaboom, and H. F. Taylor, "Fiber-optic delay line devices for RF signal processing," *Elect. Lett.*, vol. 13 (22), pp. 678-680, 1977.

[14] P. Paparao, A. Ghosh, and S. D. Allen, "Design and performance optimization of fiber optic adaptive filters," *Applied Optics*, vol. 30, pp. 1826-1838, 1991.

[15] A. Ghosh, J. Barner, and P. Paparao, "Design of Least-Mean-Square based adaptive Optical Equalizers," *Opt. Comm.*, vol. 91, pp. 280-292, 1992.

[16] A. Ghosh and P. Paparao, "Acousto-optic infinite-impulse-response digital filters for line enhancement or notch filtering," *Optical Engg.*, vol. 36 (9), pp. 2579-2585, 1997.

[17] A. Ghosh, S. Frank, "Design and performance analysis of fiber-optic infinite-impulse response filters," *Applied Optics*, vol. 31 (23), pp. 4700-471, 1992.

[18] A. Ghosh and J. Trepka, "Design of Fiber optic Adaline Neural Networks," *Optical Engg.*, vol. 36 (3), pp. 843-848, 1997.

[19] J. Capmany *et al.*, "Synthesis of fiber-optic delay-line filters," *J. of Lightwave Tech*, vol. 13 (10), pp. 2003-2012, 1995.

[20] R. I. MacDonald, "Switched optical delay-line signal processors," *J. of Lightwave Tech*, vol. LT 5 (6), pp. 856-861, 1987.

[21] D. G. Feitelson, *Optical Computing*, MIT, Cambridge, MA, 1988.

[22] B. Widrow, and S. D. Stearns, *Adaptive signal processing*, Prentice-Hall, Eaglewood Cliffs, N.J., 1985.

[23] S. Haykin, *Adaptive filter theory*, 3rd ed., Prentice-Hall Inc., Eaglewood Cliffs, N.J., 1996.

[24] Treichler, J.R., C. R. Johnson, Jr.,and M. G. Larimore, *Theory and design of adaptive filters*, Upper Saddle River, NJ USA, Prentice-Hall, 2001.

[25] H. Kenneth, and K. Ray, *Linear Algebra,* Prentice-Hall of India, 1984; see also D. K. Faddeev and V. N. Faddeeva, *Computational Methods of Linear Algebra*, Freeman, San Francisco, 1963.

[26] A. Benveniste, M. Metrivier, and P. Priouret, *Adaptive Algorithms and Stochastic Approximations*, Springer-Verlag, 1990.

[27] R. E. Kalman, "A new approach to linear filtering and prediction problems," *Trans. ASME, J. Basic Eng.*, vol. 82, pp. 35-44, 1960.

[28] R. S. Bucy and P. D. Joseph, *Filtering for Stochastic Processes, with Applications to Guidance*, Wiley, New York, 1968.

[29] M. S. Grewal, "Application of Kalman filtering to the calibration and alignment of inertial navigation system," *Proc. of PLANS '86-Position Location and Navigation Symposium*, Las Vegas, 1986.

[30] M. S. Grewal and R.S. Miyasako, "Gyro compliance estimation in the calibration and alignment of inertial measurement units," *Proc. of the Eighteenth Joint Service Conference on Data Exchange for Inertial Systems*, San Diego, 1986.

[31] C. K. Churi and G. Chen, *Kalman Filtering with Real-Time Applications*, Springer-Verlag, New York, 1987.

[32] J. Kesler and S. Haykin, "An adaptive interference canceller using Kalman filtering," *Communication Research Laboratory, McMaster University, Hamilton*, Ontario, Canada L8S 4L7, 19....

[33] D. N. Godard, "Channel equalization using a Kalman filter for fast data transmission," *IBM J. Res. Dev.*, vol. 18, pp. 267-273, 1974.

[34] M. S. Grewal, and A. P. Andrews, *Kalman Filtering Theory and Practice*, Upper Saddle River, NJ USA, Prentice-Hall, 1993.

[35] P. S. Maybeck, *Stochastic Models, Estimation, and Control*, Vol. 1, Academic Press Inc., 1979.

[36] G. Welch, and G. Bishop, "An introduction to the Kalman filter," *Deptt. of Computer Science, University of North Carolina at Chapel Hill*, Chapel Hill, NC, 2002.

[37] A. V. Oppenheim, R.W. Schafer with J. R. Buck, *Discrete time signal processing*, Prentice-Hall, Eaglewood Cliffs, N.J., 2001.

[38] K. Jackson *et al.*, "Optical Fiber Delay-Line Signal Processing," *IEEE Trans. Microwave Theory Tech.*, MTT-33, pp. 193-210, 1985.

[39] B. Nyman and P. Prucnal, "Passive Waveguide structures for Integrated Optical Signal Processing," *Opt. Engg.*, vol. 28, pp. 982-989, 1989.

[40] D. Du Toit and H. Roberts, " A single Fiber Linear Bus LAN Topology," *Proc. Soc. Photo-Opt. Instrum. Engg.*, vol. 991, pp. 170-178, 1988.

[41] D. S. Shenk and L. G. Cohan, "Fiber-Optic Tapping via Induced Scattering," *IEEE/OSA J. Lightwave Tech.*, vol. LT-7, pp. 1556-1558, 1989.

[42] P. Paparao and A. Ghosh, "Performance Optimization of Fiber Optic Adaptive filters," in *Conf. Record, 1990 International Topical Meeting on Optical Computing*, Kobe, Japan (SPIE, Bellingham, WA, 1990), pp. 311.

[43] B. E. Shwekla, and R. I. Mac. Donald, "Optoelectronic Transversal Filter," *Electronics Letter,* vol. 27, pp. 1769-1770, 1991.

[44] K. Sasayama, M. Okuno, and K. Habara, "Coherent Optical Transversal Filter using silica-based waveguides for high speed signal processing," *J. of Lightwave Tech.,* vol. 9(10), pp. 1225-1230, 1991.

[45] D. Casasent, J. Jackson, and C. P. Neuman, "Frequency-multiplexed and pipelined iterative optical systolic array processors," *Applied Optics*, vol. 22 (1), pp. 115-124, 1983.

[46] C. Caraiscos and B. Liu, " A roundoff error analysis of the LMS adaptive algorithm, "*IEEE Trans. Acoustics, Speech Signal Process.,* vol. ASSP-32, no. 1, pp. 34-41, 1984.

[47] D. Casasent and A. Ghosh, "Optical Linear Algebra Processors: Noise and Error-Source Modeling," *Optics Letter*, vol. 10, pp. 252-254, (1985). Also see A. Ghosh, D. Casasent, and C. P. Neuman, "Performance of direct and iterative algorithms on an optical systolic processor," *Applied Optics*, vol. 24 (22), pp. 3883-3892, 1985.

[48] J. M. Senior, *Optical Fiber Communications,* Prentice-Hall of India, New Delhi, 1994.

[49] D. Casasent, "Acoustooptic Linear Algebra Processors: Architectures, Algorithms, and Applications," *Proc. IEEE*, vol. 72 (7), pp. 831-848, 1984.

[50] W. T. Rhodes and P. S. Guilfoyle, "Acoustooptic Algebraic Processing Architectures, " *Proc. IEEE*, vol. 72 (7), pp. 820-830,(1984.

[51] H. J. Caufield *et al.*, "Optical implementation of systolic array processing," *Opt. Comm.*, vol. 40 (2), pp. 86-90, 1981.

[52] R. A. Athale and J. N. Lee, "Optical Processing Using Outer-Product Concepts," *Proc. IEEE.*, vol. 72 (7), pp. 931-941, 1984.

[53] P. S. Guilfoyle, "Systolic acousto-optic binary convolver," *Optical Engg.*, vol. 23, pp. 20-25,(1984.

[54] R. A. Athale, W. C. Collins, and P. D. Stilwell, "High accuracy matrix-matrix multiplication with outer product processor," *Applied Optics*, vol. 22, pp. 368-370, 1983.

[55] R. P. Bocker, S. R. Clayton, and K. Bromley, "Electrooptical matrix multiplication using the twos complement arithmetic for improved accuracy," *Applied Optics*, vol. 22 (13), pp. 2019-2021, 1983.

[56] M. Gruber, J. Jahns, and S. Sinzinger, "Planar-integrated Optical Vector-Matrix Multiplier," *Applied Optics,* vol. 39, No. 29, pp. 5376-5373, 2000.

[57] J. Jahns and A. Haung, "Planar Integration of free-space Optical components," *Applied Optics*, vol. 28, pp. 1602-1605, 1989. Also see, A.K. Ghosh, "Optical processing of signals in Surface Plasmon Resonance optical sensors," *Deptt. of Elec. Engg. IIT Kanpur*, Kanpur, India, 2000.

[58] J. Jahns, "Planar Packing of free-space Optical Interconnections," *Proc. IEEE*, vol. 82, pp. 1623-1631, 1994.

[59] J. Jackson and D. Casasent, "State estimation Kalman filter using optical processing: noise statistics known," *Applied Optics*, vol. 23 (3), pp. 376-378, 1984.

[60] D. Casasent, C. P. Neuman, and J. Lycas, "Optical Kalman filtering for missile guidance," *Applied Optics*, vol. 23 (12), pp. 1960-1966, 1984.

[61] J. L. Fisher, D. Casasent, and C. P. Neuman, "Factorized extended Kalman filter for optical processing," *Applied Optics*, vol. 25 (10), pp. 1615-1621, 1986.

[62] J. L. Fisher, D. Casasent, and C. P. Neuman, "Factorized extended Kalman filter: case study results," *Applied Optics*, vol. 27 (9), pp. 1877-1885, 1988.

[63] P. F. McManamon, *et al.*, "Optical phased array technology," *Proc. IEEE*, vol. 84, pp. 268-298, 1996.

A 145006

A145006